Function of the Cytoplasmic FMRP Interacting Protein 1 (CyFIP1) in mouse

Dissertation

zur Erlangung des Doktorgrades (Dr. rer. nat.)
der Naturwissenschaften im Fachbereich Biologie

der Mathematisch-Naturwissenschaftlichen Fakultät
der Rheinischen-Friedrich-Wilhelms-Universität Bonn

vorgelegt von

Stefanie Stöcker

aus Siegburg

Bonn, im August 2015

Angefertigt mit Genehmigung der Mathematisch-Naturwissenschaftlichen Fakultät der Rheinischen Friedrich-Wilhelms-Universität Bonn.

Gutachter:

1. Gutachter: Prof. Dr. Walter Witke

2. Gutachter: Prof. Dr. Dieter Fürst

Tag der Promotion: 30.03.2016

Erscheinungsjahr: 2016

Summary

CyFIP (Cytoplasmic Fragile X mental retardation protein Interacting Protein) is a large scaffolding protein that was shown to be a central regulatory component of the WAVE complex. The pentameric WAVE complex is a nucleation promoting factor (NPF) regulated by phosphoinositides and phosphorylation, which translates signals from the small GTPase Rac1 by exposing the VCA domain in the WAVE subunit, thus activating the Arp2/3 actin nucleation complex and initiating actin polymerization. Actin reorganization is important for cell motility, migration, locomotion, proliferation and more. Except for HSPC300/Brick, each subunit is represented by a gene family - CyFIP1 and CyFIP2 for CyFIP, Nap1/Hem2 and Hem1 for Nap, WAVE1, WAVE2, and WAVE3 for WAVE, and Abi1, Abi2, and Abi3 for Abi. In principle this allows to build many different WAVE complexes, a few of which have also been crystalized and their structure determined. Despite the extensive sequence similarity, the expression pattern of CyFIP1 and CyFIP2 in mouse tissues suggests distinct physiological roles. CyFIP1 is ubiquitously expressed, while CyFIP2 has a more specialized function in the nervous system, where it is ten-fold more abundant than its homologue. CyFIP1 has been proposed to function as a tumor suppressor gene and is a known interaction partner of FMRP in the brain (Fragile X Mental Retardation Protein), hence having a distinct role in translational control. CyFIP1 has also been linked to autism spectrum disorder phenotypes in Prader-Willi, Angelman and Fragile X Syndromes.

In this work the role of CyFIP1 during mouse embryonic development, ES cells in vitro differentiation and female fertility was analyzed, as well as the composition of the WAVE complex. The results showed that CyFIP1 has an essential role in early embryonic development and CyFIP1-/- embryos die around embryonic day 6.5. To obtain better insight into the function of CyFIP1 in development two strategies were used: 1. analysis of the embryos and 2. Generation and differentiation of ES cells. Generated CyFIP1-/- ES cells showed disturbed cell proliferation, differentiation and adhesion. Differentiation studies of CyFIP1-/- ES cells into embryoid bodies (EB) indicated that lineage determination is altered. EBs showed an increase in endodermal tissue, a decrease in meso-endodermal tissue and higher apoptosis. Importantly ES cells showed alterations in the levels of several WAVE complex components. Microarray analysis of in vitro differentiated ES cells revealed down-stream effectors and pathways affected by CyFIP1 depletion.

CyFIP1+/- females showed an infertility disorder similar to women with Fragile X-dependent POI (primary ovarian insufficiency) Syndrome. Investigations in the ovaries and follicles of wild type and CyFIP1+/- females showed some important differences. Altered follicle distribution in the ovaries of CyFIP1+/- females was observed. Antral and preovulatory follicles of CyFIP1+/- females appeared significantly smaller than wt. Studies on the ligands and composition of the WAVE complex indicated that the WAVE complex is not an irreversibly stable pentameric complex. Biochemical analyses under different ionic conditions were made and results are in agreement with the predictions from the structure determined by the Rosen lab, showing how CyFIP/Nap forms a core complex around which the other subunits assemble. Variable complexes were recognized in different tissues. Novel Cyfip1/2 ligand candidates were identified by mass spectrometry after pull-down of the complex in brain, such as Cofilin1, CapZ, Myosin1 and Myosin4. One surprising novel Cyfip1/2 ligand was POF1 (Premature ovarian failure 1B), an actin binding protein mutated in human premature ovarian failure. These latest findings expand the current view of the WAVE complex.

Table of Contents

Abbreviations

°C	degree Celsius
µg	microgram
µl	microliter
µM	micromolar
µm	micrometer
3’ UTR	3-prime untranslated region
5’ UTR	5-prime untranslated region
AB	Antibody
ABP	Actin binding protein
ADP	Adenosine diphosphate
Arp	Actin related protein
APS	Ammonium persulfate
ATP	Adenosine triphosphate
BMP	Bone morphogenetic protein
bp	Base pair
BSA	Bovine serum albumin
CAP	Cyclase-associated protein
CNS	Central nervous system
DAPI	4',6-diamidino-2-phenylindole
DEPC	Diethylpyrocarbonate
DMEM	Dulbecco's modified Eagle's medium
DMSO	Dimethyl sulfoxide
DNA	Deoxyribonucleic acid
dpc	Days post coitum
E	Embryonic day
ECL	Enhanced chemiluminescence
EDTA	Ethylenediaminetetraacetic acid
ERK	Extracellular-signal regulated kinase
ES cell	Embryonic Stem cell
Et. al.	Et alii (and others)
EtBr	Ethidium bromide
EtOH	Ethanol

FACS	Fluorescence-activated cell sorting
F-actin	Filamentous actin
FCS	Fetal calf serum
Fig.	Figure
fl	flox
G-actin	Globular actin, monomeric actin
Hepes	4-(2-hydroxyethyl)-1-piperazineethanesulfonic acid
HRP	Horseradish peroxidase
kb	kilobase
kDa	kilodalton
KO	Knockout
LIF	Leukemia inhibitory factor
MAPK	Mitogen activated protein kinase
min	minute
mm	millimeter
nm	nanometer
nt	nucleotide
N-WASP	Neural WASP
PAGE	Polyacrylamide gel electrophoresis
PBS	Phosphate buffered saline
PCR	Polymerase chain reaction
PFA	Paraformaldehyde
Pfn	Profilin
PI3K	Phosphoinositid-3-Kinase
qPCR	quantitative (real-time) PCR
RNA	Ribonucleic acid
rpm	rotations per minute
RT	Room temperature
RT	Reverse Transcription
sec	second
SDS	Sodium dodecylsulfate
TAE	Tris acetate EDTA buffer
TBS	Tris buffered saline
TBST	Tris buffered saline with Tween 20

TEMED	N,N,N',N'-Tetramethylethylenediamine
Tris	Tris(hydroxymethyl)aminomethane
TritonX-100	*t*-Octylphenoxypoly(ethoxy)$_9$-ethanol
Tween 20	Poly(oxyethylene)$_{20}$-sorbitan-monolaurate
u	units (enzymes)
UV	Ultraviolet light
V	Volt
VCA domain	Verprolin homology, Cofilin homology, Acidic region domain
v/v	volume per volume
w/v	weight per volume
WASP	Wiscott-Aldrich Syndrome protein
WAVE	WASP verprolin homologous protein
wt	wild type

List of Figures

1. Introduction

1.1 The actin cytoskeleton

The term cytoskeleton was first introduced by the French embryologist Paul Wintrebert in 1931. The cytoskeleton is composed of three major types of protein filaments: microtubules, intermediate filaments, and microfilaments. Microfilaments are polymers of actin that together with a large number of actin-binding and associated proteins constitute the actin cytoskeleton. Actin genes have been highly conserved during evolution, and actin molecules from various organisms are functionally interchangeable in vitro (Kron, Drubin et al. 1992; Nefsky and Bretscher 1992). Actin is a 42 kDa ATPase that can polymerize into filaments of 7 nm in diameter. Two different actin forms exist. G-actin is the monomeric form and F-actin is the polymeric form of actin. Globular (G) actin is able to polymerize into filamentous (F) actin which can disassemble back into the initial G-actin. Actin filaments are very dynamic and live in permanent reorganization. ATP-bound G-actin assembles into the filament. Upon binding to the end of a filament, an actin subunit rapidly hydrolyzes its bound ATP into ADP and a phosphate group (Pi) that is slowly released (Fig. 1). ADP-bound actin is prone to depolymerization. Released ADP-G-actin is recharged with ATP and ATP-G-actin is able to bind again. ATP-actin subunits preferentially bind to the fast growing "barbed" end of an actin filament (Fig. 1), although they can also bind on the other side, to the "pointed" end, at a much slower rate. In the cell, several actin binding proteins act together to control the polymerization process, which is directed towards the cell membrane.

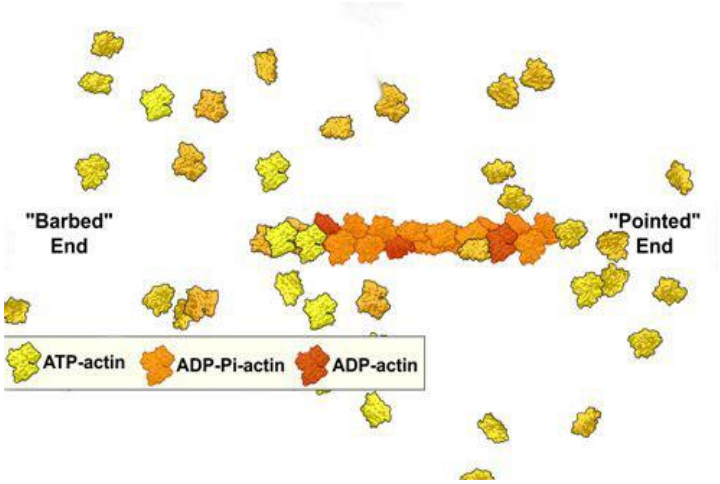

Figure 1: Actin polymerization and depolymerization.
Continuous remodeling of the actin filament at the fast growing barbed end and slow growing pointed end (Kuhn and Pollard 2005).

1.2 Actin binding proteins

Actin filaments play a crucial role in different processes such as cell migration, motility, intracellular trafficking and cell division. All of these are dynamic processes that require polarity and a continuous reorganization of the actin filament network. In cells, the assembly and disassembly of actin filaments, and also their organization into functional higher order networks, is regulated by a plethora of actin-binding proteins (ABPs) (dos Remedios, Chhabra et al. 2003). The activities of these proteins are in turn under the control of specific signaling pathways. They have the following functions: nucleation, monomer binding, capping, stabilization, severing, depolymerization, cross-linking, sequestration, and nucleotide exchange. In Fig. 2 the different classes of actin binding proteins are shown.

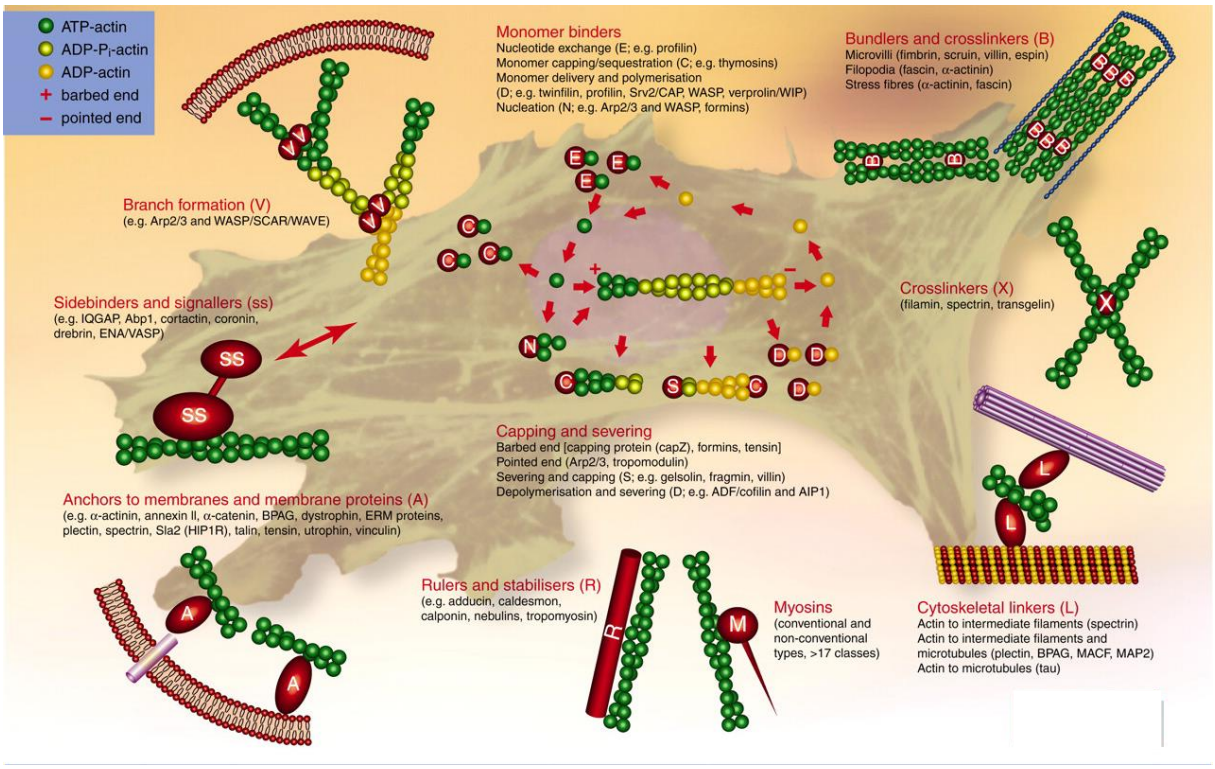

Figure 2: The actin cytoskeleton is regulated by actin-binding proteins (ABPs). Different classes of ABPs are shown (Winder 2005).

1.3 Profilin

Profilin is one of the first characterized actin binding proteins and is involved in the dynamic turnover and restructuring of the actin cytoskeleton (Carlsson, Nystrom et al. 1977). Profilin forms a 1:1 complex with G-actin and, acting as an ADP-ATP exchange factor, can regulate the rate of actin polymerization (Mockrin and Korn 1980). Today four Profilin genes are known in mice and humans (Kwiatkowski and Bruns 1988; Honore, Madsen et al. 1993; Braun, Aszodi et al. 2002; Obermann, Raabe et al. 2005). Profilin 1 and 2 are described to play a major role in actin dynamics. In mice Profilin1 is expressed ubiquitously, except in the skeletal muscle. The deletion of Profilin1 in mice results in lethality before the blastocyst stage due to a possible defect in cytokinesis (Witke, Sutherland et al. 2001). Profilin2 is mostly expressed in brain, although lower expression can be found in skeletal muscle, testis, uterus, thymus and kidney. Two splice variants, Profilin2A and Profilin2B, have been reported (Witke, Podtelejnikov et al. 1998; Di Nardo, Gareus et al. 2000). A knockout study of this gene in mice described neurological and behavioral defects (Pilo Boyl, Di Nardo et al. 2007). Profilin1 and Profilin2 form different complexes to regulate actin assembly (Witke 2004). Among others, one of the ligands in the Profilin2 complex is POP (Partner of Profilin) (Witke, Podtelejnikov et al. 1998), also named CyFIP, whose study is the main topic of this thesis.

1.4 Actin nucleators and nucleation promoting factors

Actin nucleators promote the polymerization of the different types of actin arrays formed in a variety of cellular processes, such as cell migration, cell division, cellular morphogenesis, and membrane trafficking. The first discovered actin nucleator was the Arp2/3 (actin-related protein 2/3) complex (Machesky, Atkinson et al. 1994; Mullins, Stafford et al. 1997). In the last decade the complexity of nucleation mechanisms became clear and several novel nucleators have been described. Today about 28 different nucleators are known in mammalian cells. These can be divided into three Classes (Fig. 3): (1) the Arp2/3 complex and its nucleation promoting factors (the WASP and the WAVE families), (2) formins, and (3) WH2-containing nucleators like Spire, Cobl, and Leiomodin.

WASP family members use their WH2/V (Wiskott-Aldrich homology 2/Verprolin homology) domain to recruit actin monomers and their cofilin homology (C) and acidic (A) domains to bind to one subunit of the actin-related protein 2/3 (Arp2/3) complex. This structure, created and stabilized by N-WASP, mimics an actin trimer and allows further addition of actin monomers (Takenawa and Miki 2001). Arp2/3 also allows the formation of branched actin networks (Fig. 3) (Mullins, Heuser et al. 1998). Formins are hypothesized to nucleate actin by stabilizing spontaneously formed actin dimers and/or trimers. Differently from the Arp2/3, formins remain associated with the barbed end while favouring addition of actin subunits, thus functioning also as elongation factors for the formation of long linear filaments (Fig.3) (Faix and Grosse 2006). Spire, Cobl, and Lmod contain between one and four WH2 domains each, separated by intervening linker sequences of variable length (Kerkhoff 2006). Their nucleation mechanisms are related, but each may generate an actin nucleus with distinct properties (Fig. 3), stabilized by lateral and/or longitudinal contacts between subunits, and in some cases capped at one end. In some respects, N-WASP represents a specialized form of Class 3 nucleator, in which the third actin monomer-binding domain has been replaced with a domain that binds to actin-related proteins (Chesarone and Goode 2009).

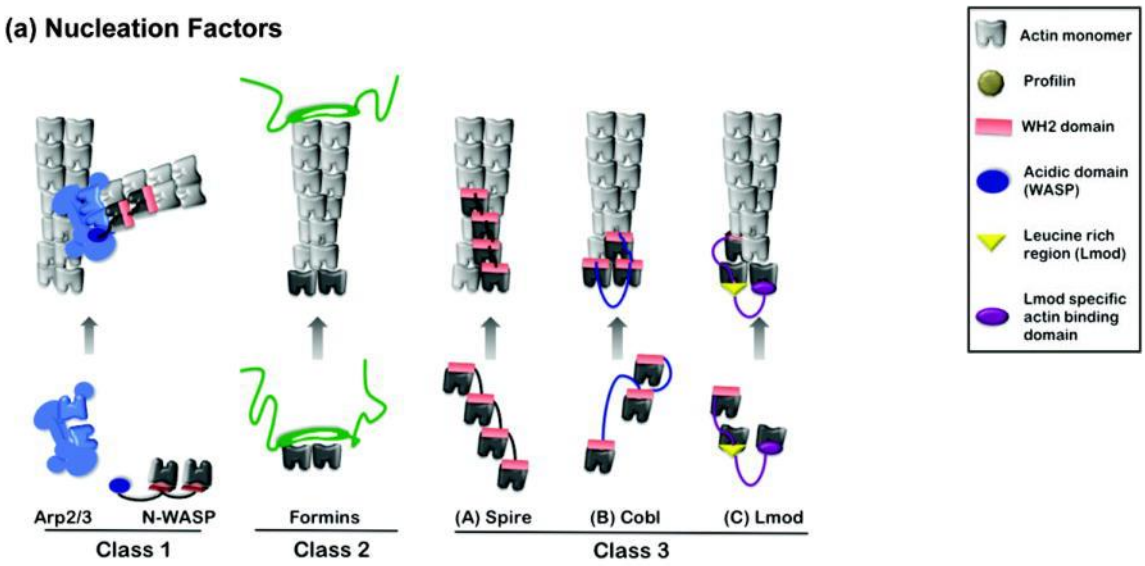

Figure 3: Mechanisms of actin nucleation. The three classes of actin nucleators and their mechanism of function are schematically represented. Nucleator domains are displayed in color, actin subunits used by nucleators to seed polymerization in black, and actin subunits polymerized from nuclei in gray (Chesarone and Goode 2009).

1.5 The Wiskott-Aldrich Syndrome protein (WASP) family

WASP has been associated with modulation of lymphocyte activation and cytoskeletal reorganization (Aldrich, Steinberg et al. 1954; Cooper, Chae et al. 1968). Indeed the Wiskott-Aldrich syndrome, an X-linked recessive disease, is characterized by immunodeficiency, thrombocytopenia and eczema (Thrasher 2002). Five proteins belong to this protein family: WASP, N(neural)-WASP, WAVE1, WAVE2 and WAVE3. WASP is only present in cells from the hematopoietic system. N-WASP shares sequence homology with WASP and shows a high expression in the nervous system (Miki, Miura et al. 1996). WAVE is the acronym of WASP-family Verprolin-homologous protein (Suetsugu, Miki et al. 1999). The three mammalian WAVE isoforms have different expression pattern. WAVE1 and WAVE3 are highly expressed in the brain, WAVE2 is ubiquitously expressed (Takenawa and Miki 2001). All WASP family members share a common C-terminal organization, the VCA region. The VCA region consists of three domains: the Verprolin homology domain (V), also known as WH2 (WASP Homology 2) domain, the cofilin homology or central domain (C), and the acidic domain (A). The N-terminus is similar in WASP and N-WASP with the WH1 (WASP Homology 1) domain and the autoinhibitory domain. WAVE proteins, instead, have a WHD (WAVE Homology Domain) also called SCAR homology domain (SHD) (Bear, Rawls et al. 1998). WASP and N-WASP possess a GTPase-binding domain (GBD), which can bind directly to the small GTPase Cdc42. Cdc42 regulates filopodia formation activating WASP/N-WASP which recruit and activate the Arp2/3 complex, triggering actin polymerization (Miki, Sasaki et al. 1998). WAVE proteins are also downstream of a small GTPase, called Rac1, but they have no possibility for a direct interaction with it, missing the GBD. Other proteins have been found to interact with WAVE and respond to Rac1 signaling, organized in the so called WAVE complex (Eden, Rohatgi et al. 2002).

1.6 The WAVE complex

The WAVE complex is formed as a heteropentamer of a molecular weight of about 500 kDa (Eden, Rohatgi et al. 2002). The components of the WAVE complex are WAVE itself, Abi (Abelson-interacting protein), Nap (Nck-associated protein), CyFIP (cytoplasmic Fragile-X mental retardation-protein interacting protein) and HSPC300 (heat-shock protein C300, also known as Brick) (Eden, Rohatgi et al. 2002). As previously mentioned, there are three WAVE isoforms in mammals, WAVE1 and WAVE2 have been reported to be part of the WAVE complex. Later studies on WAVE3 showed that WAVE3 is likely to participate in similar signaling complexes to WAVE1 and WAVE2 and that the differences between these WAVE proteins are likely to be at the level of tissue expression, differences in affinity for certain binding partners and possibly interaction with yet undiscovered binding partners (Stovold, Millard et al. 2005). The Abi family also comprises three different isoforms: Abi1, Abi2 and Abi3 (Nesh). All three can be part of the WAVE complex, but Abi3 likely plays a different role in the regulation of c-Abl (Hirao, Sato et al. 2006). Abi is a scaffolding molecule that was originally identified as an interactor for the tyrosine kinase Abl (Shi, Alin et al. 1995). Nap1 or p125Nap was reported to bind the SH3-containing protein Nck. In hematopoietic cells a different isoform is expressed called Hem1. CyFIP is the direct interaction partner of Nap1 in the WAVE complex (Fig. 4) and two isoforms exist (CyFIP1 and CyFIP2). HSPC300 is the smallest subunit of the WAVE-complex, a small peptide of approximately 75 amino acids whose function is still unclear.

The exact architecture of the WAVE complex was identified by Chen et al. in 2010 and is schematized in Figure 4. The WAVE complex consists of two sub-complexes: a dimer formed by pseudo-symmetric association of the two large, similar proteins CyFIP and Nap1, and a trimer formed by the N-terminus of WAVE1, Abi2 and HSPC300 forming a four-helix bundle.

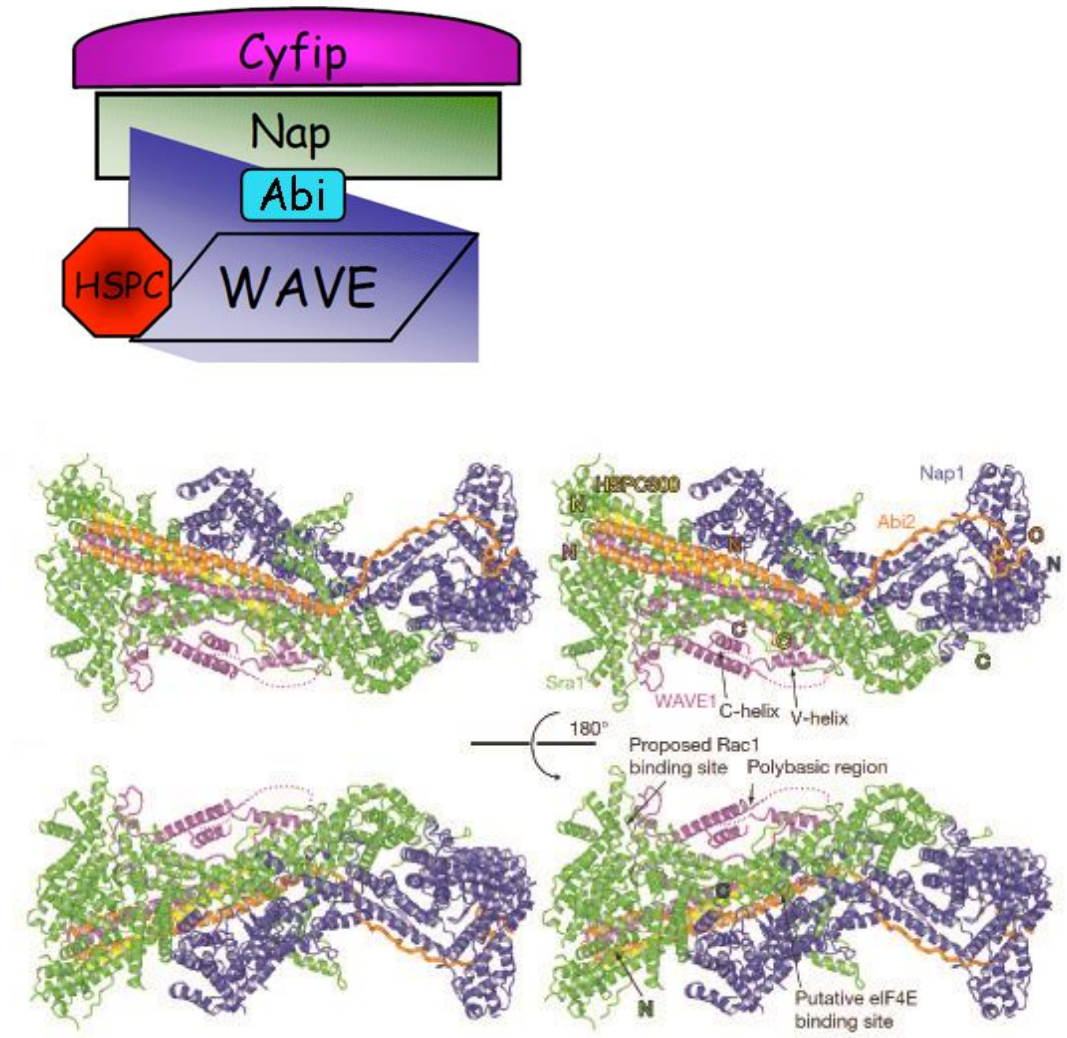

Figure 4: Structure and composition of the WAVE complex. A) Topography as determined by biochemical studies (Adapted by Marzia Massimi from Gautreau 2004). **B, C)** CyFIP/Sra1 and Nap1 build the base of the complex as a pseudo-symmetric dimer. WAVE, Abi and HSPC300 form a trimer that lies on top of the base. In case of the inactive form, Nap1 keeps the VCA region of the WAVE protein inaccessible to possible binding partners. Following activation by the Rac1 small GTPase this region is exposed **B)** Stereo view of the WAVE-complex. Sra1, Nap1, WAVE1, Abi2 and HSPC300 are green, blue, magenta, orange and yellow, respectively. **C)** 180° rotation around a horizontal axis of the structure in A). The polybasic region and the proposed Rac1 and eIF4E binding sites are indicated. (Chen, Borek et al. 2010)

1.6.1 Regulation of the WAVE complex

The WAVE complex plays an essential role in remodeling the actin cytoskeleton. The complex is by default inactive towards the Arp2/3 complex, but can be stimulated by the Rac1 GTPase, kinases and phosphatidylinositols. Within the structure of the

regulatory WAVE complex, the activity of WAVE toward the Arp2/3 complex is inhibited by intra-complex sequestration of its VCA region (Chen, Borek et al. 2010). In fact, the WAVE proteins lack the auto-inhibition feature. Therefore it depends on the other components of the WAVE complex fulfilling the inhibitory function. This is achieved through the structure of the complex. The inactive form of the complex shows WAVE's VCA region facing Nap1, which makes it unreachable to possible binding partners (Fig. 5). The regulatory WAVE complex is recruited to the membrane and triggered by extracellular signals to release its inhibition of WAVE (Padrick, Cheng et al. 2008; Lebensohn and Kirschner 2009). Activation of the WAVE complex is achieved by the small GTPase Rac1 (Fig. 4), which directly interacts with CyFIP1, or might act through a yet unknown mediator, by exposing the VCA domain (Goley and Welch 2006). The VCA region of the WAVE protein is responsible for the binding of Actin monomers and the Arp2/3 complex. The Arp2/3 complex, as previously explained, an important F-actin nucleator, is therefore recruited by the WAVE protein to finally trigger actin polymerization via a tripartite complex formed close to the cell membrane (Fig. 4) (Bogdan, Grewe et al. 2004).

However, the exact composition of the WAVE complex and the complexity of its regulation and function *in vivo* and in the different cell types and tissues remain still unclear.

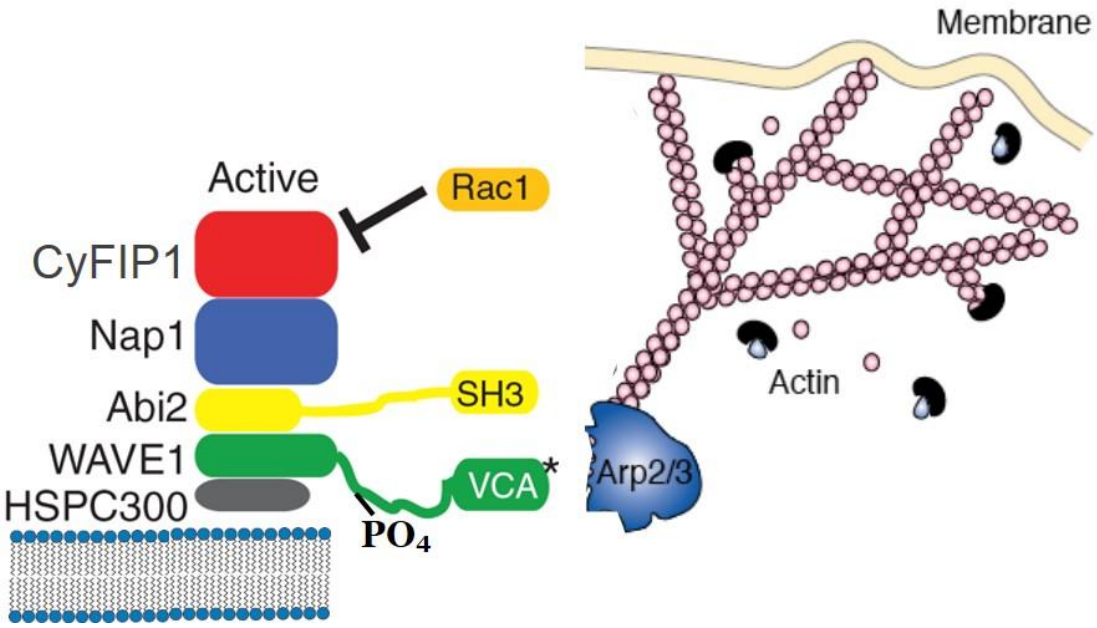

Figure 5: WAVE complex activation. Model of WAVE complex activation according to the Chen&Rosen structure (Chen, Borek et al. 2010). Activated Rac1, phosphorylation, and phospholipids are thought to unmask the VCA domain required for Arp2/3 activation (adapted from Stradal et al., TICB, 2004).

1.6.2 Genetics of the WAVE complex in the mouse

In the past years several studies on knockout mice for the different subunits of the WAVE complex have been published. There are three different studies on WAVE1 knockout mice, which were generated with two different methods. In the studies from Dahl et al. a gene trap approach was used to generate a line of mice bearing a disruption of the WAVE1 gene. Homozygous disruption of the WAVE1 gene resulted in postnatal lethality at day 20. These animals showed severe limb weakness, a resting tremor, and notable neuroanatomical malformations without overt histopathology of peripheral organs (Dahl, Wang-Dunlop et al. 2003). The same WAVE1 knockout mice were used for another study that described defects in myelin formation (Kim, DiBernardo et al. 2006). A different targeted disruption of the WAVE1 gene by homologous recombination generated viable mice with reduced anxiety, sensorimotor retardation, and deficits in hippocampal-dependent learning and memory (Soderling, Langeberg et al. 2003). WAVE2 knockout mice were created similarly by homologous recombination in one study that reported embryonic lethality at E12.5, with defects in the response of fibroblasts to platelet-derived growth factor (Yan, Martinez-Quiles et al. 2003). Another study on a different WAVE2 knockout model showed embryonic cardio-vascular defects, hemorrhages, and lethality at about embryonic day 10. Mutant endothelial cells did not form lamellipodia in response to VEGF (vascular endothelia growth factor) (Yamazaki, Suetsugu et al. 2003). One conclusion from these knockout studies could be that WAVE1 and WAVE2 have overlapping functions during early embryo development because both single mutants survive midgestation (Soderling, Langeberg et al. 2003; Yamazaki, Suetsugu et al. 2003; Yan, Martinez-Quiles et al. 2003). WAVE3 and HSPC300 knockout mice are not described yet. Abi1 knockout mice died around embryonic day 11.5 and displayed malformations in the developing heart and brain. Western blotting analysis of Abi1 ko cell lysates indicated decreased levels of WAVE2 complex components: WAVE2, Nap1, and CyFIP1. On the contrary, the expression of Abi2 was significantly increased. Apparently the presence of Abi1 is critical for the integrity and stability of the WAVE2 complex so that it cannot be restored even by enhanced Abi2 expression (Dubielecka, Ladwein et al. 2011). Homozygous deletion of the murine Abi2 gene in mice resulted in defective orientation and migration of secondary lens fibers, abnormal neuronal migration in the neocortex and hippocampus, aberrant dendritic spine morphology and density, and profound deficits

in learning and memory (Grove, Demyanenko et al. 2004). Two different Nap1 knockout mouse models are reported in the literature. In Nap1 ko mice, generated by insertional mutagenesis in the C-terminal region of the gene, embryonic lethality at E10.5 was observed, with several morphogenetic defects, such as strikingly open, undulating neural folds in the anterior of the embryo (Yokota, Ring et al. 2007). A different Nap1 mutant mouse model was generated by a missense mutation by ENU (N-ethyl-N-nitrosourea) mutagenesis at the beginning of the Nap1 coding sequence. These Nap1 knockout mice arrested embryonic development around day E9 and displayed several morphogenetic defects such as delay in endoderm and mesoderm migration, failure in heart formation and neural tube closure, duplication of the antero-posterior body axis. Interestingly, loss of Nap1 induced loss of WAVE1 expression and cellular mislocalization of Abi1 and CyFIP1/Sra1 (Rakeman 2006).

1.7 CyFIP

From previous work, CyFIP appears to have many functions and interacting partners, some of which are known and some might still be unknown. Due to this, CyFIP was given a number of names. In 1998 CyFIP was described under the name p140Sra1. It was purified from bovine brain cytosol and identified as a 140 kDa molecular mass Rac1-interacting molecule. Therefore it was named Specifically Rac-associated protein 1 (p140Sra1) (Kobayashi, Kuroda et al. 1998). At the same time CyFIP was found as an interactor of Profilin2 and named POP (Partner of Profilin) (Witke, Podtelejnikov et al. 1998). The name PIR121 (121F-specific p53-inducible RNA) was given in a work in which the level of a specific messenger RNA, identified as the CyFIP mRNA, was found increased in cell lines expressing the apoptosis-inducing p53 mutant, 121F (Saller, Tom et al. 1999). PIR121 is normally used for the Dictyostelium orthologue. Another name for CyFIP, derived from a work on a C. Elegans mutant phenotype, is Gex2 or Gut on the Exterior 2 (Soto, Qadota et al. 2002). Finally, the name CyFIP1 and 2 (Cytoplamic FMRP Interacting Protein) was given in 2001 when a yeast two-hybrid screening yielded two novel interactors of FMRP (Schenck, Bardoni et al. 2001). Related to this, a novel role for CyFIP1 was recently reported, that might be independent from its role in the WAVE complex. CyFIP1 can behave as an eIF4E inhibitor, a novel 4E-BP (eukaryotic translation initiation factor 4E Binding Protein),

cooperating with FMRP in down-regulating translation in neurons (Napoli, Mercaldo et al. 2008). In lower organisms only one CyFIP gene is present, while in human and mouse two genes, encoding for CyFIP1 and CyFIP2, are found. In the mouse these genes are located on chromosome 7 and 11, respectively, showing the same genomic organization of 31 exons encoding for 1253 amino acids. CyFIP1 and 2 share 88% amino acid sequence identity and have the same molecular weight of 145 kDa. In the mouse CyFIP2 was shown to be approximately 10 fold more abundant in brain than CyFIP1 at the mRNA level (Massimi 2008). CyFIP1 is the predominant isoform expressed in ES cells and early embryonic stages, while CyFIP2 is expressed later during development and then restricted to the brain (Massimi 2008), but the specific role of CyFIP1 in development is still unknown.

1.7.1 The physiological role of CyFIP1 and CyFIP2

Several studies have been carried on model organisms such as Dictyostelium, C. Elegans, and Drosophila and also on different cell types in order to understand the physiological role of CyFIP. In Dictyostelium the pirA gene which encodes PIR121/CyFIP was disrupted and defects in migration and chemotaxis were observed (Blagg, Stewart et al. 2003). Ablation of the worm gene Gex2 resulted in embryonic lethality with defects in morphogenesis of the hypodermis. In Gex2 mutants, neither dorsal intercalation nor ventral migration (including leading cell migration) occurred, resulting in the complete loss of ventral closure (Soto, Qadota et al. 2002). Drosophila Sra1 null mutants were also embryonic lethal and showed defects in synaptic architecture and bristle development (Schenck, Bardoni et al. 2003; Bogdan, Grewe et al. 2004). Studies in zebrafish showed that CyFIP2 is required to maintain positional information by dorso-nasal axons as they project through the optic tract and the tectum (Pittman, Gaynes et al. 2010). Bozdagi et al. showed that haploinsufficiency of CyFIP1 mimics key aspects of the phenotype of Fmr1 knockout mice and is consistent with the hypothesis that these effects are mediated by interaction of CyFIP1 and FMRP in regulating activity-dependent translation. They observed that in CyFIP1 heterozygous mice metabotropic glutamate receptor (mGluR)-dependent long-term depression (LTD) induced by paired-pulse low frequency stimulation (PP-LFS) was significantly increased in comparison to wildtype mice. In addition, mGluR-mediated LTD was not affected in the presence of protein synthesis inhibitors in the CyFIP1 heterozygous

mice, while the same treatment inhibited LTD in wildtype littermate controls. Behavioral studies of CyFIP1 heterozygous mice showed enhanced extinction of inhibitory avoidance (Bozdagi, Sakurai et al. 2012). In mammalian cell culture studies, using siRNA, CyFIP1 was shown to be essential for lamellipodia formation and the entire WAVE complex could no longer be detected in CyFIP1 knockdown cells (Steffen, Rottner et al. 2004).

1.7.2 CyFIP1 knockout mouse

A CyFIP1 conditional knockout mouse was generated by Dr. Marzia Massimi in a C57BL/6J mouse genetic background. The targeting vector carrying the CyFIP1 genomic sequence and LoxP sites flanking exon 4 and exon 6, together with a Neomycin resistance cassette, was created as shown in Fig. 6. Excision of the LoxP flanked region upon Cre recombination resulted in a frame shift leading to premature translation termination soon after exon 3, producing a knockout allele. The Neomycin resistance cassette was also flanked by FRT sites, which allowed its removal upon FLP recombination (Massimi 2008) to produce a clean Flox allele.

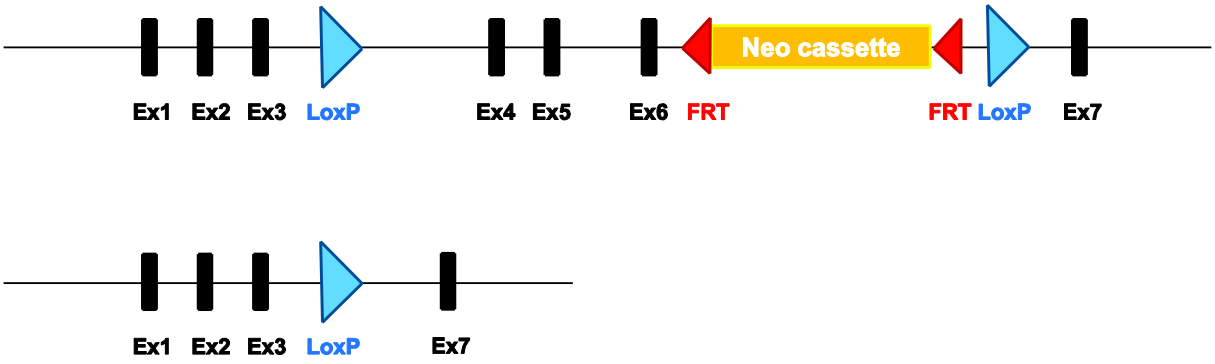

Figure 6: CyFIP1 targeted allele and the Cre-mediated recombination event leading to the CyFIP1 knockout allele. Exon 4 and exon 6 are flanked by LoxP sites. These can be used for the conditional removal of the flanked region by Cre recombination. A Neomycin resistance cassette, flanked by FRT sites, was also inserted for the selection of recombinant ES cell clones. The Neomycin cassette can be removed by FLIP recombination (Massimi 2008).

To generate the CyFIP1 complete knockout mouse, CyFIP1+/targeted mice were crossed with a Cre-deleter strain. Heterozygous CyFIP1 deleted mice (CyFIP1+/-) were then mated among themselves to obtain CyFIP1 null mutants (CyFIP1-/-). The

CyfFIP1 complete knockout resulted embryonic lethal, with embryos dying around embryonic day 8.5 due to severe developmental defects (Fig. 7). Somites were absent in the mutant embryos and the tissues appeared to be degraded. Some components of the WAVE complex were no longer detectable in homozygous CyFIP1 ko embryos by Western blotting (Massimi 2008). The generation of the conditional CyFIP1 mouse model is still in progress.

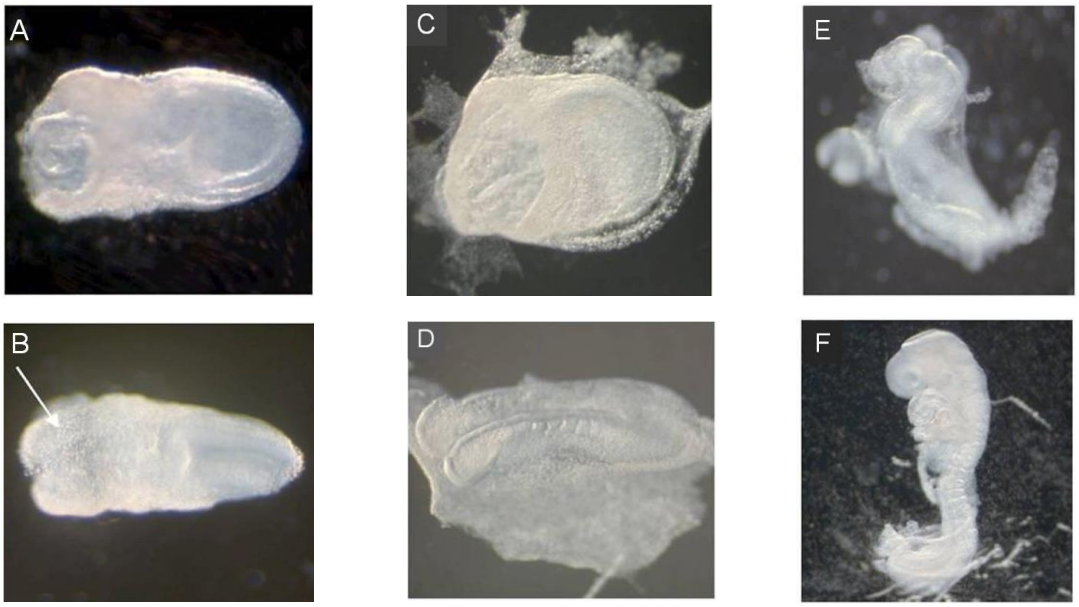

Figure 7: CyFIP1 null mutants and control littermates. (**A**) E8.5 CyFIP1-/- embryo. (**B**) E8.5 CyFIP1+/+ embryo that has started to differentiate the neural plate (indicated by an arrow). (**C**) E9 CyFIP1-/- embryo. (**D**) E9 CyFIP1+/+ embryo. The differences between mutant and wild type are more evident at this stage: it is evident the lack of differentiated somites in the mutant, while in the control 6 pairs of somites are visible. (**E**) E9.5 CyFIP1-/- embryo. (**F**) E9.5 CyFIP1+/+ embryo. Only a few mutants reached this stage, had an overall degenerated aspect, and their tissues appeared degraded (Massimi 2008).

1.7.3 CyFIP1 in Autism Spectrum Disorders

In humans, CyFIP1 has been genetically linked to a number of Autism Spectrum Disorders (ASDs), which suggests that CyFIP1 might be a central component of the different ASD pathways. The CyFIP1 gene in humans is located on chromosome 15q11.2, this is a critical region of high susceptibility to deletion and duplication (Pathania, Davenport et al. 2014). For example paternal or maternal deletion occurs in the Prader-Willi and Angelman Syndromes, respectively. The CyFIP1 gene falls within the range of chromosomal deletion responsible for the syndromes (Ben-Shachar,

Lanpher et al. 2009), and if included in the deletion increases the occurrence of the autistic phenotype in the syndromes. CyFIP1 has also been implicated in the autistic phenotype of patients with Fragile X syndrome (Clifford, Dissanayake et al. 2007). Apart from point mutations, gene dosage and copy number variation also play an important role in autism spectrum disorder (Nishimura, Martin et al. 2007). Two pathways that affect the maturation of excitatory synapses and therefore disrupt neuronal connectivity were shown to be affected by CyFIP1: the protein translation pathway (FMRP, PTEN and TSC1/2) and the actin cytoskeletal/adhesion molecule pathway (e.g Neuroligins, Neurexins, Shank and Integrin-β3) (Walsh, Morrow et al. 2008).

1.7.4 POF/POI (Premature Ovarian Failure / Premature Ovarian Insufficiency)

Besides the neurological syndromes, CyFIP1, through one of its ligands, might be indirectly involved in another disease affecting the reproductive system. Studies have suggested that females who show premature ovarian insufficiency of unknown cause have a 1/50 chance of being a premutation carrier of the FMR1 gene, the same gene that causes Fragile X syndrome (Macpherson, Murray et al. 1999) and whose protein product FMRP is a well-known binding partner of CyFIP1. Females who have premature ovarian insufficiency have problems with ovarian function which can lead to infertility and early menopause. Indeed, two chromosomal regions involved in POF have been located on the long arm of the X chromosome at Xq13-21 (Omim: POF2) and at Xq26-28 (Omim: POF1) (Ennis, Ward et al. 2006) and FMR1 is found at Xq27.3. Blood testing of affected females showed high levels of the pituitary hormone FSH (follicle stimulating hormone) and low levels of the ovarian hormone AMH (anti-Müllerian hormone). Recent studies suggest that the FMR1 gene can exert controlling functions on ovarian recruitment and ovarian reserve (Gleicher and Barad 2010). While POF has not been studied yet in FMR1 ko mice, in other studies germ cell deficient (gcd) mice were generated, which reproduced premature ovarian failure. Germ cell deficient mice underwent normal puberty and complete sexual development but by 6-8 weeks of age their estrous cycle became irregular. Mice aged 12-16 weeks became reproductively senescent, as defined by the apparent absence of estrous cycling. The

ovaries of wild type mouse feature white spots that correspond to corpora lutea, while the ovaries of the germ cell deficient mice were much smaller with no gross evidence of ovarian activity (Duncan, Cummings et al. 1993).

1.8 Ovarian and follicular development

The mouse ovary is a very complex structure with tight regulation machineries between the different cell types. At birth, the ovary is a solid organ. It consists of only two different cell types: the oocytes and the stroma cells. Then the ovary undergoes massive changes in morphology in the five to eight weeks between birth and fertility. While the oocytes grow, the stroma cells differentiate into theca cells, lutein cells, granulosa cells and many others. The granulosa cells surround the oocytes, and form follicles that grow and differentiate while in constant interplay with the oocyte (Eppig 2001). The concept of a regulatory loop between oocyte and follicles was proposed by Eppig et al. in 2001. He showed that follicular cells maintain oocytes in meiotic arrest until the pre-ovulatory surge of gonadotropins and, at the same time, promote growth and maturation of the oocyte. On the other hand the oocyte is crucial for follicle formation, as well as for granulosa cell proliferation and differentiation. During the fertile life of a female a constant maturation of follicles and oocytes takes place, starting with recruitment of primordial follicles and going on to ovulation or atresia, programmed follicular death. A mature ovary is structured with a compact cortical layer, where the follicles are localized, and a loose medulla in the middle of the organ, where blood vessels and lymphatic vessels can be found (Figure 8).

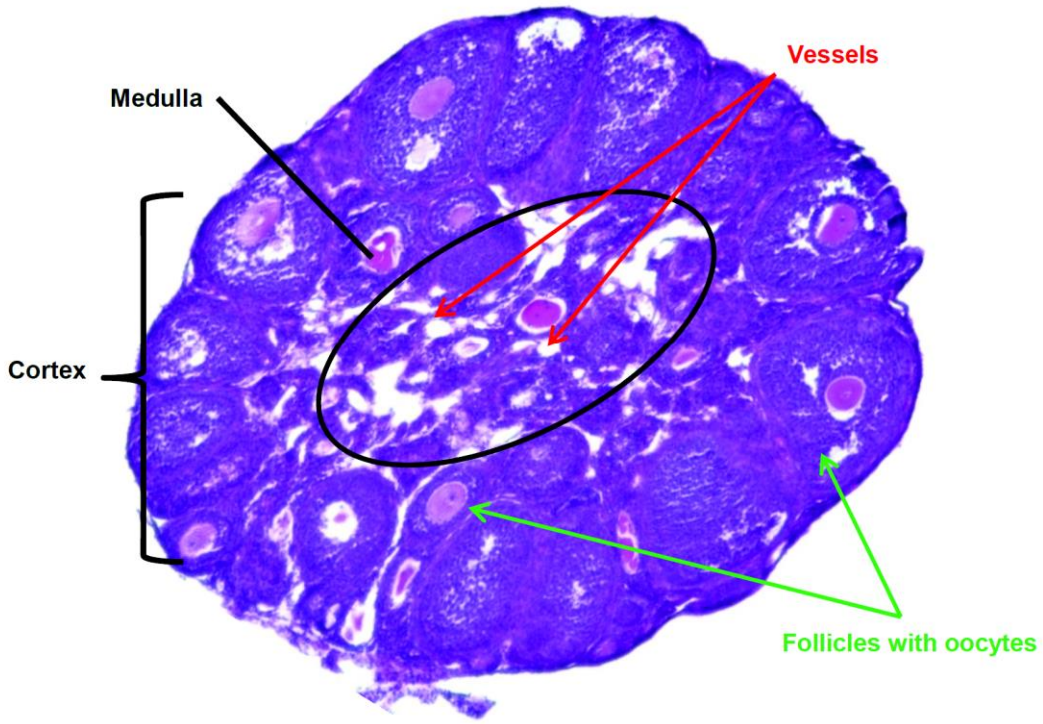

Figure 8: Organization of a mouse ovary. H&E staining of a frozen section from an adult mouse ovary. Indicated in the figure are the compact outer layer (Cortex) containing the follicles (green arrows) and the medulla in the center of the organ, a loose structure dense with vessels (red arrows).

1.8.1 Follicle development and classification of the developmental stages

In mature ovaries all follicular developmental stages are present at the same time. Several classification systems for oocytes and follicles have been published in the past years. The classification proposed by Pedersen & Peters 1968 and adapted later by Myers et al. (2004) is shown in Figure 9. Myers et al. classification is marked in red in Figure 9. It is a more simplified system, and was used in this thesis for the analysis of the ovaries of CyFIP1 heterozygous mice.

Three big groups of follicles, small, medium and large, are subdivided in different Types. In the group of small follicles, Type 1 and Type 2 consist of non-growing small oocytes with no or only few granulosa cells attached. Small follicles, but surrounded by a whole layer of squamous granulosa cells, were named Type 3a follicles. All these were also called primordial follicles, and form the pool from where growing follicles are recruited. After recruitment, the oocyte starts growing and the granulosa cells become

cuboidal and start to proliferate. Type 3b or primary follicles contain a growing oocyte with a single layer of granulosa cells. Follicles with more than one layer of cells around the growing oocyte are called secondary follicles (Types 4 to 5b).

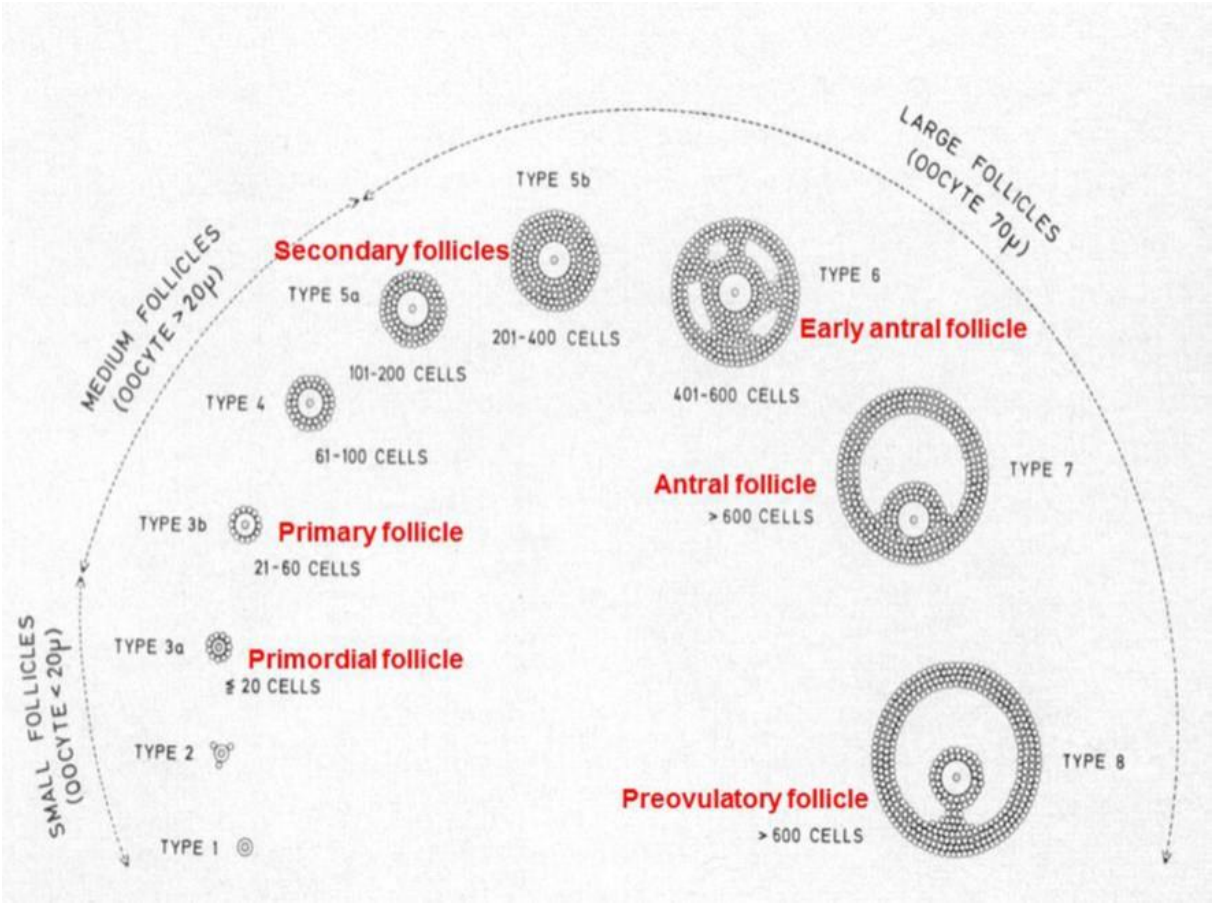

Figure 9: Classification of the different developmental stages of a follicle. Small follicles: bare oocyte (type 1 and 2) and primordial follicle consisting of the oocyte and one layer of squamous granulosa cells (type 3). Medium follicles: primary follicle surrounded by one layer of cuboidal granulosa cells (type 3b); secondary follicle with two to five layers of granulosa cells (type 4 to 5b). Large follicles: early antral follicle with small dispersed cavities in the granulosa cell layers and a fully mature oocyte (type 6); antral follicle with a large antrum filled with follicular fluid (type 7); pre-ovulatory follicle with a large antrum and a ring of granulosa cells encircling the oocyte (type 8) (modified from (Pedersen and Peters 1968)).

The transition from medium to large follicles is marked by the formation of cavities containing follicular fluid. Oocytes in large follicles are fully grown and meiotically competent, which means that they can resume meiosis after a gonadotropin surge. Type 6 or early antral follicles, sometimes called tertiary follicles, display scattered cavities with follicle fluid. In Type 7 or antral follicles one large cavity (antrum) is present and divides the granulosa cell types into two different classes: (1) the oocyte-associated cumulus cells and (2) the follicle-associated mural cells. The last class of

follicles is the pre-ovulatory or type 8 follicles. Following a pre-ovulatory gonadotropin surge, the oocyte resumes meiosis and the cumulus cells start to express hyaluronic acid, leading to cumulus expansion and finally to ovulation.

1.9 Embryonic stem cells

A useful tool to study early mouse development is to culture and in vitro differentiate Embryonic Stem cells (ES cells). ES cells are derived from the inner cell mass of blastocysts (Evans and Kaufman 1981; Martin 1981) but can also be isolated from 8-cell stage embryos (Wobus, Wallukat et al. 1991) or from morulae (Eistetter 1989). Under optimal conditions ES cells can be expanded almost indefinitely in cell culture. Furthermore, embryonic stem cells are pluripotent cells and thus are able to differentiate into cells of the three germ layers: mesoderm, endoderm, and ectoderm. ES cells can be cultured into so-called “embryoid bodies” (EBs) that represent aggregates of differentiating ES cells in non-adherent cultures and consist of a core of ectoderm, mesoderm and endoderm surrounded by visceral and parietal endodermal cells (Maye, Becker et al. 2000). Using this approach ES cells can be differentiated into cardiogenic (Wobus, Wallukat et al. 1991; Maltsev, Rohwedel et al. 1993; Maltsev, Wobus et al. 1994), myogenic (Rohwedel, Maltsev et al. 1994), adipocytic (Dani, Smith et al. 1997), chondrogenic (Kramer, Hegert et al. 2000), osteogenic (Hegert, Kramer et al. 2002), hematopoetic (Schmitt, Bruyns et al. 1991), insulin-producing (Schroeder, Rolletschek et al. 2006), epithelial (Bagutti, Wobus et al. 1996) and also neuronal (Fraichard, Chassande et al. 1995; Strubing, Ahnert-Hilger et al. 1995; Rujano, Pina et al. 2004) cell types. The differentiation of mouse ES cells into non-somatic germ cells including oocytes and sperm cells has also been done (Hubner, Fuhrmann et al. 2003; Kehler, Hubner et al. 2005). During in vitro differentiation ES cells-derived cells differentially express developmentally regulated genes encoding transcription factors, enzymes, receptors or ion channels, mimicking expression patterns that are seen in vivo during embryo development (Wobus, Wallukat et al. 1991; Rohwedel, Maltsev et al. 1994; Guan, Rohwedel et al. 1999).

1.10 Embryoid bodies

The name embryoid bodies was given to these cell aggregates due to their similarities to post-implantation embryos. Embryoid bodies are three-dimensional structures generated by the aggregation of pluripotent stem cells when they are cultured in the absence of feeder cells and on low attachment surfaces. It was shown in 1985 that mouse ES cells can form EBs in vitro (Doetschman, Eistetter et al. 1985). The morphogenic events in EBs mimic multiple aspects of the post-implantation mouse embryo, including primitive endoderm formation (Grabel and Casanova 1986; Shen and Leder 1992), germ layer differentiation (Keller 1995; Itskovitz-Eldor, Schuldiner et al. 2000), and epithelial to mesenchymal transition (Shukla, Nair et al. 2010). The process of cavitation in mouse embryogenesis has also been examined using EBs (Coucouvanis and Martin 1999; Maye, Becker et al. 2000). The specific mechanism of cavitation in developing embryos and EBs is thought to be regulated by programmed cell death induced by factors secreted by the visceral endoderm, and survival of cells based on basement membrane attachment (Coucouvanis and Martin 1995; Coucouvanis and Martin 1999). EBs can be formed using a variety of techniques, including hanging drop (Maltsev, Wobus et al. 1994), static suspension (Doetschman, Eistetter et al. 1985), semi-solid methylcellulose culture (Ling and Neben 1997; Dang, Kyba et al. 2002), and stirred-culture bioreactors (Gerecht-Nir, Cohen et al. 2004). Each system has specific advantages and disadvantages (Kurosawa 2007); for example, the hanging drop method is relatively controlled, but not suitable for producing large amounts of EBs, while static suspension is simple and scalable, but not well controlled. Rotary suspension culture provides a middle ground between hanging drop and static suspension, in that it produces EBs uniform in size and shape, yet with a high yield (Carpenedo, Sargent et al. 2007). Directed differentiation of EBs is most commonly accomplished through addition of soluble factors to the culture medium. Growth factors such as vascular endothelial growth factor (VEGF) (Nourse, Halpin et al. 2010), brain derived neurotrophic factor (BDNF) (Takaki, Nakayama et al. 2006), basic fibroblast growth factor (bFGF) (Yamada, Kioussi et al. 1994), epidermal growth factor (EGF) (Kang, Cho et al. 2007), and platelet-derived growth factor (PDGF) (Kang, Cho et al. 2007) have been studied in the context of EBs differentiation. Other morphogens such as bone morphogenetic proteins (BMPs) (Bruce, Gardiner et al.

2007), Wnts (ten Berge, Koole et al. 2008) and retinoic acid (Bain, Ray et al. 1996) have also been assessed for directed EB differentiation.

1.11 Embryonic development

Since the CyFIP1 knockout mouse model is embryonic lethal, a detailed analysis of early embryonic developmental events is required in order to understand which is the cause of lethality and, subsequently, the role of CyFIP1 and the WAVE complex in developmental events. Early embryonic development can be divided into two phases, a preimplantation and a postimplantation phase.

1.11.1 Preimplantation development

Preimplantation development is characterized by a fast cell division process from a one-cell embryo to a blastocyst stage embryo and lasts 4-5 days in mice (Fig. 10). Early cellular doubling divisions occur without a perceptible increase in embryo size.
The zona pellucida surrounds the embryo until implantation (Comiskey, Goldstein et al. 2003). Mammalian embryos need to establish a permanent connection to maternal tissues to grant nutrient and oxygen supply. Timing of implantation in the mouse is at around 4.5 days of embryonic development (E4.5). The E4.5 mouse blastocyst contains three cell types: epiblast, trophoblast and primitive endoderm. Lineage studies, mostly using chimeras and reconstituted blastocysts, have shown that the three cell types give rise to distinct tissues later in development (Rossant 1987). The primitive endoderm and the epiblast lineage are the major cell lineages which are important for gastrulation (Srinivas 2006).

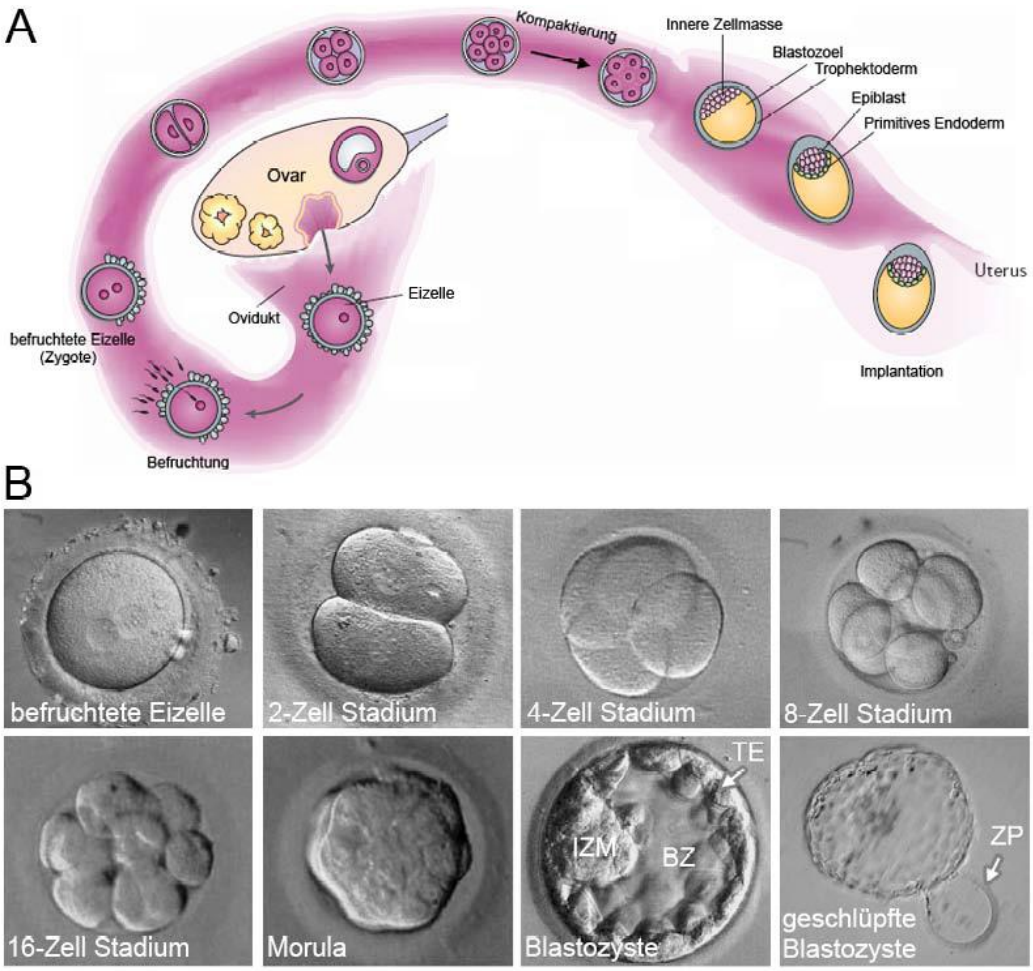

Figure 10. Preimplantation embryo development. (**A**) Schematic view of the development of the preimplantation embryo in mice from day 0 (E0) to day 5 (E5.0) (Wang und Dey, 2006, modified by Wörsdorfer). (**B**) Light microscopy images of early embryonic development stages. IZM: inner cell mass, BZ: blastocoele, TE: trophectoderm, ZP: zona pellucida (Braude, Pickering et al. 2002, modified by Wörsdorfer)

1.11.2 Postimplantation development

The early postimplantation development involves dynamic processes resulting in dramatic rearrangements in the embryo. At around E5.0, soon after implantation, the early postimplantation mouse embryos are divided into two regions and display a proximal-distal body axis (Fig. 11A).

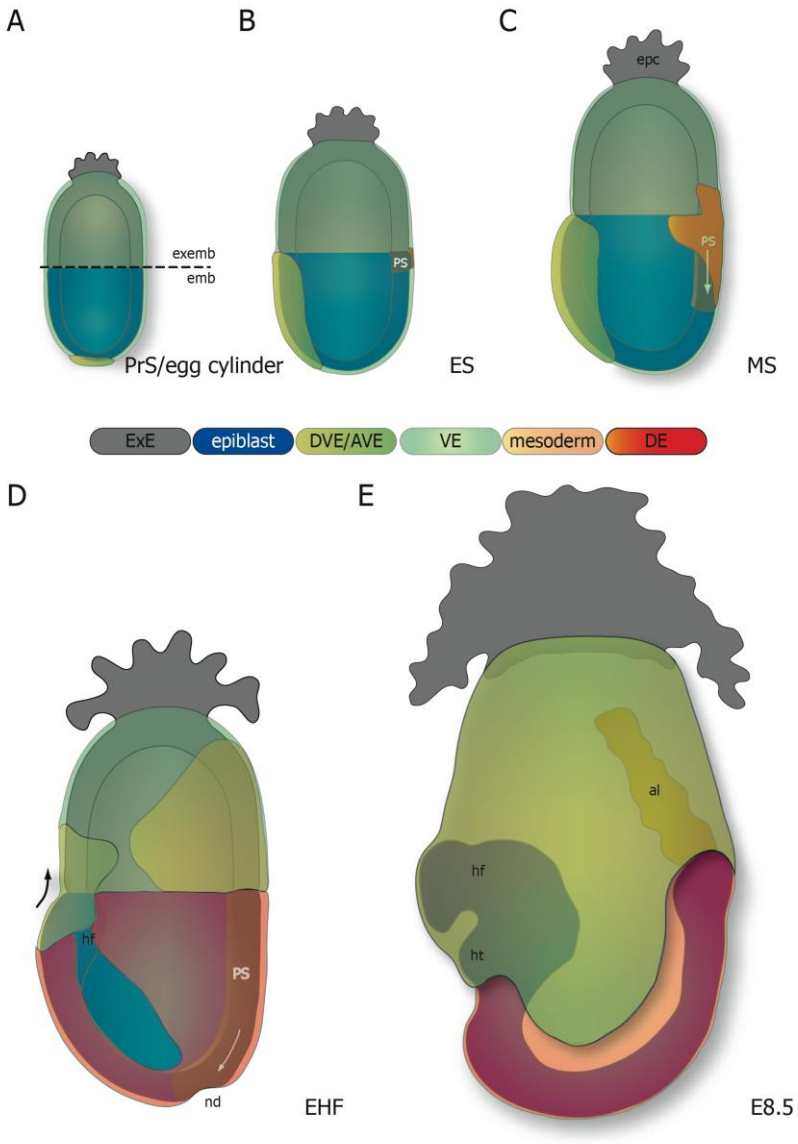

Figure 11. Early postimplantation development in the mouse. (**A**) At PrS/egg cylinder stage, the embryo consists of two cell layers, the epiblast (blue) and the surrounding Visceral Endoderm (VE, light green) and is characterized by a proximal-distal (PD) axis. The differentiation of VE cells at the distal tip of the embryo into DVE (Distal VE, bright green) marks the first visible sign of the forming asymmetry. (**B**) Just prior to the beginning of gastrulation, the DVE migrates anteriorly (becoming Anterior VE, AVE) and marks the future anterior pole of the embryo. On the opposite side, at the very proximal end of the embryonic region, the primitive streak (PS) forms. (**C**) Mesoderm (yellow) and Definitive Endoderm (DE, orange) are formed in the PS. The PS progresses further distally and the produced DE and Mesoderm migrate laterally. Mesoderm also expands into the extraembryonic region, to form the visceral yolk sac (VYS) mesoderm. (**D**) At the early head fold (EHF) stage, almost the entire VE region has been replaced by DE and the VE displaced towards the extraembryonic region. The ectoderm in the anterior is specified to become neuroectoderm and the head folds start to extrude. At the anterior end of the PS, the node (nd), an embryonic organizer region, has formed. (**E**) At E8.5, the head folds have formed and the ventral body side of the embryo begins to close and thereby the embryo will be incorporated into the VYS. The mesodermal derived allantois establishes a contact to the chorion. Abbreviations: al: allantois, AVE: anterior visceral endoderm, DE: definitive endoderm DVE: distal visceral endoderm, EHF: early head fold

stage, emb: embryonic region, epc: ectoplacental cone, ES: early streak stage, ExE: extraembryonic ectoderm, exemb: extraembryonic region, hf: head fold, ht: heart, MS: mid streak stage, nd: node, PrS: pre-streak stage, PS: primitive streak, VE: visceral endoderm, VYS: visceral yolk sack (Kaufman 1992, modified by Erlacher).

This is the egg-cylinder stage of the mouse embryo, so called because of a cup shaped structure. About 20 to 24 hours later, at early streak stage (~E6.5), the body axis shifts from proximal-distal to anterior-posterior and the embryonic germ layers begin to form: this is the process of gastrulation (Beddington 1981; Tam and Beddington 1987) (Fig. 11B,C). The initiation of gastrulation is indicated by the primitive streak (PS), a transient structure that is located in the posterior of the embryonic region. Through the primitive streak epiblast cells can flow and form mesoderm and definitive endoderm. These cells then migrate to their respective destinations in the embryonic, and in the case of early-generated mesoderm, also into the extraembryonic region (Parameswaran and Tam 1995) (Fig. 11D,E). In consequence of the cylindrical shape of rodent embryos, the early postimplantation embryo requires a rotation along the longitudinal (antero-posterior) axis that results in an inversion of the order of the germ layers: in fact before E8.0 the endoderm forms the outermost and the ectoderm the innermost cell layer, while at E9.5 the endodermal layer is on the inside of the embryo and the ectoderm is on the outside (Kaufman 1992). The inversion occurs in concert with the closure of the ventral and parts of the dorsal body walls in order to form a closed primitive gut and neural tube, respectively, and is referred to as embryonic turning (Kaufman 1992). This turning happens between E8.5 and E9.5 and together with the ventral closure gives rise to the folding of the midline endoderm and results in arranging the primitive gut tube (Fig. 12). This also induces the fusion of the two lateral heart primordia, which have already formed by E7.5, and the complete enclosure of the embryo by the visceral yolk sac. The visceral yolk sac is composed of cells of the extraembryonic region, which are the extraembryonic visceral endoderm and the extraembryonic mesoderm (Kaufman 1992; Erlacher 2009).

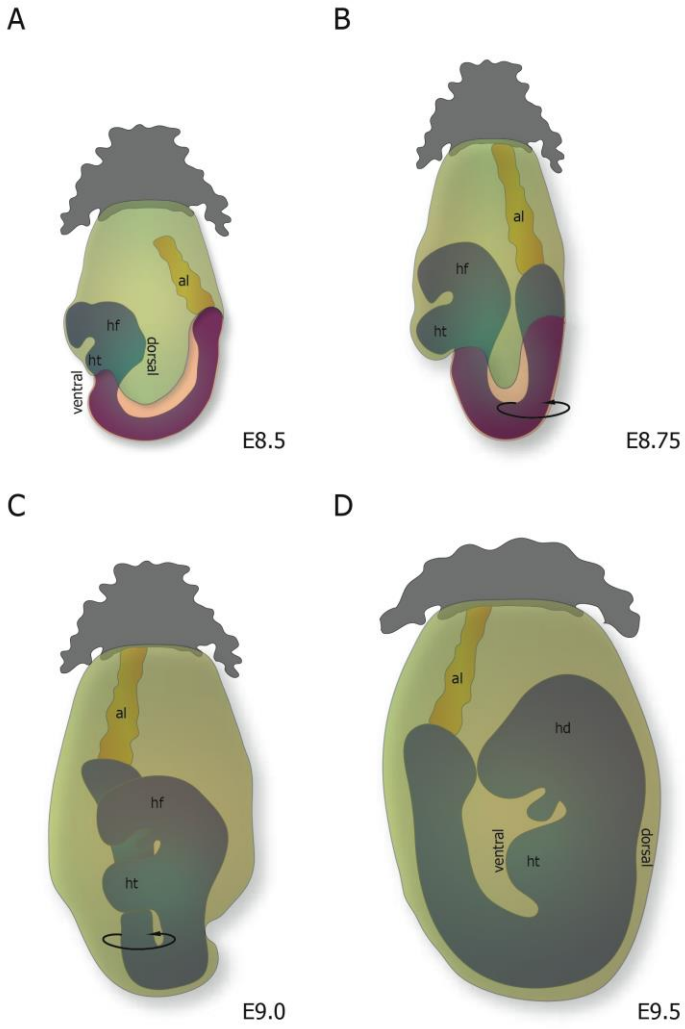

Figure 12. Embryonic turning in the mouse embryo. During early postimplantation development, the mouse embryo exhibits an inversion of germ layers. Chordate development requires the turning of the embryo in order to establish the embryonic body plan. (**A**) At E8.5, the embryo exposes its ventral body side, consisting of endoderm, to the outside and starts to be enclosed in the VYS. (**B**) While the enclosure in the VYS proceeds, the caudal end begins to "roll" in an anticlockwise motion around the rostral part of the embryo. (**C**) At E9.0, the embryo is almost entirely enclosed within the VYS. (**D**) The turning process is completed at around E9.5, and the embryo has achieved the fetal position, which is typical in chordate embryos. Abbreviations: al: allantois, hd: head, hf: head fold, ht: heart, VYS: visceral yolk sac (Kaufman 1992, modified by Erlacher).

With the inception of gastrulation the basis for proper development of neural and head structures is already laid down. The anterior ectoderm is structured to form the prospective brain structures. At head fold stage (E8.0), the neuroectoderm can already be distinguished from close-by surface ectoderm and elevates into clearly visible head folds (resulting in the stage name). Between E8.0 and E9.5, the time of embryonic turning, the head folds and the more caudal neuroepithelium folds up. The folds close and fuse in an exactly regulated mode which is starting at the hindbrain level and continues both rostrally and caudally forming the future fore- mid- and hindbrain regions and the neural tube. Subsequently, the neural tube generates the spinal cord (Kaufman 1992). During further development, many different cell types, structures and organs are specified at their designated location. All developmental stages are subject to exact regulatory machineries, consisting of a large number of different gene products that are present at a given time in a certain environment (Erlacher 2009).

1.11.3 Theiler stages

Theiler stages have been used for a more detailed classification of embryonic development than the normal “days post coitum” or “embryonic day” classification. The mouse development is divided into 26 prenatal and 2 postnatal Theiler stages. Each Theiler stage is identified with one 'average' age, and a range of variation of real ages, centered on this average, that can be seen when actual developing embryos are studied. In fact, embryos of the same gestational age may differ in their stage of development. Especially during preimplantation and early postimplantation development, the embryo is involved in dynamic processes and dramatically rearranged in one day, so that the Theiler stages can quantify these changes in a better way. Theiler's criteria are, for example, cell number or somite number and therefore allow to distinguish many of the important phases of early development.

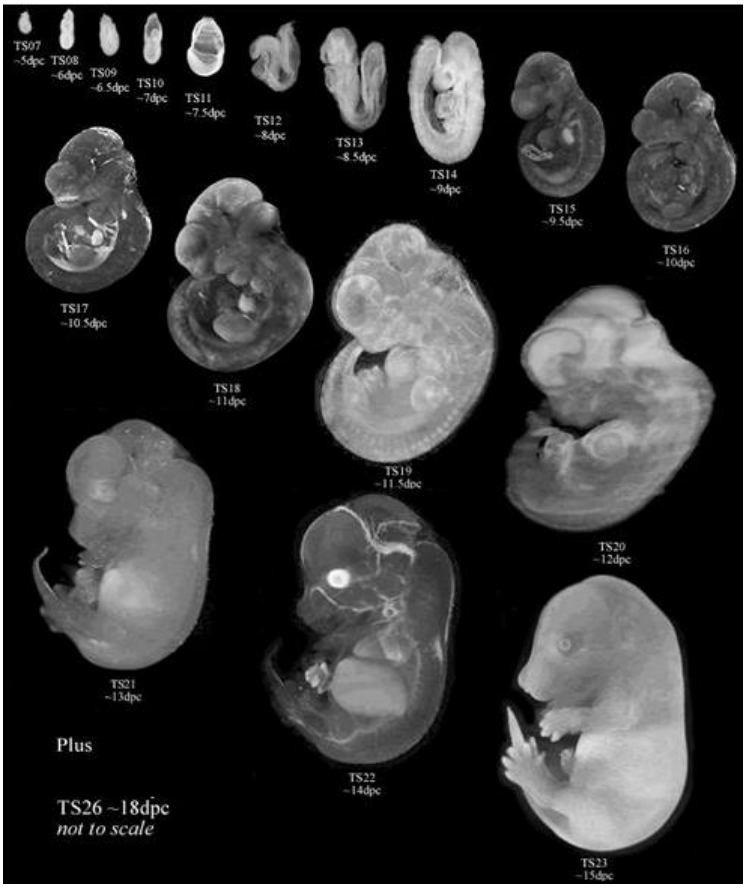

Figure 13. Theiler stages and their relationship to “days post-coitum” (dpc). The 25 Theiler stages and the corresponding development of the embryo are shown (Kaufman 1992)

1.12 Aim of the Thesis

The aim of this thesis is to obtain better insight into the functions of CyFIP1 and the WAVE complex during oogenesis and early mouse development: how the actin nucleation function is reconciled with cellular events such as cell survival, apoptosis, membrane trafficking and cell lineage programming; how the composition of the WAVE complex is regulated and which could be the relevant upstream and downstream signaling pathways.

The starting point was the observation that CyFIP1 heterozygous females showed a reduction of fertility at as early as 10-12 weeks of age. Therefore the role of CyFIP1 in ovarian and follicular maturation was analyzed.

Previous studies showed that embryos lacking CyFIP1 die at E6.5. The role of CyFIP1 and the WAVE complex was studied during early embryonic development by using the CyFIP1 knockout mouse model. A focus was put on the genetic background and mutation inheritance in the mouse. In parallel to the analysis of early mutant mouse development, CyFIP1 ko ES cells were employed in an in vitro paradigm of embryonic development, the embryoid bodies. In this in vitro model of development, cell proliferation, differentiation and adhesion were analyzed. Germ layer formation mimicked in the embryoid bodies approach was analyzed by flow cytometry using specific developmental markers.

Finally, the complexity of the composition of the WAVE complex was studied and new possible ligands were identified with biochemical and spectroscopic methods.

2. Material

2.1 General stock solutions, buffers and media

2.1.1 General solutions

Solution	Concentration	Substance
10x PBS (1l)	1.5 M (87.68 g)	NaCl
	162 mM (23 g anhydrous)	Na_2HPO_4
	38 mM (4.56 g)	NaH_2PO_4
	pH 7.4	
PBT	0.1 %	Tween-20
		in PBS
4% Paraformaldehyde (100 ml)	60 ml	PBS
	4 g	PFA
	dissolve at 65 ºC	
	adjust volume to 100 ml	PBS
	sterile filtrate	
TBS (1l 10x)	1.5 M (87.68 g)	NaCl
		(1 M) Tris/HCl pH
	0.25 M (25 ml)	7.4
TBS-T	0.2%	Tween-20
		in TBS

2.1.2 Solutions for the analysis of nucleic acids

Solution	Concentration	Substance
50x TAE-Buffer (1l) pH 8.3	2 M (242.2 g)	Tris base
	57.1 ml	Glacial acetic acid
	0,05 M (100 ml)	EDTA 0.5 M (pH 8,0)

Proteinase K (stock in H_2O)	10 µg/µl	
Tail DNA extraction buffer	50 mM	Tris/HCl pH7.4
	100 mM	NaCl
	1%	SDS
	5 mM	EDTA
	0.5 µg/µl	Proteinase K
ES cells DNA extraction buffer	20 mM	Tris/HCl pH7.4
	150 mM	NaCl
	2 mM	EDTA
	1%	SDS
	0.5 µg/µl	Proteinase K
DNA loading buffer	40%	Sucrose
	0.5%	SDS
	0.25%	Bromophenol blue
DNA ladder 1 kb Plus (500 µl)	50 µ	DNA ladder 1 kb Plus
	83 µl	DNA loading buffer
	367 µl	H_2O
RNA lysis buffer	100mM	NaCl
	10mM	$MgCl_2$l
	5mM	EDTA
	50mM	Tris/HCl pH 7.4
	1%	Triton-X100
	40U/ml	RNAseOut (added just prior to use)

2.1.3 Solutions and Media for ES cell culture

Solution	Concentration	Substance
ES cell medium	410 ml	DMEM medium
(500 ml)	15% (75 ml)	ES cell-tested Fetal Calf Serum
	1 mM (5 ml)	Non essential amino acids (100x stock)
	1 mM (5 ml)	Sodium Pyruvate (100x stock)
	10 mM (5 ml)	HEPES pH 7.2 (100x stock)
	1 mM (5 ml)	Glutamine (100x stock)
	5 ml	Pen/Strep antibiotics (100x stock)
	4 µl	β-mercaptoethanol
	1 ml	LIF conditioned media (contains leukemia inhibitory factor)
ES cell differentiation medium	ES cell medium without LIF and only 10% FCS	
ES cell freezing medium	10%	DMSO in ES cell medium
Gelatine (0.2%)	0.2% (w/v)	‘Porcine skin gelatine’

2.1.4 Solutions and media for flow cytometry

Solution	Concentration	Substance
MACS buffer	2mM	EDTA
	1%	Fetal calf serum
		PBS
0,1%	TritonX	
1%	Fish gelatine	

2.1.5 Solutions for biochemical analysis

Solution	Concentration	Substance
Coomassie solution	50%	Methanol
	10%	Acetic acid
	0.1%	Coomassie Brilliant Blue
		stir O/N, filtrate
ECL solution A (200 ml)	0.1 M	Tris/HCl pH 8.6
	4 ml	Luminol stock
	0.1 ml	P-hydroxy-coumarin stock
ECL solution B (200 ml)	0.1 M	Tris-HCl pH 8.6
	0.2 ml	H_2O_2 (30%)
Luminol stock solution (10 ml)	0.44 g	Luminol
		in DMSO
P-hydroxy-coumarin stock (1 ml)	150 mg	P-hydroxy-coumarin
		in DMSO
IF blocking solution	10%	Goat serum
	0.2%	Triton-X100
		in TBS
IF washing solution	0.2%	Triton-X100
		in TBS
10x NCP (Western blot washing buffer)	1.47 M	NaCl
	0.4 M	Tris base
	0.5 %	Tween-20
	pH 8-8.2	

10x SDS running buffer	0.25 M	Tris base
	1.92 M	Glycine
	1%	SDS
5x SDS loading buffer	110 mM	Tris/HCl pH 6.8
	20%	Glycerol
	3.8%	SDS
	8%	β-mercaptoethanol
	ad libitum	BPB (Bromophenol blue)
Towbin transfer buffer	25 mM	Tris base
	192 mM	Glycine
	20%	Methanol
Western blot blocking solution	5%	Non-fat Milk powder in 1x NCP
Triton lysis buffer	150 mM	NaCl
	50 mM	Tris/HCl pH 7.4
	1%	Triton-X100
	1x	EDTA-free Complete protease inhibitor (Roche)
SDS stacking gel (4%) (for 2 gels) 10 ml	6.1 ml	H_2O
	1.3 ml	30% Acrylamide (1:38)
	2.5 ml	0.5 M Tris/HCl pH 6.8
	50 µl	20% SDS
	70 µl	10% APS (Ammonium Persulphate)
	5 µl	TEMED

SDS separating gel (8%)	10.7 ml	H_2O
(for 2 gels) 20 ml	5.3 ml	30% Acrylamide (1:38)
	3.8 ml	2 M Tris/HCl pH 8.8
	100 µl	20% SDS
	140 µl	10% APS (Ammonium Persulphate)
	10 µl	TEMED
Coupling buffer	0.1 M	$NaCO_3$
	0.5 M	NaCl
	pH8.5	
Blocking buffer (for Profilin2	0.1 M	Tris pH 8.0
beats)	0.5 M	NaCl

2.2 Commercial solutions

2.2.1 Commercial solutions for nucleic acid analysis

Name	**Manufacturer**
dNTPs 100 µM each	Promega
$MgCl_2$ 25 mM	Promega
PCR-flexi-buffer (5x)	Promega
Go-Taq Polymerase 5 u/µl	Promega
SuperScriptIII First Strand Synthesis System for RTPCR	Invitrogen

2.2.2 Commercial solutions for tissue culture

Name	**Manufacturer**
DMEM	Gibco
DMSO	Sigma

FCS	PAA
HEPES pH 7.2 (100x)	Gibco
L-Glutamine (100x)	Gibco
LIF	Gibco
Non essential amino-acids (100x)	Gibco
PBS	Gibco
Pen/Strep antibiotics (100x)	Gibco
Sodium pyruvate (100x)	Gibco
Trypsin (2.5%)	Gibco
Trypsin-EDTA (2.5%-0.05%)	Gibco

2.2.3 General tissue culture materials

Name	**Manufacturer**
Cell culture flasks (75 cm^3)	Corning
Cryotubes	Nunc
Pipetteman	Eppendorf
Filters	Millipore
Lab-Tek™ Chamber Slides™	Thermo Scientific
Petri dishes (diameter 3 cm, 10 cm)	VWR
Pipettes (1 ml, 2 ml, 5 ml, 10ml, 25 ml, 50 ml)	BD Falcon
Plastic tubes (15 ml, 50 ml)	Sarstedt
Well plates (96-, 48-, 24-, 6-well)	Corning

2.2.4 Further material

Name	**Manufacturer**
Protein transfer membrane Immobilon-P	Millipore
Bio Max XAR Film	Kodak
Microspin columns G-50	GE- Healthcare
1.5/2 ml tubes	Roth

2.3 Commercial chemicals and reagents

2.3.1 Liquids

Name	Manufacturer
Acrylamide (30%)	BioRad
Bovine serum albumin (BSA) (10 mg/ml)	New England Biolabs
Bradford reagent (5x)	BioRad
Chloroform	Merck
CyQUANT® Cell Proliferation Assay Kit	Life Technologies
Dimethylsulfoxide (DMSO)	Merck
Eosin (0.05% Eosin in 96% Ethanol)	Merck
Ethanol (technical)	Merck
Ethanol, absolute	Merck
Ethidiumbromide (10 mg/ml)	BioRad
Film developer solution G153	AGFA
Film fixer solution G354	AGFA
Formamide	Sigma
Glacial acetic acid	Merck
Glutaraldehyde (25%)	Sigma
Glycerol	Sigma
HCl 37%	Merck
Hemalaun	Merck
Heparin	Sigma
Hydrogen peroxide (30%)	Sigma
Isopropanol	Merck
β-Mercaptoethanol	Sigma
Methanol	VWR
NBT (Nitroblue tetrazolium chloride 100mg/ml)	Sigma
Phenol	Merck
RNase Inhibitor	Roche
TaqMan® probes	Life Technologies
TEMED	Sigma

Transcription buffer (for Digoxigenin labeling)	Roche
Triton-X100	Roche
TRIzol®	Life Technologies
Tween 20	Sigma

2.3.2 Reagents

Name	**Manufacturer**
Agar	AppliChem
APS	Fischer Scientific
Bromophenol blue	BioRad
BSA	Merck
Coomassie Brilliant Blue	BioRad
dpN_6	Pharmacia
DTT	Sigma
EDTA	Sigma
Glucose	Merck
Glycine	Grüssing
Luminol	Sigma
$MgCl_2$	Sigma
Milk powder (non-fat)	Roth
NaH_2PO_4	Sigma
Na_2HPO_4	Sigma
NaOH pellets	Sigma
P-hydroxy-Coumain	Sigma
Poly-L-proline (MW 40.000)	Sigma
Protease inhibitor cocktail tablets,Complete, EDTA free	Roche
Proteinase K	Sigma
SDS	Merck
Sodium chloride	Merck
Tris base Ultra	Roth

2.4 Technical equipment

Description	Manufacturer
Axiovert + AxioCam Color 412-312	Zeiss
Binocular MS 5 +	Leica
Camera ConProgRes C10 plus +	JENOPTIK Germany
Light source KL 1500 LCD	Leica
Centrifuge 5415 D	Eppendorf
Centrifuge 5417 R	Eppendorf
Centrifuge J2-HS	Beckman
Centrifuge J2-MC	Beckman
Centrifuge tissue culture	Beckmann
CTR 5500 + camera DFC 420 C	Leica
Electric homogenizator	Bosch
Film developer Curix 60	AGFA
Freezer (-80 °C)	Thermo Scientific
Gel documentation UV	Herolab
Gel electrophoresis running chambers	BioRad/EMBL
Glass-Teflon tissue grinders	Co
Heating blocks	Grant/QBT
Hybridization oven	Bachofer
ImageQuant LAS4000 Mini	GE Healthcare
Incubators for bacterial culture	Heraeus
Incubators for tissue culture	Heraeus
Magnetic stirrers	Heidolph
Microscopes for tissue culture	Leitz
Multi-channel pipettes	Eppendorf
Ovens	Heraeus
PTC-200 Peltier Thermal Cyclers	MJ Research
pH-meter	InoLab
Pipette tips	Molecular Bio Products
Pipettes	Gilson
Pipetteboy	Eppendorf
Power supply PowerPAC300	BioRad

Power supply PowerPAC200	BioRad
Rocker	Heidolph
Scale	Sartorius
Scale (analytic)	Kern & Sohn
SDS PAGE apparatus	Pharmacia Biotech
Shaker	New Brunswick Scientific
Spectrophotometer	Beckmann
Thermomixer	Eppendorf
UV-Table	Bachofer
Vortex	Scientific Industries
Water purifier	Millipore
Western blotting apparatus	BioRad

2.5 Antibodies

2.5.1 Primary antibodies

Antigen	Isotype	Dilution	Manufacturer
Abi1	rabbit polyclonal	1:1000	Sigma
Abi2	mouse polyclonal	1:500	Sigma
Actin C4	mouse monoclonal	1:2000	MP Biomedicals
Akt	rabbit polyclonal	1:1000	Cell signaling
phoshpho Akt (Ser473)	rabbit monoclonal	1.1000	Cell signaling
Erk1/2 (p44/42 MAPK)	rabbit polyclonal	1:1000	Cell signaling
phoshpho Erk1/2 (p44/42 MAPK)	rabbit monoclonal	1:1000	Cell signaling
FAK	rabbit polyclonal	1:1000	Abcam
GAPDH	mouse monoclonal	1:5000	Callbiochem
Nap1	rabbit polyclonal	1:1000	Millipore (Upstate)
PI3-Kinase p85 (N-SH3)	mouse monoclonal	1:1000	Millipore (Upstate)
POP 5C9-E12 (Hybridoma supernatant)	mouse monoclonal	1:1.5	Witke Lab (Massimi)
WAVE1	mouse monoclonal	1:500	BD Bioscience
WAVE2	rabbit polyclonal	1:500	Cell signaling
Smad1	rabbit monoclonal	1:1000	Cell signaling
phoshpho Smad1/5	rabbit monoclonal	1:1000	Cell signaling
SOS1	rabbit polyclonal	1:1000	Cell signaling
Sra1	rabbit polyclonal	1:500	Millipore (Upstate)
α-Tubulin	mouse monoclonal	1:5000	Sigma
γ-Tubulin	mouse monoclonal	1:2000	Sigma

2.5.2 Direct labeled Antibodies for flow cytometry

Antigen	Conjugate/Host	Dilution	Manufacturer
Beta-catenin	PE/mouse	1.100	eBioscience
CD184 (CXCR4)	PerCP-eFluor 710/rat	1:100	eBioscience
Cleaved Caspase 3	Alexa Fluor 488/rabbit	1:50	Cell signaling
Sca-1	FITC/rat	1:100	eBioscience
SSEA1	PE/mouse	1:100	eBioscience

2.5.3 Secondary Antibodies

Secondary antibody	Isotype	Dilution	Manufacture
HRP goat anti-mouse	polyclonal	1:5000	Merck
HRP goat anti-rabbit	polyclonal	1:5000	Merck

2.6 Oligonucleotides

The Oligonucleotides in this thesis were produced by Eurofins MWG Operon.

2.6.1 Oligos for mice genotyping

Oligo	Sequence (in 5'-3' direction)
Cre 1 (sense) (346)	GCC TGC ATT ACC GGT CGA TGC AAC GA
Cre 2 (antisense) (345)	GTG GCA GAT GGC GCG GCA ACA CCA TT
Cre 3 (antisense) (356)	TCG TTG CAT CGA CCG GTA ATG CAG GC
CyFIP 1-flox1 for (492)	GTT TTA AGG AAG TCT TTG CC
CyFIP 1-flox1 rev (493)	TAA CTA AAA GAG GTA CC
CyFIP 1-floxed rev (576)	AAG ACT GAT AAG TAG CTC C

2.7 ES cell lines

CyFIP1+/+ CyFIP1+/- CyFIP1-/-	Embryonic stem cell lines, obtained from blastocysts from CyFIP1 heterozygote matings.	Generated and first described in this thesis.

2.8 Animals

All animals used for this thesis were bred under optimal conditions, following the German and EU guidelines (2010/63/UE) for welfare of laboratory animals. The mice were in C57/Bl6N or CD1 genetic background.
The following mouse lines were used for the experiments:

Line	Reference
CyFIP1-/- ko	Massimi (PhD Thesis), 2008

2.9 Molecular Weight Markers

Name	Manufacture
SeaBlue Plus2 Pre-Stained Standard	Invitrogen
1 kb Plus DNA Ladder	Invitrogen
Broad Range marker	BioRad
Precision Plus Protein™ Dual Color	BioRad

3. Methods

3.1 Molecular Biology

3.1.1 Isolation of genomic DNA from mouse tail biopsies

A 3 mm tail biopsy was cut from 17-21 days-old pups. The tail biopsy was digested in 200 µl of Genomic DNA extraction buffer over night at 56°C. On the next day, ½ volume (100 µl) of saturated NaCl solution was added to the digested tails. The tubes were shaken vigorously for 90 seconds and centrifuged for 14 minutes at 14000 rpm. 220 µl of the supernatant were used to precipitate the DNA by transferring them to a new tube containing ~2.5 volumes (500 µl) of Ethanol. The DNA, visible by flocculation, was spun for 1 min at 14000 rpm and the supernatant was removed. The DNA pellet was dried at 37°C for a few minutes and resuspended in 200 µl of MilliQ water by shaking at 37°C for one hour. For PCR reaction, 1 µl of the resuspended DNA was used, while for southern blotting 50 µl per digestion were used.

3.1.2 Isolation of genomic DNA from ES cells

ES cells derived from blastocysts were genotyped according to the following method. ES cells were cultured on gelatine-coated 6 well plates for two passages to dilute out the feeder cells. In order to lyse ES cells, 1 ml of ES cell lysis buffer was added and incubated for 2 hours at 37°C. Then the lysates were recovered with a cut 1 ml tip (due to genomic DNA viscosity) and transferred into a 2 ml Eppendorf tube. The lysates were incubated over night at 56°C. On the following day, DNA was extracted by adding ½ volume (500 µl) of a saturated NaCl solution, shaking very energetically for 90 seconds and centrifuging for 14 min at 14000 rpm. The supernatant was transferred into 2.5 volumes (3.75 ml) of ethanol in a 5 ml snap cap tube. The DNA flocculated and after a short spin, the supernatant was removed with a pulled Pasteur-Pipette. The DNA pellet was dried at 37°C for a few minutes and resuspended in 500 µl of MilliQ water and shaken at 37°C for one hour to obtain complete dissolution. 1 µl of a 1/10 dilution was used for the PCR reaction.

3.1.3 Isolation of genomic DNA from amnion or yolk sac

Genomic DNA was extracted from the amnion or yolk sac by Proteinase K digestion (0.5 mg/ml) of the tissue in 20 µl of MilliQ water overnight at 56°C. The following day Proteinase K was inactivated by increasing the temperature to 98°C for 10 min. After cooling and a short centrifugation, 1 µl of the supernatant was used for the PCR reaction.

3.1.4 Phenol-chloroform extraction of DNA

Phenol-Chloroform extraction is a way to remove proteins from nucleic acid samples. It was employed on some genomic DNA samples if the PCR reaction was not clear to increase the purity of the template DNA.
Phenol/Tris-(pH 7.4)-Chloroform (1:1) was added with a ratio of 1:1 to the DNA solution, and thoroughly shaken for 30 sec. The emulsion was centrifuged for 10 min at 14.000 rpm to obtain a separation of the phases. The aqueous, DNA-containing, phase on top was carefully transferred into a new Eppendorf tube. The DNA was precipitated adding 2.5 volumes of Ethanol and centrifuging for 10 min. After removal of the supernatant, the pellet was dried and dissolved in H_2O.

3.1.5 Genotyping of mice, ES cells, and embryos by PCR

The polymerase chain reaction (PCR) is a widely used technique in molecular biology. It is an enzymatic way to amplify a DNA template in replicative cycles using short oligonucleotide primers and free deoxynucleotides. Specific sense and antisense primers flanking the desired target sequence were used. There are three main steps in each PCR cycle: denaturation, annealing and extension. The reaction mixture is first heated to a temperature between 95-98°C that ensures DNA denaturation. The mixture is then cooled to a temperature (generally, between 55-65°C) that permits annealing of the primers to the complementary sequences in the single-stranded DNA. The short, typically 18 to 24 bases, oligonucleotide primers should have a defined GC content (40-60%) that determines the annealing temperature. The extension step typically occurs at 72°C. In the presence of the four dNTPs the *Taq* Polymerase synthesizes new DNA strands starting at the 3'-end of the annealed primers. These steps are

repeated for 25-35 cycles. A final extension step at 72°C for 3-10 min is usually performed to ensure that the new DNA fragments are complete.
The amplified DNA products can be visualized by gel electrophoresis using agarose gels after staining with ethidium bromide or other fluorescent intercalating agents.

3.1.5.1 Genotyping of CyFIP1 ko mice

Oligo sequences are found in the Materials (2.6.1).
PCR Mix for 20 µl of Total Reaction Volume:

- 11.2 µl H_2O
- 4.0 µl 5 × Flexi Buffer
- 1.2 µl $MgCl_2$ (25mM)
- 0.4 µl dNTPs (10mM)
- 1.0 µl Oligos 492/493 (20 mM)
- 1.0 µl Oligos 492/576 (20 mM)
- 0.2 µl Taq-Polymerase
- 1.0 µl Genomic DNA

Programme (CKO-Pfn2)

98°C for 2 min	
96°C for 30 sec 55°C for 1 min 15 sec 72°C for 30 sec	**35 cycles**
72°C for 5 min	
15°C forever	

Expected PCR products:
wild type band: 270 bp
deletion band: 410 bp

3.1.5.2 Genotyping of Cre-deleter mice

PCR Mix for 20 µl of Total Reaction Volume:

11.2 µl	H_2O
4.0 µl	5x Flexi Buffer
1.2 µl	$MgCl_2$ (25mM)
0.4 µl	dNTPs (10mM)
0.5 µl	Oligos 346/345 (20 mM)
0.5 µl	Oligos 149/150 (20 mM)
0.2 µl	Taq-Polymerase
1.0 µl	Genomic DNA

Programme (Cre-P)

98°C for 2 min	
96°C for 30 sec 58°C for 30 sec 72°C for 40 sec	**30 cycles**
72°C for 5 min	
15°C forever	

Expected PCR products:
wild type (gelsolin) band: 264 bp
Cre band: 600 bp

3.1.6 Gel electrophoresis

The DNA products amplified by PCR can be visualized by gel electrophoresis. Gels were prepared, depending on the size of DNA fragments, by melting 0.8-2% (w/v) agarose in 1× TAE buffer and adding 7 µl of ethidium bromide per 100 ml of gel. In the electrophoresis chamber the gel was covered with 1× TAE buffer. DNA loading buffer was added to the DNA (PCR products have the loading buffer included in the PCR mix) and samples were pipetted in the gel slots. The gel was run at constant voltage (20-90V) for 30-90 min. Finally, gels were documented using a gel documentation system with UV illumination (BioRad).

In order to measure the RNA concentration and determine the purity of the RNA, 1 µl of this solution was measured with the NanoVue (GE Healthcare) spectrophotometer.

3.2 Cell Biology

3.2.1 ES cell culture

Cell culture was performed under sterile conditions in a sterile laminar flow hood with sterile media, glass and plastics. Cells were cultured in a humidified incubator at 37°C in 5% CO_2 atmosphere.

ES cells were grown in tissue culture plates or flasks coated with gelatine, on a layer of mouse embryonic fibroblasts (MEFs) inactivated by γ-irradiation in ES Cell Medium, which was changed daily. ES cells were passaged every 3-4 days. For passaging ES cells, medium was removed, and then cells were washed twice with PBS and incubated in Trypsin-EDTA for 5 min at 37°C. In order to inactivate trypsin, at least 1 volume of ES Cell Medium was then added and the cells were resuspended to a single-cell suspension, transferred to a 15 ml tube and centrifuged at 760 rpm for 5 min. The pellet was resuspended in an appropriate volume of ES Cell Medium and cells were plated on new gelatine coated plates with freshly plated MEFs.

3.2.2 Freezing and thawing of ES cells

ES Cells can be stored for long periods of time in liquid N_2.

In order to freeze ES cells, they were treated with trypsin and centrifuged as previously described (3.2.1 Cell Culture). Afterwards the cell pellet was resuspended in ice-cold ES cell freezing medium and transferred into cryo-vials. Vials were frozen overnight at -80°C. The following day, the vials were transferred into liquid nitrogen.

ES cells were thawed in a 37°C water bath. Immediately after thawing, cells were complemented with ES Cell Medium, transferred in a tube, and centrifuged (760 rpm, 5 min).

The pellet was resuspended in ES Cell Medium and plated onto a 10 cm dish coated with gelatine, on a monolayer of freshly plated mitotically inactivated MEFs.

3.2.3 Generation of mouse Embryonic Stem (ES) cells

3.2.3.1 Blastocysts preparation from mice

Time-mated females were sacrificed at embryonic day 3.5. The uteri were dissected and transferred to a petri dish containing ES Cell Medium. With scissors and forceps the uteri were cleaned from fat. A clean uterus was transferred to a 35 mm dish and the blastocysts were flushed out of the uterine horn using a 3 ml syringe with a 27G needle, using ES Cell Medium. The whole process was performed on an inverted microscope. Blastocysts were collected with a capillary tube and pipette and transferred singularly into the wells of a 48-well plate containing a layer of mitotically inactivated MEFs.

3.2.3.2 ES cell derivation

Blastocysts were incubated at 37°C with 5% CO_2 for approximately two days in 48-well plates. During this period it is important to avoid any interference. After attachment to the feeder layer, the blastocysts hatch and the ES Cell Medium can be changed. The inner cell mass (ICM) then expanded and 5 or 6 days after plating of the blastocyst a defined ES cell-like population could be seen in the expanded ICM. The cells were then trypsinized for the first time and plated again on a new 48-well plate on fresh MEF feeder layer. The typical appearance of mouse ES cell clones was normally seen 4-5 days after the first trypsinization. The following days the ES cells grew and were finally trypsinized a second time and plated on a 6-well plate and finally expanded to 75 cm^2 flasks. ES cells can then be frozen in ES cell freezing medium. Normally eight 1 ml aliquots were frozen from a 75 cm^2 flask of each established mouse ES cell line.

3.2.3.3 ES cell differentiation

Mouse embryonic stem cells are derived from the ‘inner cell mass’ of blastocysts and have pluripotent properties. Embryonic stem cells of mouse can differentiate into different embryonic tissues depending on culture conditions.

3.2.3.3.1 Spontaneous differentiation into embryoid bodies

ES cells were trypsinized from a cell culture dish and pipetted to obtain a single-cell suspension. The cells were then transferred onto a Petri dish in ES cell differentiation medium to induce differentiation. After a few days in culture they formed cell aggregates of different sizes. The cells could not attach to the surface of the Petri dish and grew in suspension. The medium was carefully changed every second day. Culture was stopped after 7 days. The derived embryoid bodies varied greatly in size.

3.2.3.3.2 Hanging-drop method for embryoid bodies

To control the size of the cell aggregates more precisely, the hanging drop method was used. After trypsinization, ES cells were resuspended in ES cell differentiation medium and counted with a haemocytometer. Fifty drops of 20 µl, containing approximately 1500 cells, were deposited on the interior of a cover of a 10 cm Petri dish and the cover was set over the bottom part containing PBS. After two days in culture at 37°C each drop contained a small aggregate of cells, which was transferred to a Petri dish and cultured for additional 4 days. During this period, medium was changed carefully every second day.

3.3 Flow cytometry analysis

Flow cytometry is a widely used method for characterizing and separating individual cells. With Flow cytometry it is possible to measure certain physical and chemical characteristics of cells or particles as they pass in a fluid stream by a beam of laser light. Cells or EBs in this work were grown like described previously and analyzed by flow cytometry.

3.3.1 Preparation of ES cells for flow cytometry analysis

ES cells were trypsinized from a cell culture dish and pipetted in ES cell Medium to obtain a single-cell suspension. After centrifugation the ES cells were resuspended in MACS Buffer and stained as followed in 3.3.3 or 3.3.4.

3.3.2 Preparation of EBs for flow cytometry analysis

The EBs, which were grown in suspension in Petri dishes, were transferred carefully into 50 ml falcon tubes. For 10 min the EBs were allowed to settle down to the bottom of the falcon tube. The supernatant was removed and EBs were washed two times with PBS. A gentle spin for 5 minutes at 500 rpm was done to collect the EBs at the bottom of the tube when in PBS. Supernatant was discarded. An appropriate volume of MACS buffer (approximately 15-25 ml per falcon depending on the amount of EBs) was added and incubated at RT for about 15 min with pipetting in between until a single cell suspension was visible under the microscope. Around 10^6 cells were transferred to an eppendorf tube for each antibody staining and flow cytometry assay. The cells were kept on ice at 4°C.

3.3.3 Extracellular antibody staining for flow cytometry

All steps were performed at 4°C.The cells in Eppendorf tubes were spun down for 5 min at 1000 rpm, the supernatant discarded and the pellet resuspended in 100 µl of MACS buffer. 1 µl of the appropriate fluorescently-labelled primary antibody was added and incubated at 4°C in the dark for 45 min. After 45 min, 500 µl of MACS buffer were added to dilute the antibody and spun down at 1000 rpm for 5 min. The supernatant was discarded and the cells were washed once in 500 µl of MACS buffer and spun down again. After the supernatant was removed the cells were resuspended in 200 µl of MACS buffer and analyzed by flow cytometry (BD Accuri C6).

3.3.4 Intracellular antibody staining for flow cytometry

All steps were performed at 4°C. The cells collected in Eppendorf tubes were spun down for 5 min at 1000 rpm, the supernatant discarded and, in order to fix the cells, resuspended in 300 µl 2% PFA and incubated for 10 min at 4°C. Then 500 µl of MACS buffer were added to dilute the PFA. After fixation centrifugation must be performed at 3000 rpm for 5 min to minimize cell loss. Supernatant was discarded and cells washed once with 500 µl of MACS buffer and treated as previously described. The cells were resuspended in in 300 µl of MACS Buffer with 0,1% TritonX and 1% fish gelatine and incubated for 45 min to permeabilize and block the cells. Afterwards cells were spun down and resuspend in 100 µl of MACS buffer. 1 µl of the appropriate fluorescently-labelled primary antibody was added and the cells were incubated at 4°C for 45 min in the dark. After 45 min, 500 µl of MACS buffer were added to dilute the antibody and cells were spun down at 1000 rpm for 5 min. The supernatant was discarded and the cells were washed once in 500 µl of MACS buffer and spun down again. After the supernatant was removed the cells were resuspended in 200 µl of MACS buffer and analyzed by flow cytometry (BD Accuri C6).

3.4 CyQuant assay

The CyQuant assay (Life Technologies) uses DNA quantification as a measure to determine the number of cells, so it can be used for proliferation, differentiation and adhesion assays. The cells were seeded in triplicates in 96-well-plates at a defined density with 200 µl of medium. One plate was prepared for each time point. For the proliferation and differentiation assays cells were cultured for 1, 2, 3, 4 and 5 days, with medium changes every second day. For the adhesion assay cells were cultured for 1, 2, 3 and 4 hours. The time point zero was done by spinning cells down at the moment of plating for 5 min at 1000 rpm to attach them mechanically to the plate. After the respective incubation period, the medium was removed from the plates. The wells were carefully washed twice with PBS. The plates were then frozen at -80°C. The freezing step is critical for cell lysis. The plates can be stored at -80°C for up to 4 weeks. For the assay, a working solution was prepared by adding 50 µl of CyQuant GR stock solution (Component A) to a mixture of 1 ml cell lysis buffer stock solution

(Component B) and 19 ml of nuclease-free water in a 50 ml tube protected from light. After the 96-well-plates were thawed at room temperature, 200 µl of the working solution were added to each well and the plates were incubated for 5 minutes. The fluorescence was determined by a microplate reader (Victor, Perkin Elmer) at an excitation wavelength of 480 nm and an emission wavelength of 520 nm.

3.5 Microarrays

The RNA expression levels of large numbers of genes can be analyzed by Microarrays. Illumina BeadChip arrays were used. The BeadChip arrays are constructed by introducing oligonucleotides bearing 3-micron beads to microwells etched into the surface of a slide-sized, silicon substrate. During the manufacturing process, beads self-assembly into the microwells of the BeadChip arrays. Each bead contains hundreds of thousands of copies of covalently-attached, oligonucleotide probes and is represented with an average of 30-fold redundancy (Illumina). Cells were grown as described previously and trypsinized from a 10 cm cell culture dish. One wash in PBS was performed. Cells were lysed in 1ml of TRIzol® with pipetting up and down several times and immediately frozen at -20°C until processing.
The Microarray and data analysis was done in the Microarray facility of Joachim Schulze, LIMES Institute.

3.6 Biochemistry

3.6.1 Protein Lysates

3.3.6.1 Preparation of protein lysates from mouse tissues

Mouse organs were dissected on ice, shock-frozen in liquid nitrogen and stored at-80°C. Fresh organs were also used for protein lysates. The organ was placed in Triton Lysis buffer in a Glass-Teflon douncer and homogenized at constant speed (250-500 rpm) on ice until the tissue was completely dissociated.
The homogenized tissue was centrifuged for 15 min at 14000 rpm at 4°C. The supernatant was transferred to a fresh tube and the protein concentration was determined using the Bradford assay. Protein lysates were shock-frozen and stored at -80°C. Diluted lysates in 1× SDS loading buffer were denatured by heating at 95°C for 10 min and stored at -20°C.

3.3.6.2 Preparation of protein lysate from cultured cells

Adherent growing cells were trypsinized (see protocol), culture medium was added and the cell suspension was collected in a 15 ml Falcon tube. The cells were spun down for 5 minutes at 7600 rpm and washed twice with 5 ml of ice cold PBS.

3.3.1.6.1 Cytoplasmic and nuclear cell lysates

To prepare cytoplasmic and nuclear extracts, the cells were lysed in Triton lysis buffer (see 3.3.1.1) for 10 min on ice, after resuspending the cell pellet by pipetting up and down with a blue tip, and transferred into a 1.5 ml tube. Normally, for a 10 cm dish growing to confluence, 300 µl of Triton lysis buffer were used. The lysate was then spun down for 10 min at 14000 rpm at 4°C. The supernatant, which contained the cytoplasmic fraction, was transferred into a new tube. SDS loading buffer was added to a final concentration of 1x. Protein concentration was determined using the Bradford

assay. The pellet, which contained the nuclei, was washed once in Triton lysis buffer and lysed in 20-50 µl 2x SDS loading buffer. The lysates were denatured and genomic DNA sheared with 3-4 cycles of 2 minutes at 99°C and 15-30 seconds vortexing, cooled on ice and stored at -20°C. Protein concentration was determined using the Bradford assay.

3.3.1.6.2 Total lysates

For total protein extraction, cells were lysed in 2x SDS loading buffer. In order to shear genomic DNA and denature the proteins, the lysates were boiled for 2 min at 99°C and vortexed for 15-30 seconds for 3-4 times. Protein concentration was determined with the Bradford essay. Lysates were stored at -20°C.

3.6.2 Western blotting

3.6.2.1 Discontinuous SDS-Polyacrylamide Gel Electrophoresis (SDS-PAGE)

SDS-PAGE (Sodium Dodecyl Sulfate PolyAcrylamide Gel Electrophoresis (PAGE) (Laemmli 1970)) is a method to separate proteins according to their molecular weight. Since proteins with similar molecular weights may migrate differently due to their difference in structure or net charge, SDS, an anionic detergent, and β-Mercaptoethanol, a reducing agent, are used to denature proteins to their primary (linearized) structure and coat them with a uniform negative charge.

Acrylamide gels are composed of two layers: an upper layer about 2 cm long and with a fixed acrylamide concentration of 4%, called “stacking gel”, needed to compact proteins in one line; a lower layer about 5 cm long, called “resolving gel”, needed to separate the proteins: the size of the proteins of interest determine the acrylamide percentage to be used for this gel. The components of the WAVE complex (except for HSPC300) were analyzed using 8% acrylamide gels. Samples in 1X SDS loading buffer were loaded on the gel. To identify the size of the proteins, 7 µl of See Blue Plus2 Pre-Stained Molecular Weight Standard (Invitrogen) or 6 µl of Broad Range Unstained MW Standard (BioRad) were also loaded. Electrophoretic separation was

obtained in 1x running buffer at 80 V through the stacking gel and at 130 V through the resolving gel. The electrophoresis was stopped when the 50 kDa marker band reached the bottom of the gel.

3.6.2.2 Blotting (wet blot)

The high molecular weight proteins of the WAVE complex were transferred to a membrane with wet blots. Following SDS-PAGE, the gel was equilibrated in transfer buffer. 3MM Whatman sheets and a PVDF membrane were cut to the size of the gel and soaked in transfer buffer. The PVDF membrane was first activated by immersion for a few seconds in methanol. The gel and the membrane were packed between the soaked 3MM paper pieces and two sponge pads in perforated plastic plates as follows:

Anode (+)
Sponge pad
2 Whatman sheets
PVDF membrane
Polyacrylamide gel
2 Whatman sheets
Sponge pad
Cathode (-)

The transfer was performed in a blotting tank for 90 min at 110 V at 4°C or overnight at 20 V at room temperature.

3.6.2.3 Protein detection

After transfer of the proteins to the PVDF membrane, the membrane was blocked for 30 min in blocking solution. The primary antibody was diluted in blocking solution to an appropriate concentration and the blot was incubated either for 2 h at room temperature or overnight at 4°C. The membrane was washed three times for 10 min in 1x NCP. Incubation of the blot with the secondary antibody conjugated to horseradish peroxidase (HRP) was carried out for 1 h at room temperature in blocking solution with a dilution of 1:5000. The membrane was again washed three times for 10 min in NCP 1x. The protein of interest was detected by enhanced chemical luminescence (ECL)

utilizing the reaction of Luminol and H_2O_2, which is catalyzed by the HRP. For this purpose, the membrane was incubated with the ECL reagent for 1 min and the chemiluminescent signal was acquired with a LAS4000 Mini (GE Healthcare) imager.

3.6.3 Coomassie staining

Coomassie reagent was used to stain proteins on an acrylamide gel in order to estimate the protein concentration and the quality of the lysates.
Gels were first fixed by incubation in 40% Methanol and 10% Acetic acid in Milli-Q water for 30 minutes (this step was only necessary for gels that were not previously blotted, in fact the transfer buffer contains methanol, therefore blotted gels are already fixed). Then the gels were stained in Coomassie solution for 30 min at room temp. Finally the gels were washed twice for 15 minutes in 40% Methanol and 10% Acetic acid in H_2O and twice for 30 minutes in 20% Methanol and 10% Acetic acid in H_2O. Coomassie stained gels were stored in distilled water.

3.6.4 Coupling of Profilin2 to sepharose beads

Profilin2 beads were made by dissolving 50 mg of Profilin2 in 12 ml of coupling buffer (0.1 M $NaCO_3$, 0.5 M NaCl, pH8.5). 1,5 g of dry CNBr-activated sepharose 4B were weighted (1 g of lyophilized powder gives about 3.5 ml final volume of medium) and suspended in 1 mM HCl. The medium was swelling immediately and then washed for 15 minutes with 1 mM HCl on a sintered glass filter (porosity G3). Then the beads were washed briefly with cold water and coupling buffer. The beads were added immediately to the dissolved Profilin2 and incubated on a test tube rotator overnight at 4°C.
The next day, the beads were washed three times with 40 ml of coupling buffer and blocked with 0.1 M Tris pH 8.0, 0.5 M NaCl for 2 hours at RT. Then the resin was washed 4 times (alternating with 0.1 M sodium acetate pH 4.0, 0.5 M NaCl and 0.1 M Tris pH 8.0, 0.5 M NaCl). The beads were stored in 20 mM Tris pH 8.0, 5 mM EDTA, 0.1 M NaCl, 0.1% NaN_3 at 4°C.

3.6.5 Profilin2-beads pull-down

The pull-down assay was performed in a cold room at 4°C. First columns were washes with 500 µl of lysis buffer. Then Columns were filled with 100 µl of lysis buffer. Afterwards a solution containing 100 µl of Profilin2-beads and 100 µl of water was added on top of the lysis buffer. The beads were left to settle and then washed twice with 500 µl of lysis buffer before the protein lysates with a total protein amount of 250 mg were added. The flow-though was collected and added two more times to the column. The last flow-through, (unbound fraction) was transferred into a new tube and stored in 1x SDS loading buffer. To remove unbound proteins from the columns, they were washed 5 times with 800 µl of lysis buffer. After washing, 150 µl of 2x SDS-loading buffer were added to each column and the beads were thoroughly mixed by pipetting up and down. The solution containing the beads (bound fraction) was transferred into a new tube and stored. All fractions were boiled at 99°C and vortexed in between (the bound fraction had to be vortexed carefully). The unbound and the wash fraction were shortly spun down and stored at -20°C. The bound fraction was spun down at 1000 rpm for 5 min to separate the beads from the supernatant. The supernatant was transferred into a new tube and both were stored at -20°C.

3.7 Histology

3.7.1 Paraffin embedding of ovaries for morphological studies

For paraffin embedding, the ovaries were fixated in an eppendorf tube with 1 ml of 2% PFA in PBS overnight at 4°C with shaking. The next day the tissues were washed three times for 30 minutes in PBS at 4°C and then again in fresh PBS overnight. Dehydration was performed at 4°C on a shaker in increasing alcohol concentrations. After two hours in 50% ethanol/H_2O the tissues were placed in 75% ethanol. The ethanol was replaced after two hours and the ovaries were incubated at least overnight at 4°C. The dehydration process was completed at room temperature with two 30 minutes incubations in 96% ethanol and two 30 minutes incubations in absolute ethanol. After dehydration the ovaries were transferred in glass vials and cleared incubating for three times 30 minutes in xylene. Then xylene was replaced with paraffin at 60°C. The ovaries were incubated in paraffin in a heating block at 60°C twice for at least 45

minutes, then in fresh paraffin overnight and the next day again 45 minutes in new paraffin. At last the each ovary was oriented in a small embedding mould, covered with an appropriate amount of paraffin and allowed to solidify at room temperature. The hardened paraffin block was then taken out of the mould, trimmed with a razor blade and mounted on a tray with melted paraffin ready to be cut with the microtome.

3.7.2 Hemalaun and Eosin (H&E) staining

The H&E staining was performed on paraffin sections of the mouse ovary. First the sections were deparaffinated and rehydrated, all steps taking place under the fume hood. The slides were placed in a glass shuttle and dipped three times for 10 minutes in a glass tray with xylene and then transferred to trays with decreasing alcohol concentrations for four minutes each: absolute ethanol, 96%, 75% and 50% ethanol. Then the slides were submerged in distilled water for 10 minutes before the staining. First the sections were stained with Meyers Hemalaun for 15 seconds and subsequently blued for 30 seconds to one minute under flowing tap water (nuclear staining). The counterstaining was realized with eosin/ethanol for two minutes. Then the slides were rinsed under flowing tap water until no more color came off and dipped for 30 seconds in 96% ethanol, then two minutes in absolute ethanol and finally for 2 minutes in xylene. The sections were mounted with Entellan and left to dry overnight under the fume hood and the imaged under the microscope.

.

4. Results

4.1 Analysis of the infertility phenotype in CyFIP1+/- females

4.1.1 CyFIP1+/- females show infertility

Previous observations showed that CyFIP1 heterozygous (+/-) females, starting at the age of about three months, were less fertile than wild type females of the same age. Only 19% of CyFIP1+/- plugged females were pregnant in contrast to 72% of wild type females (figure 14, (Stoecker 2010)).

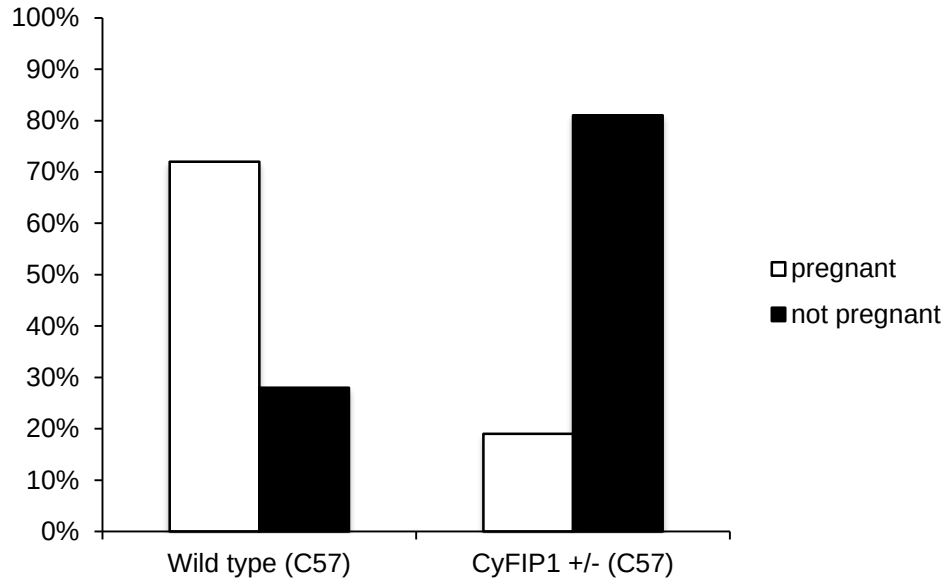

Figure 14: Comparison between CyFIP1+/- and wild type pregnancies of plugged females. Percentage representation of pregnant females in CyFIP1+/- matings (n=31) and wild type matings (n=25). Females were older than 3 months and in a C57BL/6N genetic background (Stoecker 2010).

In order to identify the role that CyFIP1 plays in ovaries and the reason for premature infertility in CyFIP1 heterozygous female mice, their ovaries were analyzed in comparison to wild type ovaries from age-matched littermates.

4.1.2 WAVE complex stability in ovaries

Previous experiments showed that the entire WAVE regulatory complex was down-regulated in the CyFIP1 knockout embryos (Stoecker 2010). Therefore the first question was if and how the components of the WAVE complex would also be affected

in the ovaries of CyFIP1+/- females. CyFIP1, as expected, was found reduced in protein extracts from heterozygous ovaries (figure 15). Surprisingly also the other three WAVE complex components analyzed showed a reduction in their levels (figure 15). Although Nap1 appeared expressed at much lower levels than in brain it was further reduced in extracts from heterozygous ovaries. Abi1 showed a double band running slightly higher compared to the two bands in the brain control, but it is well known that Abi1 has different splice isoforms in different tissues (at least 15 isoforms have been characterized in total). WAVE2 appeared very weak in the brain control, which is normal since WAVE1 and 3 are the predominant isoforms in the brain, and it was very clearly reduced in heterozygous ovaries. Overall more than 50% of the WAVE complex was lost in CyFIP1 heterozygous ovaries (figure 15).

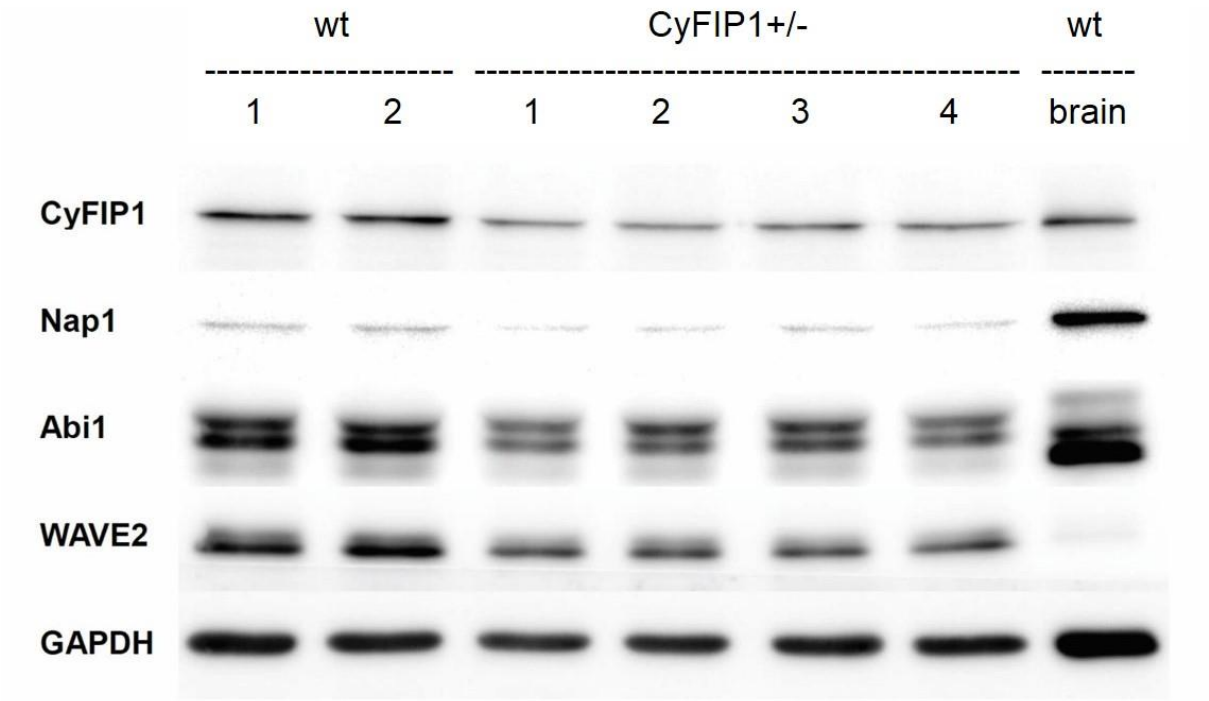

Figure 15: Western blot analysis of the WAVE complex in CyFIP1 heterozygous ovaries. Two wild type lysates and four CyFIP1 heterozygous lysates of ovaries from 3 months old females were loaded as indicated. A brain lysate was used as positive control. Examined proteins: CyFIP1, Nap1, Abi1, and WAVE2. Reference protein for loading control: GAPDH. A reduction of CyFIP1, Nap1, Abi1 and WAVE2 is evident in the heterozygous ovaries.

4.1.3 Morphological analysis of the ovaries

In order to understand what effect the reduction of WAVE complex availability was having on the ovaries, firstly ovaries from 3 weeks old CyFIP1+/- and wt females were analyzed to see if any morphological differences could be detected at this early stage, considering that female mice become fertile at about 5-6 weeks of age. Therefore, the ovaries were taken and analyzed before the mice became fertile and had an estrous cycle. Ovaries were embedded in paraffin, sectioned and stained with H&E. The gross morphology of wt and CyFIP1+/- ovary sections after H&E staining resulted very similar (figure 16).

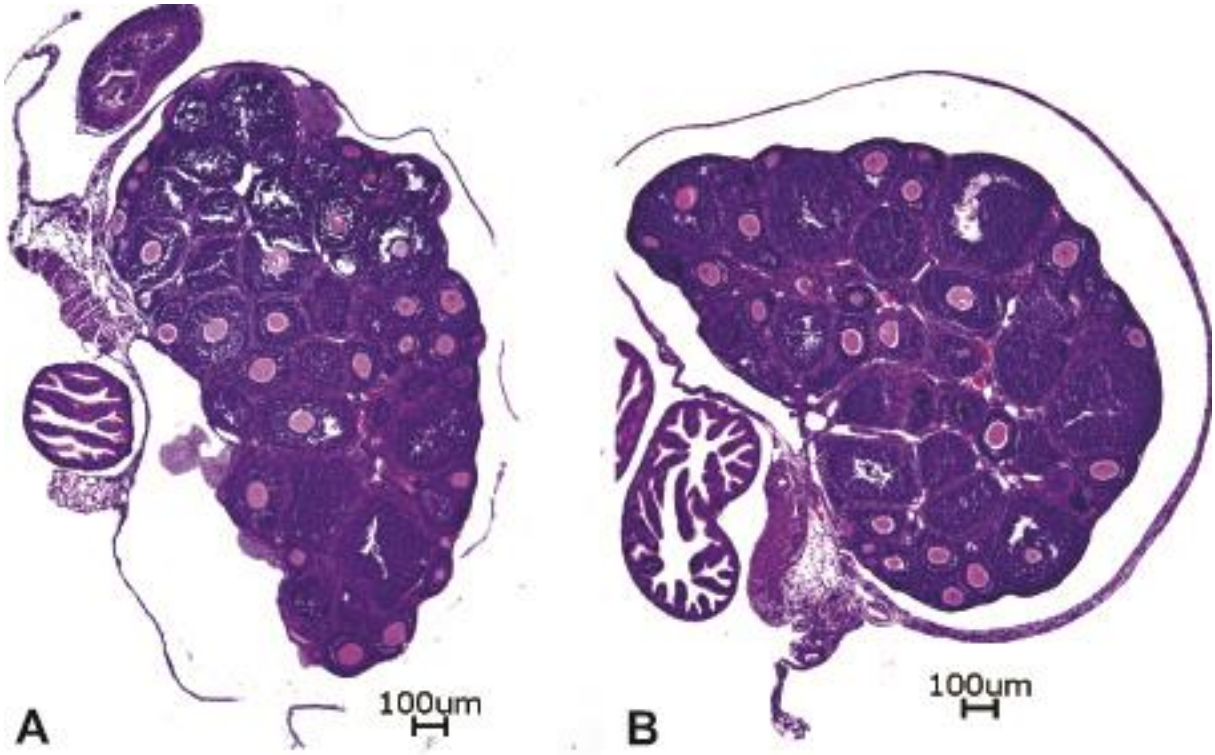

Figure 16: Sections of wild type and CyFIP1+/- ovaries from 22 days old mice. (A) Sample section from a wt ovary stained with H&E shows the presence of follicles at different stages of development. **(B)** Sample section from a CyFIP1+/- ovary similarly stained shows no difference from the wt at this time point.

Then ovaries from mature 3 month old mice were embedded in paraffin, sectioned and stained with H&E. Prior to embedding, the ovaries were imaged at the dissection microscope and measured. Measuring the ovary surface area showed in average no significant difference between wild type and CyFIP1 heterozygous ovaries (see appendix figure 38).

4.1.4 Follicle development analysis

At early time point before fertility no major differences in morphology could be detected in follicles. Ovaries from sexually mature mice were analyzed more in depth. Follicle development is essential for fertility, therefore a detailed analysis of the number of follicles at each developmental stage was performed in CyFIP1+/- ovaries from females of 2-3 months of age. Follicles are classified according to their developmental stage as previously explained (Introduction 1.8.1) and for this study a classification in five types was chosen (figure 17).

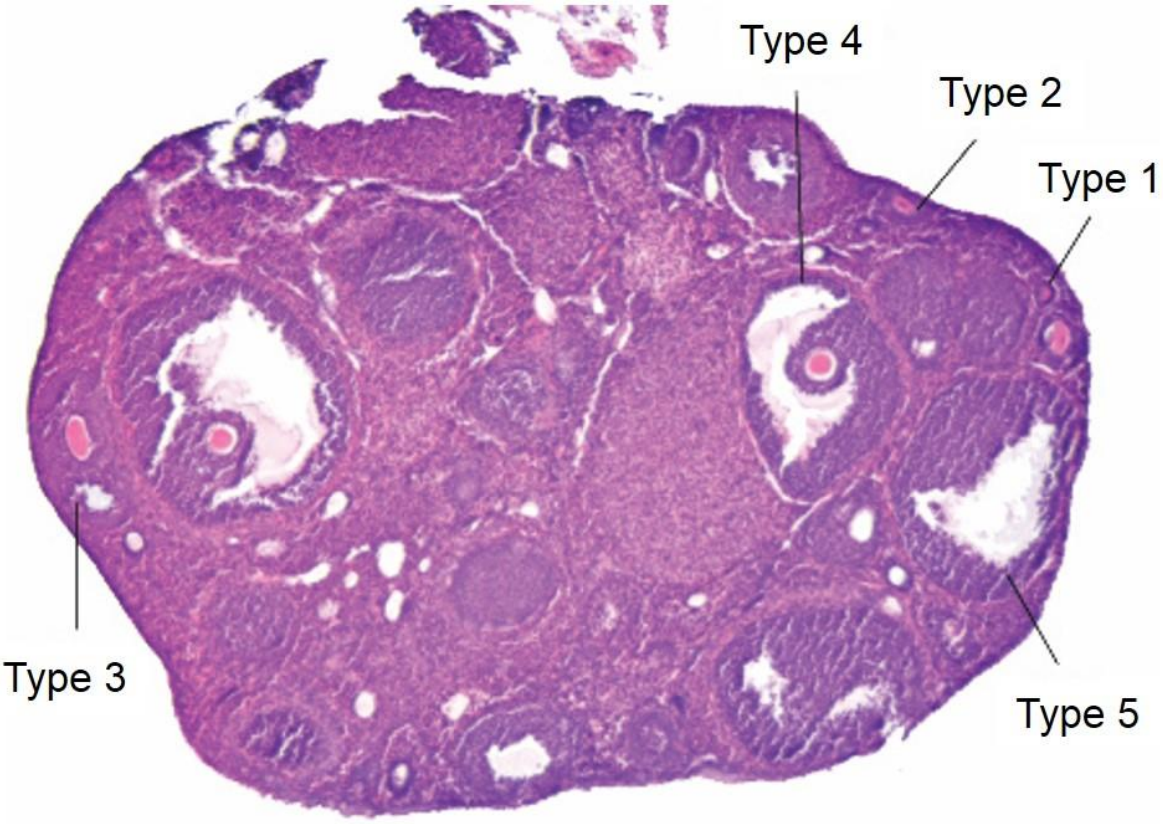

Figure 17: Classification of follicle types in H&E stained paraffin sections of the ovary. Type 1: primordial and primary follicles. Type 2: secondary follicles. Type 3: early antral follicles. Type 4: antral and pre-ovulatory follicles. Type 5: follicle-like structures without oocyte.

Groups of three consecutive wt and CyFIP1+/- 10 μm thick ovary sections at intervals of 100 μm were stained by H&E in order to properly identify all the follicles in the ovary and minimize double counting.

The numbers of Type 1 to Type 4 follicles showed no significant difference between CyFIP1+/- ovaries and wt ovaries. Nevertheless, the quantity of Type 1 and Type 3

follicles tended to be slightly lower in CyFIP1+/- ovaries, while a reverse trend was observed in follicles of Type 2 and Type 4. The comparison of Type 5 follicles, however, showed a significant difference (p=0.018) with 64 follicles in the ovaries of heterozygous animals compared to only 36 in the wild type littermates (figure 18).

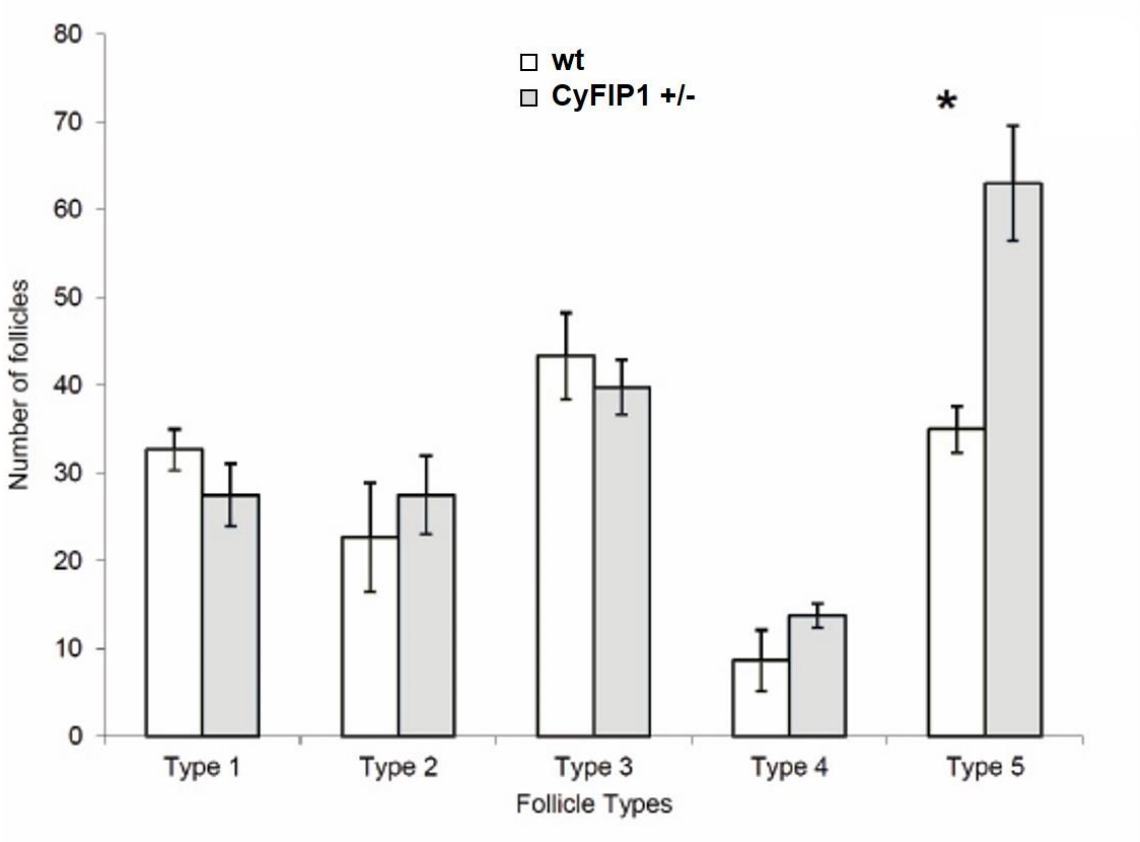

Figure 18: Comparison of the number of follicles of the 5 types present in the ovaries of wild type and CyFIP1 heterozygous females. Bars represent number of follicles classified according to their developmental stage. Type 1: primordial and primary follicles. Type 2: secondary follicles. Type 3: early antral follicles. Type 4: antral and pre-ovulatory follicles. Type 5: follicle-like structures without oocyte. The difference in the number of Type 5 follicles between wt and het is significant (wt n=3 and CyFIP1+/- n=4, t-test * 0.05>p>0.01).

4.1.5 Follicle dimensional analysis

Another possible indicator of follicular developmental defects is the size of the different types of follicles. The diameter of every Type 1 to Type 4 follicle counted in the previous section was measured, in order to compare their size distribution within each type in wild type and CyFIP1 heterozygous mice. Type 5 follicles were too heterogeneous in size to be included in this analysis. No significant differences in size were found in

Type 1-3 follicles (data not shown). Type 4 follicles, on the contrary, showed a significant difference in size distribution between wt and CyFIP1+/- animals. CyFIP1+/- type 4 follicles appeared to be in the majority of cases smaller than the controls (figure 19, where the distribution is represented as a survival graph respect to follicle diameter). It appeared clear that only 1 heterozygous female showed higher percentage of larger Type 4 follicles while only 1 wt had significantly less of the larger Type 4 follicles. Note that females were not synchronized in hormone cycle, therefore a certain variability is expected.

In summary, ovaries of CYFIP1+/- females showed a reduction of the WAVE complex components: CyFIP1, Nap1, Abi1, and WAVE2. Accordingly, follicle number and size was affected in CyFIP1+/- females: the follicle analysis showed higher number of Type 4 follicles and significantly higher numbers of Type 5 follicles in CyFIP1+/- ovaries. Also, the size of Type 4 follicles was reduced in CyFIP1+/- mice.

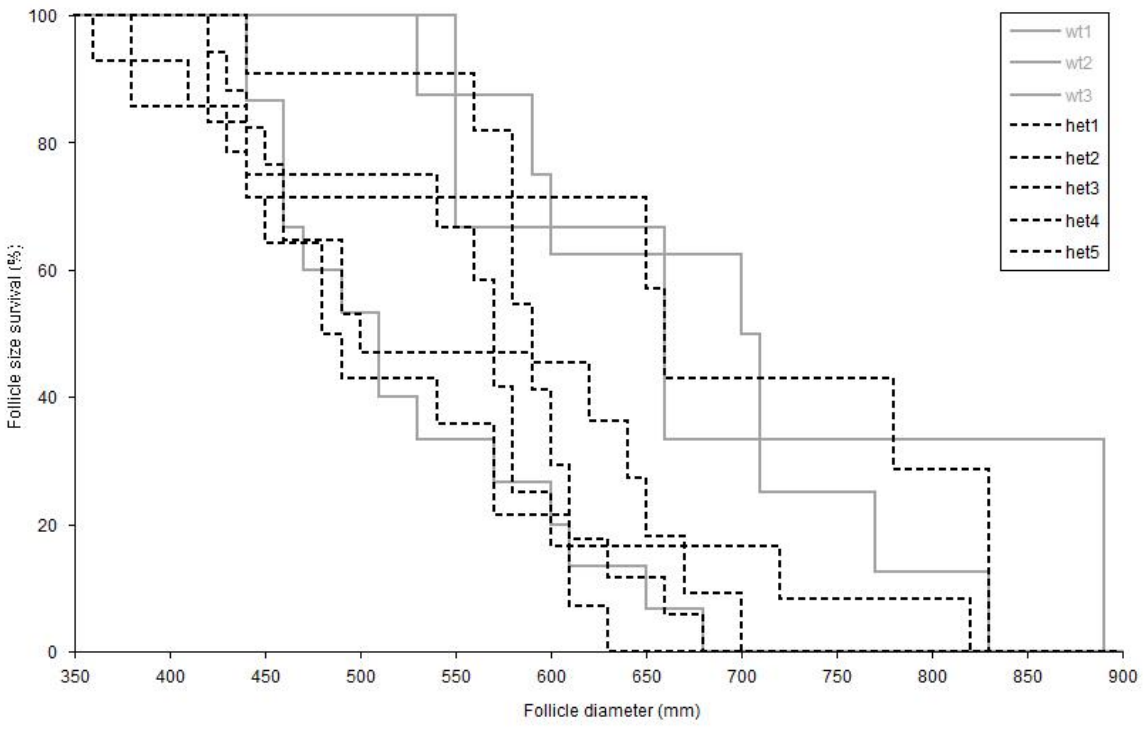

Figure 19: Survival analysis of the size of antral and preovulatory (Type 4) follicles of CyFIP1+/- females. Individual survival curves of follicle size (average diameter) showed that in the majority of CyFIP1+/- females follicles were significantly smaller than in wt. Statistical analysis using Logrank (Mantel-Cox) test gave p=0.0217.

4.2 Analysis of the CyFIP1 knockout mouse

4.2.1 Genetic background and mutation inheritance

As previously shown by Massimi, CyFIP1 is ubiquitously expressed in most adult tissues and during all embryonic stages as early as the embryonic stem cell stage. Since it was known that the knockout mouse was early embryonic lethal, to minimize the genetic variability and better define the window of lethality, heterozygous CyFIP1 knockout mice originally in a C57BL/6J background were crossed into C57BL/6N background. CyFIP1-/- embryos were then obtained by intercrossing CyFIP1+/- animals. These knockout mice appeared to die much earlier than described in previous work from Massimi (see Introduction 1.7.2), around embryonic day 6.5 (E6.5). Moreover, in this background, the phenotype of CyFIP1 heterozygous females described above (section 4.1) became evident: a highly reduced fertility. In an attempt to overcome this problem the CyFIP1 knock out mouse was backcrossed into a CD1 background. The CD1 mice are characterized by higher fertility, better maternal behavior and bigger litter size. After five generations of backcrossing with CD1 mice, timed matings between CyFIP1 heterozygous mice were resumed. Embryos were collected at E6.5, E7.5 and E8.5, imaged and genotyped by PCR. All three possible genotypes were found at these stages in CD1 genetic background with an overall correct Mendelian distribution (figure 20). Nevertheless the morphological analysis of the mutant embryos at the same stages as wild types indicated severe developmental differences.

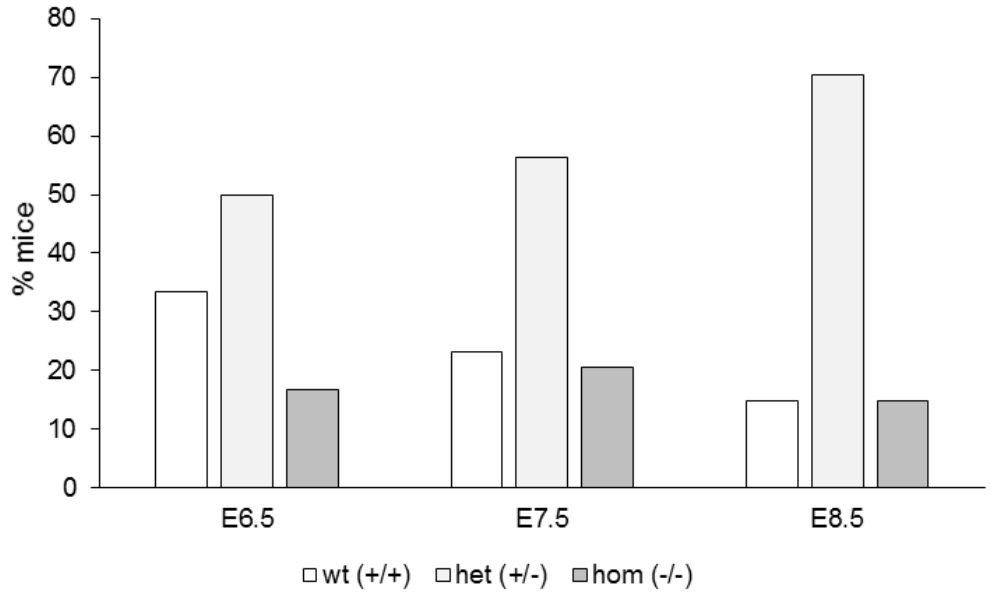

Figure 20: Distribution of the genotypes obtained from heterozygous matings in CD1 background at different early embryonic stages. Percentage representation of the genotypes of embryos dissected at E6.5, E7.5 and E8.5 showed a normal Mendelian ratio with slight preference for heterozygosity. E6.5: 1 litter, 12 pups; E7.5: 4 litters, 49 pups; E8.5: 3 litters, 27 pups.

4.2.2 Morphological analysis of Cyfip1 null mutant embryos

A morphological analysis of the embryos was performed to better define the time point of embryonic lethality. At time point E6.5, the differences between the mutant and the control were already quite obvious: CyFIP1-/- embryos appeared delayed in development. E6.5 wt embryos had reached Ts10 (see Introduction 1.11.3 for the definition of Theiler stages), while CyFIP1-/- embryos were still around Ts7 (figure 21A,B). CyFIP1-/- embryos at E7.5 were much smaller than controls and don´t develop properly (figure 21C,D). Finally at E8.5 CyFIP1-/- embryos had an overall degenerated aspect and the tissues appeared degraded. The mutants showed no morphology similarities to the controls anymore (figure 21E,F).

In conclusion CyFIP1-/- embryos showed severe developmental problems starting at the time point where gastrulation and germ layer formation take place.

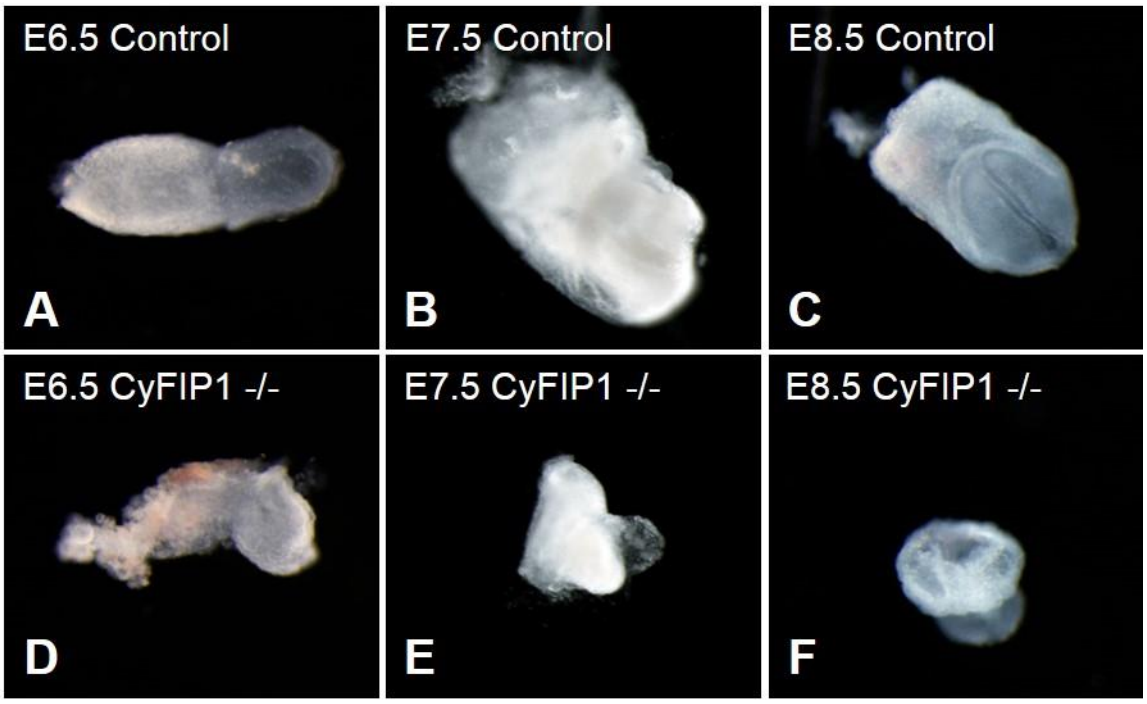

Figure 21: Morphology of control sample and CyFIP1-/- embryos at developmental day E6.5, E7.5 and E8.5. Control sample embryos (**A**,**C**,**E**), and Cyfip1-/- sample embryos (**B**,**D**,**F**). The genotype was determined by PCR on the whole embryo after imaging.

4.3 Characterization of CyFIP1 ko mouse-derived ES cells

In order to study early embryogenesis events, an alternative approach to embryonic analysis is the establishment of ES cell lines where defects in adhesion, proliferation, and differentiation can be analyzed. This approach was, therefore, chosen to elucidate the relevance of CyFIP1 in these processes and infer its function(s) in early embryonic development, since in vitro assays are a reproducible, easier to handle and validated system, and allow a substantial reduction of the use of experimental animals. For this reason ES cells were prepared from blastocysts (E3.5) collected after mating CyFIP1+/- mice of the C57Bl/6N genetic background. Briefly, blastocysts were singularly deposited on a feeder layer (mitotically arrested fibroblasts) and hatched for 5-6 days, then trypsinized and re-plated for 4-5 more days, when they were trypsinized a second time and finally plated as an established line. ES cells were kept on feeder cells and with LIF (Leukemia inhibitory factor) to maintain their pluripotency. To induce differentiation, ES cells were plated on gelatine coated dishes without feeders or cultured in suspension.

4.3.1 The WAVE complex in CyFIP1 knockout ES cells is reduced

After being generated, the ES cells were first characterized by analyzing the expression of CyFIP1 and the other components of the WAVE complex in total cell extracts, in order to establish if there was any biochemical difference.

In all CyFIP1-/- ES cells no CyFIP1 protein could be detected, as expected (figure 22). The faint band visible in the WB could likely be ascribed to the feeder cells, which normally represent a 10% of the lysate. Also no CyFIP2 was expressed at this stage. Nap1, the direct interaction partner of CyFIP1 in the WAVE complex, was strongly down-regulated as well as WAVE2 and Abi2, which seemed to be the dominant Abi form in ES cells. Abi1 and WAVE1 appeared to be less expressed, compared to brain control, but equally affected by the loss of CyFIP1.

Vinculin, a cytoskeletal adapter protein and FAK, the Focal Adhesion Kinase, which both play a role in focal adhesions, showed no differences between wt and knockout cells. SOS1 a binding partner of Abi1 in a different complex (Fan and Goff 2000) was not affected in the knockout. Total actin levels also did not appear to be altered by Western Blotting.

In summary, the major biochemical alterations that could be identified in ES cells depleted of CyFIP1 concerned the WAVE complex.

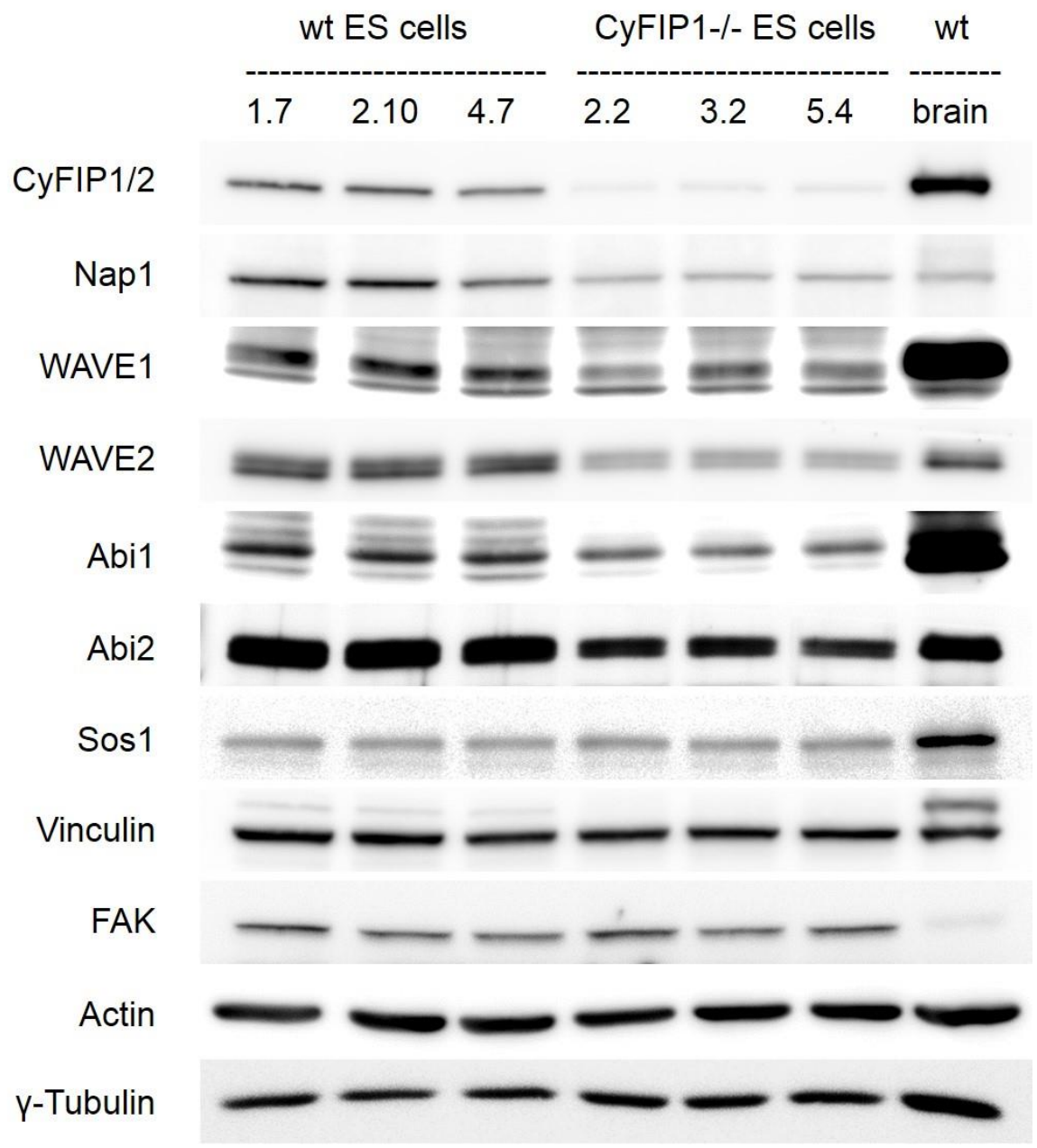

Figure 22: Expression of the WAVE complex components in CyFIP1 knockout ES cells total protein extracts. Deletion of CyFIP1 resulted in a significant reduction of the complex subunits Nap1, WAVE1, WAVE2, Abi1 and Abi2. SOS1, Vinculin, FAK and Actin seemed not to be affected by CyFIP1 depletion. γ-Tubulin is used as reference gene.

4.3.2 Genome-wide expression studies

To obtain a comprehensive insight about the genes and the pathways altered in CyFIP1 ko ES cells and their differentiation, an RNA microarray approach was performed. Microarrays, a high-throughput method, allow generating massive amounts

of molecular biology data. Three different clones for each genotype of undifferentiated ES cells and ES cells cultured for 3 days on gelatine were analyzed on beadchip arrays containing more than 29000 annotated genes. Two main strategies were followed in data analysis: 1) Identifying the differentially expressed transcripts at the level of individual genes; and 2) Assessing the differential expression of transcripts grouped into modules related to functional pathways. In order to consider a single gene differentially expressed, it had to fulfill a dual-criterion of magnitude change over reference (arbitrary minimum fold change (FC) ±1.5) and statistical significance of $p<0.05$. For gene group analyses, the expression distribution of the whole gene group had to be significantly different between the control and knockout ($p<0.05$). All data were log2 transformed because log-transformation decouples a random multiplicative error from a true signal.

4.3.2.1 CyFIP1 and CyFIP2 mRNA expression in wt and knockout undifferentiated and gelatine-differentiated ES cells

First, expression levels of CyFIP1 and CyFIP2 mRNAs were analyzed. CyFIP1 mRNA expression in the knockout cells was only 2/3 of the wt. This could be explained by the fact that although exons 4-6 are deleted, the other exons are still in place, so an mRNA could be transcribed. Although it should be prevented from nuclear export by the NMD (non-sense mediated decay) mechanism, a leakage is always possible. However no functional CyFIP1 protein could be translated and was ever detected, as shown, for example, in figure 22. CyFIP1 mRNA expression levels did not differ between ES cells and differentiated cells, both in the wt and the knockout genetic background.
On the contrary, CyFIP2 mRNA expression was affected by the knockout of CyFIP1. CyFIP2 in wt ES cells was low. Interestingly, in CyFIP1-/- ES cells CyFIP2 expression was about 20% higher than in the wt cells (figure 23). In the wt differentiated ES cells, after three days on gelatine, the expression of CYFIP2 increased about 1.5 fold in comparison to ES cells. The expression of CyFIP2 in CyFIP1-/- differentiated cells increased only slightly compared to undifferentiated cells and remained less than in wt cells.

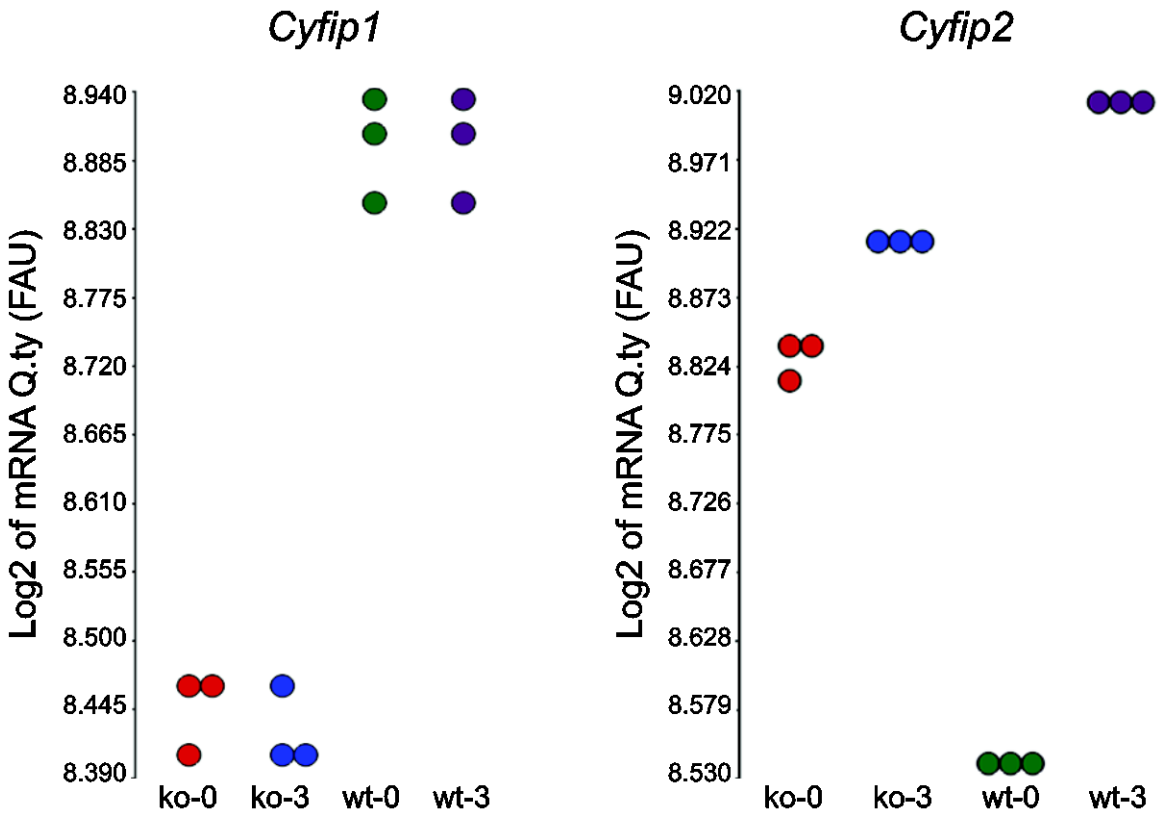

Figure 23: Log2 transformed expression levels of CyFIP1 and CyFIP2 mRNA. The triplicates for every genotype and condition are shown as circles in different colors. Each circle represents one cell clone. Expression level of CyFIP1 in the knockout is only 2/3 of wt level. CyFIP1 expression did not change between ES cells and differentiated cells. CyFIP2 expression is affected by the knockout of CyFIP1 and increases during differentiation only in wt background. wt-0 (green): Wild type ES cells; ko-0 (red): CyFIP1-/- ES cells; wt-3 (purple): Differentiated wild type ES cells for 3 days on gelatine; ko-3 (blue): Differentiated CyFIP1-/- ES cells for 3 days on gelatine.

4.3.2.2 Transcription factors altered by CyFIP1 deletion

The mainly phenomenological data generated by microarrays are often difficult to relate with the activation/inhibition of particular signal transduction pathways. The gene expression changes measured using microarrays in different cellular states, in fact, reflect just an "echo" of real molecular processes in the cells. A way to facilitate data interpretation is to look for transcription factors. Transcription factors are essential for the regulation of gene expression. They are proteins that control which genes are turned on or off in the genome by binding to DNA and other proteins. Bound to DNA, these proteins can promote or block the gene transcription holoenzyme, increasing or decreasing the availability of specific mRNAs. In CyFIP1-/- ES cells eleven

transcription factors were found significantly up-regulated and one transcription factor was significantly down-regulated compared to wild type ES cells (figure 24).

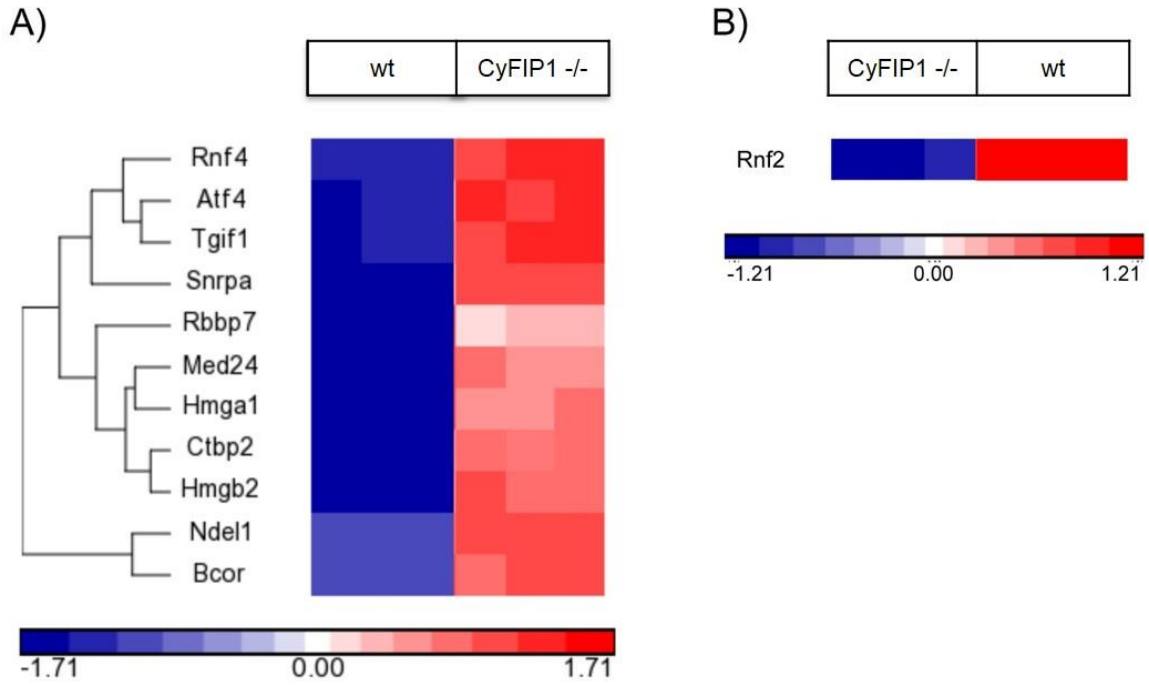

Figure 24: Gene expression heat map of transcription factors affected by CyFIP1 deletion in ES cells. The heat map displays **(A)** significantly up-regulated genes in 3 wild type ES cell clones (blue) compared to CyFIP1-/- ES cell clones (red) **(B)** significantly down-regulated genes in 3 CyFIP1-/- ES cell clones (blue) compared to 3 wild type ES cell clones (red).

Among the up-regulated transcription factors, Tgif1 and Hmgb2 are known to play an important role in embryonic development and germ layer formation (Rodriguez, Velkey et al. 2007; Powers, Taniguchi et al. 2010; Abraham, Bronstein et al. 2013). Rnf4 (RING finger protein 4), Atf4 (Activating transcription factor 4) and Hmga1 are known to play a positive role in regulating proliferation (Li and Wang 2006; Wang, Lian et al. 2009; Wang, Qian et al. 2010; Hirota, Tsuda et al. 2014). Hmga1 also has role in cancer and tumor invasiveness (Wang, Qian et al. 2010). Ctbp2 ability to direct cell migration has been previously linked to its ability to repress PTEN expression and thereby stimulate phosphatidylinositol 3-kinase (PI3K) activity, resulting in Rac-dependent migration (Paliwal, Kovi et al. 2007). Ctbp2 and Ndel1 are known to play a role in adhesion. Ndel1 is essential for cell proliferation and cell survival (Sasaki, Mori et al. 2005). Rbbp7 seems to play a role in differentiation and proliferation but more in the opposite direction compared to Rnf4 and Atf4: it inhibits cell growth by negatively

regulating β-catenin expression and the β-catenin/TCF signaling pathway, presumably through positive regulation of GSK-3 expression (Li and Wang 2006). Rbbp7 can induce apoptosis through activation of the c-Jun N-terminal kinase (JNK) signaling pathway (Zhang, Yu et al. 2003). Med24 is a component of the mediator complex (also known as TRAP, SMCC, DRIP, or ARC), a transcriptional coactivator complex thought to be required for the expression of almost all genes (Gustafsson and Samuelsson 2001). Med24 is also discussed in the hematopoietic system and for Med1 it is shown that it has influence on the hematopoietic stem cells (Stumpf, Waskow et al. 2006) and that Med1-/- bone marrow cells proliferate less (Sumitomo, Ishino et al. 2010). Snrpa is essential for splicing and is present in the spliceosome associated with Sm complex (Hetzer and Mattaj 2000). Bcor is a transcriptional corepressor and is a key transcriptional regulator during early embryogenesis (Ng, Thakker et al. 2004).

Rnf2 is the only significantly down-regulated transcription factor in CyFIP1-/- ES cells. Rnf2 is an essential component of a Polycomb group (PcG) multiprotein PRC1-like complex, a complex class required to maintain the transcriptionally repressive state of many genes, including Hox genes, throughout development.

In differentiated cells after 3 days on gelatine only one transcription factor was found to be significantly up-regulated, Rhox9, and no one was significantly down-regulated compared to wt cells (figure 25). Rhox 9 is a member of the Homeobox gene family and important in embryonic development and the reproductive system (Lee, Lee et al. 2013), which is affected already in the CyFIP1+/- mouse (see results 4.1 and 4.2). In hematopoietic stem cells Rhox9 is highly expressed compared to endothelial cells (Solaimani Kartalaei, Yamada-Inagawa et al. 2015)

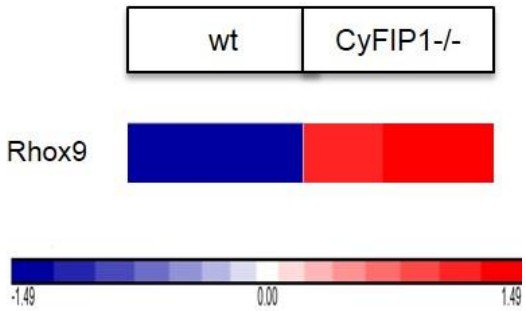

Figure 25: Gene expression heat map of transcription factors affected by CyFIP1 deletion in differentiated cells. The heat map displays one significantly up-regulated gene in 3 CyFIP1-/- cell clones differentiated for 3 days on gelatine compared to 3 wild type differentiated cell clones. No significant down-regulated genes were found.

4.3.2.3 Pathway enrichment analysis in CyFIP1-/- ES cells

Pathway enrichment analysis (PEA) was used to identify statistically significant gene sets affected by the deletion of CyFIP1. Interestingly, among others, the PI3K-Akt signaling pathway appeared up-regulated in the absence of CyFIP1 (figure 26). The PI3K-Akt signaling pathway is involved in a wide variety of cellular events including mitogenic signaling, regulation of growth and survival, vesicular trafficking, and control of the cytoskeleton.

Pathway Name	Enrichment Score	Enrichment p-value
Phagosome	7.30273	0.0006737
Viral carcinogenesis	7.20936	0.00073963
RNA transport	5.93268	0.00265137
PI3K-Akt signaling pathway	5.70258	0.00333735
SNARE interactions in vesicular transport	5.57952	0.00377439
Spliceosome	5.34357	0.00477878

Figure 26: Pathway enrichment analysis in CyFIP1 knockout vs. wt ES cells: up-regulated pathways. Significantly up-regulated gene sets/pathways are shown with the enrichment Score and p-value.

No significant differences resulted for the PEA of the entire TGFβ pathway in CyFIP1-/- ES cells in comparison to the wt cells, but the overview heat map of the pathway with all TGFβ genes showed clear differences in expression levels of a subset of genes (figure 27). For example one can see in the bottom half of the map Smad5, Smad2 and Nodal are down in the CyFIP1-/- ES cells compared to wild type ES cells. The TGFβ superfamily is known to be one of the most ubiquitous regulators of embryonic development (Gordon and Blobe 2008). For example it regulates germ layer formation via the BMP/Smad signaling (Coucouvanis and Martin 1999; Pangas, Li et al. 2008). Because of the early embryonic phenotype of the CyFIP1 knockout it seemed a plausible candidate pathway that could be affected by CyFIP1 depletion.

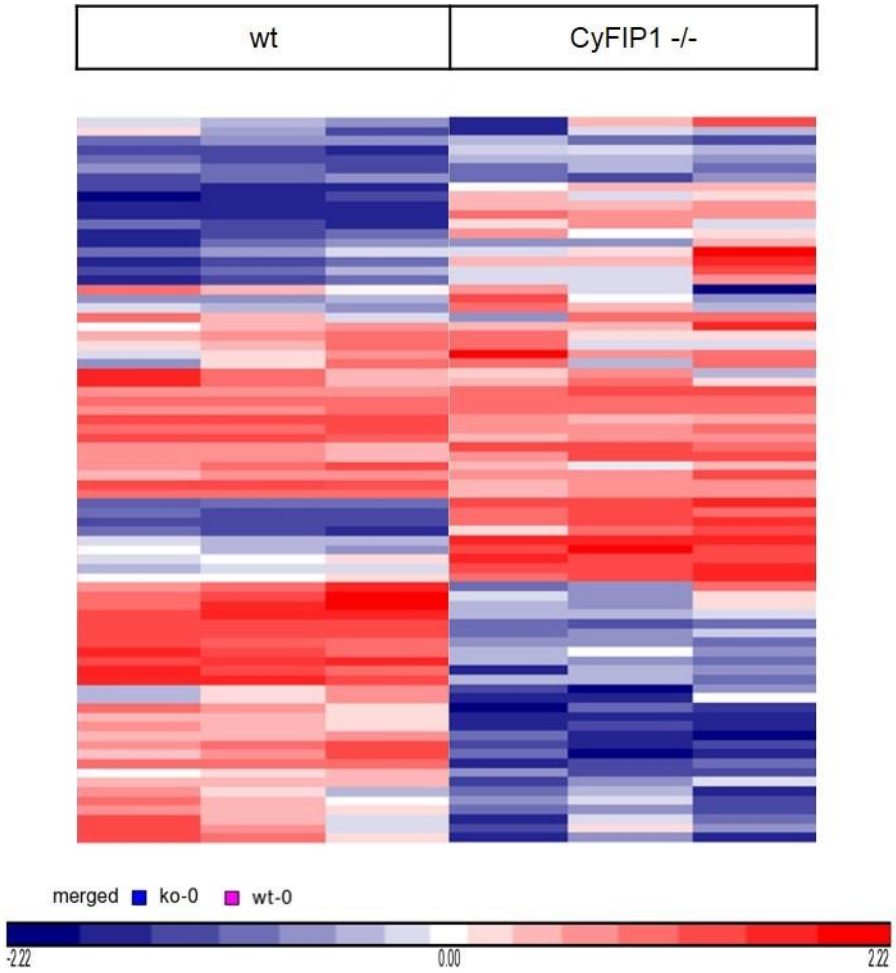

Figure 27: Gene expression heat map of TGFβ superfamily genes affected by CyFIP1 deletion. Heat map of all genes involved in the TGFβ network in the 3 CyFIP1-/- ES cell clones compared to the 3 wild type ES cell clones. A clear difference is observed in the bottom half of the map, besides some dysregulation of some of the genes in the upper part of the map.

In summary the microarray analysis showed that transcription factors mRNAs as well as pathways involved in apoptosis, cell growth, proliferation, adhesion and transcription are significantly up-regulated in CyFIP1 knockout cells. Also genes which are important in development and differentiation were significant altered in the CyFIP1-/- cells. These findings represented a starting point for further analysis of the mutant ES cells to experimentally verify any defects in apoptosis, proliferation, differentiation and adhesion.

4.4 Proliferation and adhesion properties of CyFIP1-/- ES cells

The microarray data for the CyFIP1-/- ES cells showed altered mRNA levels of transcription factors which regulate cell proliferation and adhesion. Proliferation and adhesion are important functions in cells and are necessary for the cell and the whole organism survival. To check proliferation and adhesion in CyFIP1-/- ES cells the so called CyQuant assay was used. Proliferation and adhesion can be easily and reproducibly measured with this assay because it is based on counting the cells that grow on plates using DNA quantification as a measure to determine the number of cells. The CyQuant dye intercalating nucleic acids was quantified by fluorometric measurement. For the proliferation assay, ES cells were grown on feeders for five days and every day a plate was frozen for quantification. At the end of the time course all plates were stained and read together in a plate reader. A second protocol was used to study combined adhesion and proliferation properties by growing ES cells for five days on gelatine without feeders. Adhesion capacity was examined after seeding equal numbers of ES cells on gelatine, a collagen-derived substrate, with a short time course, freezing one plate every hour for a total of 4 hours.

In the proliferation assay, Cyfip1-/- ES cells rapidly grew into a stationary phase where probably the proliferation rate was equal to the apoptosis rate, the two processes balancing each other. Instead, wt ES cells grew slower and after reaching maximal density underwent cell death with a net decrease in cell number (figure 28A). Indeed, while handling the ES cells for the experiments, it was always necessary to passage CyFIP1-/- ES cell clones earlier than wt clones although the same number of cells was plated on the dish.

In a different proliferation protocol on a collagen substrate the results were very different. While wt cells proliferated massively, up to 100 times the initial adhered number (although this high increase could be partially due to the zero time point preparation, where simple centrifugation of the cells on collagen might not efficiently adhere all seeded cells), CyFIP1-/- cells were 4 to 5 times slower (figure 28B).

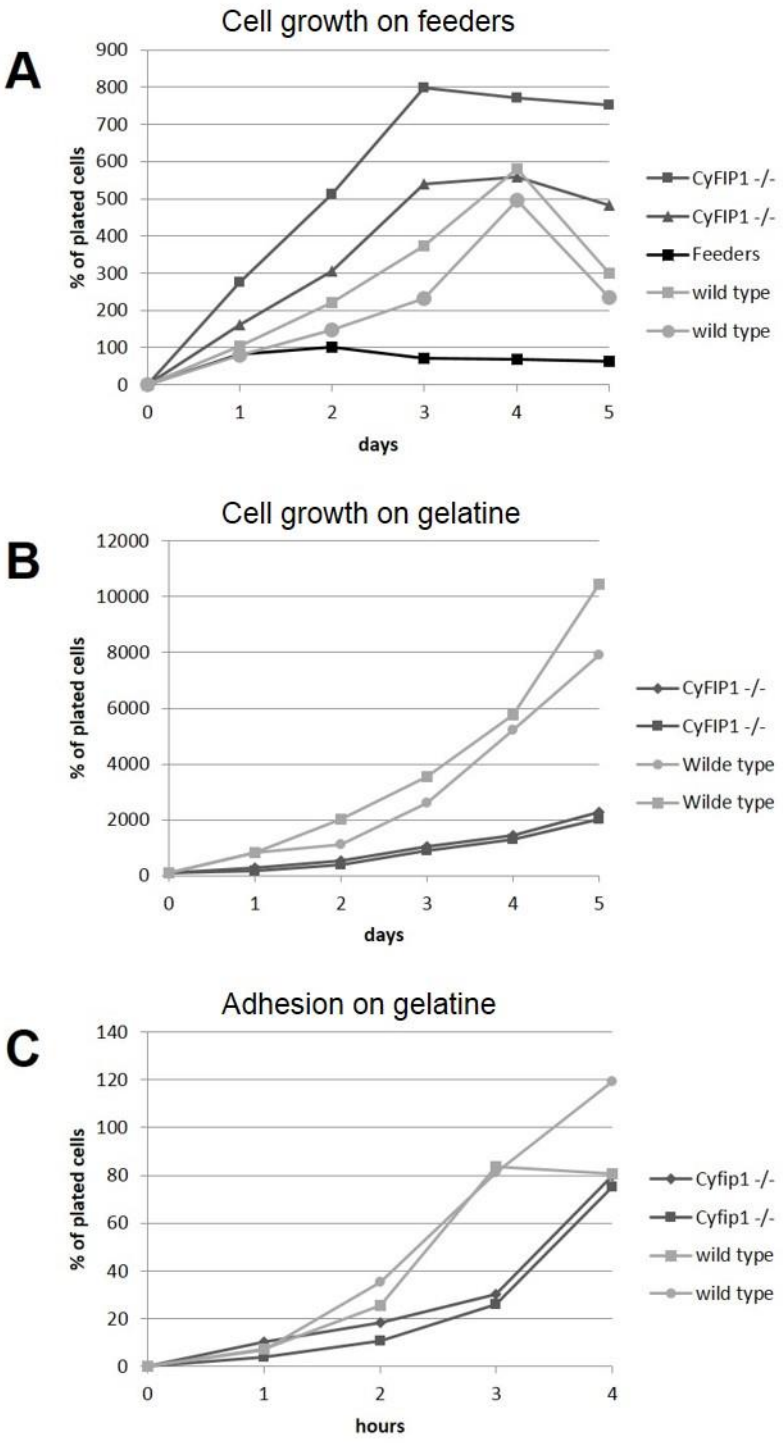

Figure 28: Proliferation and adhesion properties of CyFIP1-/- ES cells. (**A**) CyFIP1-/- ES cells showed an increased proliferation rate, as seen by the steeper slope, reaching steady state after three days on feeders (**B**) Without feeders wild type ES cells proliferated very efficiently while CyFIP1-/- ES cells were much slower. (**C**) CyFIP1-/- ES cells showed deficits in adhesion to collagen.

Analyzing raw numbers showed a much smaller number of CyFIP1-/- cells at every time point compared to wt, possibly indicating adhesion deficits on the collagen substrate, or a requirement of growth factors from feeder cells, or a cell density effect, or a combination of all factors that could all justify the different result from the previous experiment.

For this reason, the adhesion capacity of CyFIP1-/- ES cells on a collagen-derived substrate was tested and it was found reduced in the first 4 hours after plating, although only by a factor of about 2 (figure 28C). This was in line with the previous experiment, partially explaining the low growth on gelatine, since cells might be continuously lost in the medium due to adhesion deficits. But the much larger effect observed in the cell proliferation assay implies other reasons, as proposed above.

4.5 Morphological characterization of CyFIP1 knockout embryoid bodies

The morphological analysis of CyFIP1-/- embryos showed defects in development at the time point of gastrulation (see Introduction 1.7.2). The microarray data provided some hints concerning differentiation and germ layer formation. Genes from the TGF beta pathway like Smad 1 and 5, which have been shown to be important for mesoderm formation and for endoderm organization in the embryo were affected. The up-regulation of the transcription factors Tgif1 and Hmgb2 in CyFIP1-/- ES cells also suggested possible germ layer formation defects. For a detailed analysis of germ layers, an in vitro differentiation system was chosen, the embryoid body formation from ES cells, due to its sustainability compared to embryo analysis that would require a high rate of animal sacrifice. It is a well-established protocol where ES cells cultured in suspension without anti-differentiation factors spontaneously differentiate and form three-dimensional multicellular aggregates called embryoid bodies (EBs) (Nishimura, Martin et al. 2007). In the EBs, the three embryonic germ layers, ectoderm, endoderm and mesoderm, are developed. EBs grossly resemble early embryos at the blastocyst-primitive streak stage (see Introduction 1.11), having an endodermal exterior and a mesodermal and ectodermal interior. Furthermore, the cells of the EBs are surrounded by a large cystic yolk sac-like cavity. Accordingly, the outer columnar epithelium is of endodermal origin (visceral endoderm). This model system, therefore, allows to study early developmental stages in vitro.

In a first approach, in order to morphologically characterize them, EBs obtained from wt and CyFIP1-/- ES cells were imaged in wide field microscopy and measured. Evident differences could be detected in their size. Cyfip1-/- EBs were significantly

larger than control EBs (figure 29), suggesting that Cyfip1-/- cells have a higher proliferative activity, in line with the previous proliferation assay (see figure 28A).

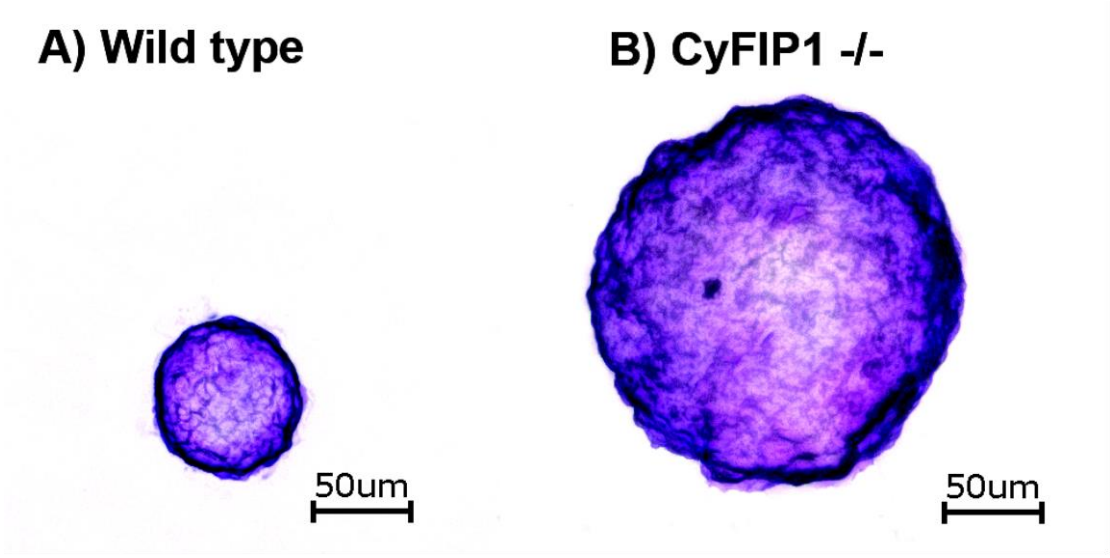

Figure 29: Comparison between wild type and CyFIP1-/- EBs after 7 days of differentiation. H&E Staining of (**A**) wt and (**B**) CyFIP1-/- EBs showed that mutant EBs are much bigger than wt controls.

4.5.1 Germ layers defects in CyFIP1-/- EBs

The question, therefore, was what could be wrong in the development of the mutant EBs. Were all layers present with increased cell numbers, or were some layers missing to the expense of other layers, or would there be no layering at all? Germ layers can be identified by specific markers. CD184 is known to be expressed in endodermal cells (Drukker, Tang et al. 2012) while beta-catenin is important for meso-endoderm formation through the Wnt-signaling pathway (Davidson, Adams et al. 2012). Cleaved caspase 3 is expressed during apoptosis and can mark the cell death rate in the blastocoele-like cavity of EBs (Porter and Janicke 1999). To address the question how the germ layer formation in CyFIP1-/- is affected, a quantitative FACS-based method was developed to analyze differentiation of individual cell lineages in CyFIP1-/- versus wt EBs. Flow cytometry has the advantage that many cells can be analyzed in a short time and quantitative data were obtained. EBs were generated from three independent clones of CyFIP1-/- and wild type (wt) ES cells after 7 days in suspension culture. They were then collected and a single cell suspension was produced with a gentle dissociation treatment. Cells were then immunostained with fluorescently-labeled

primary antibodies raised against the germ layers markers described above and analyzed with a BD Accuri flow cytometer.

The results of this analysis showed that CyFIP1-/- EBs were impaired in their differentiation program. In fact the endoderm showed a significant 40% expansion, while the meso-endoderm was decreased by 20% in comparison to wt EBs (figure 30A,B). Moreover, the apoptosis rate was increased by 60% in CyFIP1-/- EBs (figure 30C).

In summary, these data showed a considerable impairment of mesodermal lineage determination in Cyfip1-/- EBs while the endodermal lineage was found to be increased at the expense of mesodermal cells and EB size. Ectoderm seemed not to be influenced in the knockout, but it represented a very small percentage of cells in EBs (data not shown).

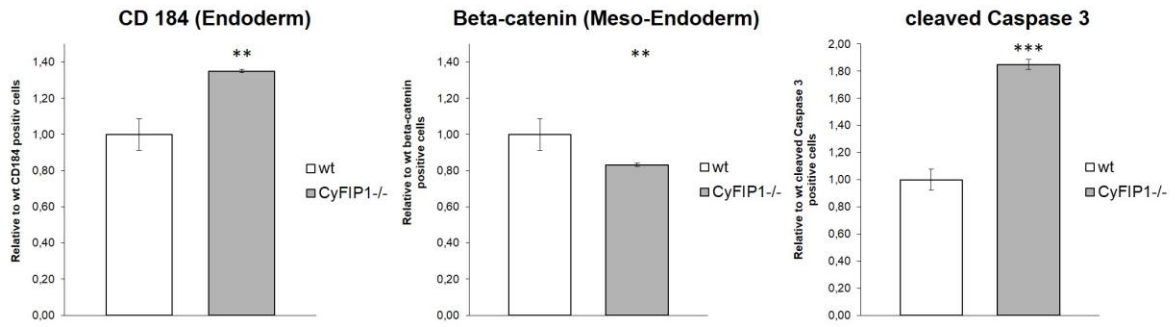

Figure 30: Quantification of endoderm, meso-endoderm and apoptosis in CyFIP1 knockout embryoid bodies. Flow cytometric analysis from 7 days old embryoid bodies. Results are displayed as fold increase (>1) or decrease (<1) respect to wt controls. **(A)** Significant increase of endodermal cells in CyFIP1-/- EBs. **(B)** The amount of mesodermal cells is significantly decreased in CyFIP1-/- EBs. **(C)** CyFIP1-/- EBs show a much higher number of apoptotic cells. For each genotype, n=3 (independent ES clones). Statistical analysis by T-test: ** P<0.01, *** P<0.001.

4.6 Differentiation of CyFIP1-/- ES cells on gelatine

While EBs formation reproduces a directed differentiation into the three germ layers, another approach to study differentiation is undirected differentiation of ES cells on a substrate, for example culturing ES cells for 3 days on gelatine without feeders in regular ES cell culture medium. This simple differentiation protocol was used also for

the microarray analysis, therefore it appeared necessary to study it from a morphological and biochemical point of view.

The wild type ES cells, despite the presence of the LIF, directly started to differentiate. In fact, under these conditions, they lost the typical round shape of the colonies, spread out and flattened. The CyFIP1-/- cells, on the contrary, mostly kept the round colony form and differentiated much less (figure 31). Even after 3 days on gelatine they looked more like ES cell clones compared to the wt where no single clone could be detected.

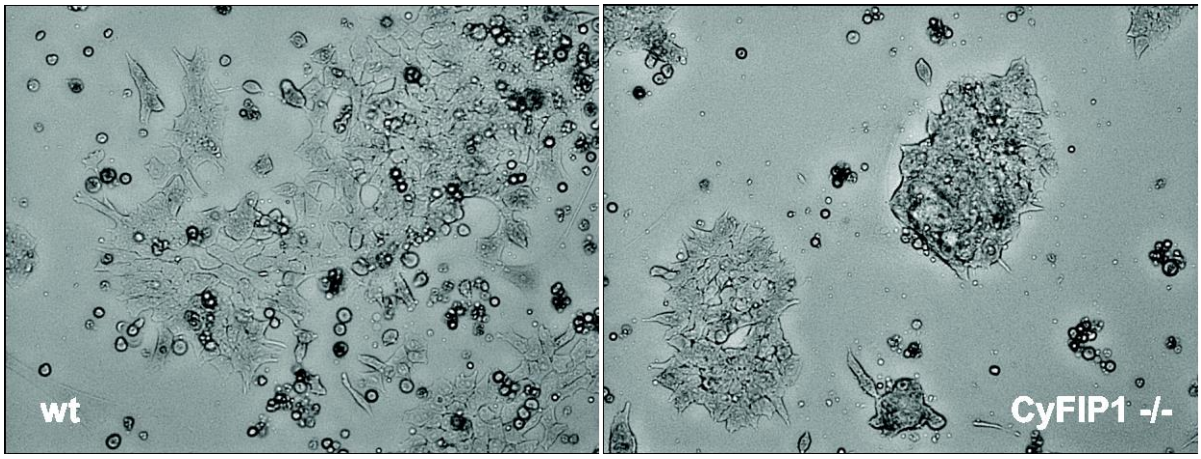

Figure 31: Wide field imaging of wild type and CyFIP1-/- ES cells after 3 days in culture on gelatine. CyFIP1-/- ES cell colonies were resistant to differentiation after 3 days in culture without feeder layer.

4.6.1 Molecular characterization of CyFIP1-/- ES cells on gelatine

As it was shown by visual analysis (4.6 and figure 31), CyFIP1-/- ES cells differentiated less than wt cells when cultured for three days on gelatine. To characterize the type of cells which were growing on the collagen-like surface, two markers were used: SSEA1, Stage-Specific Embryonic Antigen 1, a well-known marker for murine pluripotent stem cells (Ginis, Luo et al. 2004) and Sca-1, Stem cell antigen-1, a member of the Ly-6 antigen family in mouse expressed in hematopoietic stem/progenitor cells (Holmes and Stanford 2007). The cultured cells were detached from the plate, brought to a single-cell suspension, and analyzed by FACS after labeling them with the stem cell markers. This method, as previously mentioned, provides reliable quantitative data.

CyFIP1-/- cultures were tendentially richer in SSEA1 positive cells (figure 32A), indicating the presence of more stem cell-like cells than in the wt culture. This is in good accordance with the previous findings obtained analyzing the morphology of the

colonies on the dish. In addition, Sca-1 positive cells were significantly decreased in CyFIP1-/- cultures (figure 32B). Hematopoietic stem cells are the progenitor cells that give rise to all blood and immune cells and are derived from the mesodermal lineage. It was already shown using an in vitro embryo developmental paradigm that CyFIP1-/- ES cells are defective in mesoderm formation (see Results 4.5.1 and figure 30B), and these data strongly confirm the previous findings.

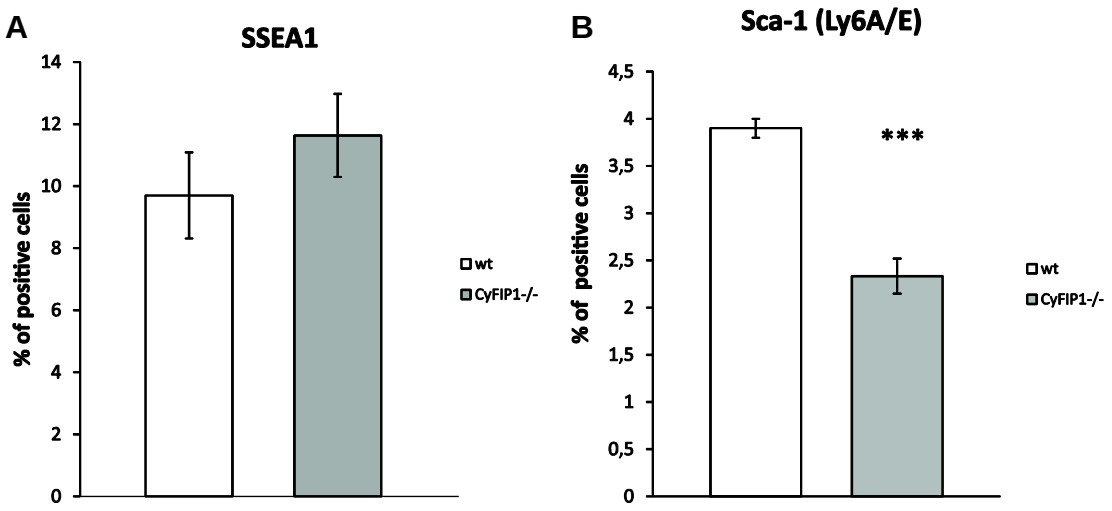

Figure 32: Quantification of different types of stem cells after culturing CyFIP1 knockout ES cells on gelatine. A) SSEA1, a stem cell marker, is increased in CyFIP1-/- cultures. **B)** Sca-1, a hematopoietic stem cell marker, is significantly decreased in CyFIP1-/- cultures. N=3 for each genotype. Statistical analysis with t-student's test: *** $p<0.001$.

4.7 Analysis of kinases involved in growth, survival and apoptosis pathways

Proliferation, cell growth and adhesion have been shown to be altered in CyFIP1-/- ES cells. These cell functions, when abnormal, play an important role in cancer formation and progression, therefore it appeared a key question to identify the signaling pathways responsible for the described phenotype. The microarray data showed an overall increase of the PI3K pathway in CyFIP1-/- ES cells. The PI3K pathway regulates many cell functions such as proliferation, cell growth and adhesion and consequently its dysregulation is also the main known cancer pathway. Nevertheless, the MAPK pathway also regulates cell proliferation and survival and is another

important cancer pathway in case of alterations. The TGFβ pathway controls apoptosis and proliferation, also resulting to have a role in cancer when altered. Important proteins of the TGFβ pathway are the Smads. Smads are intracellular proteins that transduce extracellular signals from TGFβ ligands to the nucleus where they activate downstream gene transcription (Heldin, Miyazono et al. 1997). Smad1/5 and also 8 have been shown to be important in early embryonic development (Faure, Lee et al. 2000).

The activity of these pathways correlates with the phosphorylation state of many of their components. Therefore, the phosphorylation state of key proteins of these pathways was analyzed by western blotting in cell extracts from ES cells grown on feeders to possibly uncover the molecular mechanisms leading to the defects described in the previous sections when CyFIP1 is depleted.

Western Blot analysis of PI3K, MAPK and TGFβ pathways related proteins showed no clearly visible differences in protein levels (figure 33A). Therefore a statistical approach was adopted, quantifying the protein levels in the three clones and calibrating with the γ-tubulin expression, to detect even subtle changes in the protein levels. The analysis showed only a significant decrease of phospho-Smad1/5 in CyFIP1-/- ES cells (figure 33 B). All other proteins showed no significant differences between wt and CyFIP1-/- ES cells. Only tendencies were visible. The PI3K pathway appeared down-regulated at the protein level in CyFIP1-/- compared to wt ES cells, in contradiction with the microarray analysis. A tendential down-regulation was also seen for phospho-Erk1 and phospho-Erk2 although data showed high variability among the three clones (figure 33B).

In summary, the analysis showed that P-Smad1/5 are significantly decreased, while the PI3K pathway as well as the MAPK pathway are overall not significantly affected.

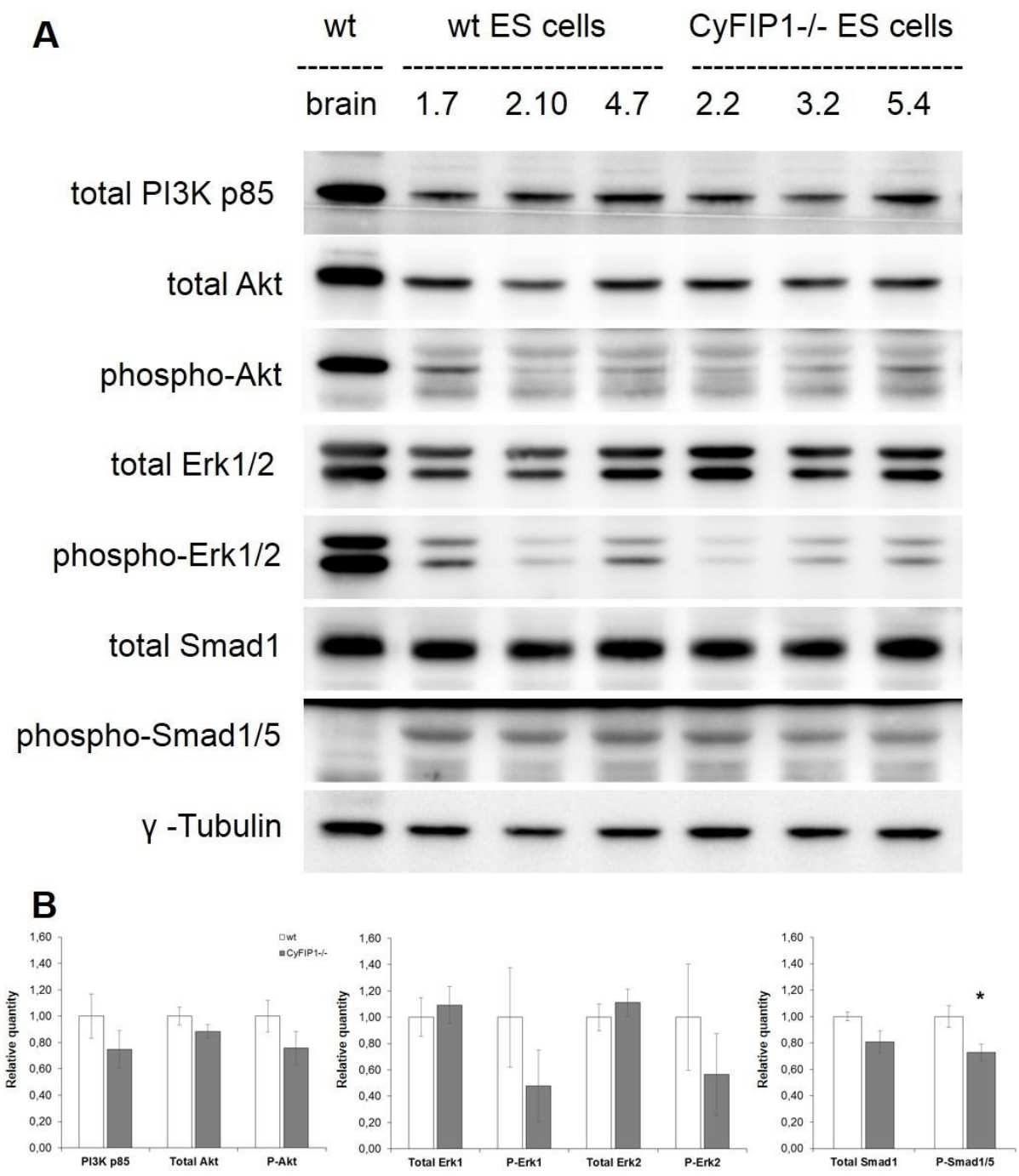

Figure 33: Total protein and phosphorylated protein levels of components of the PI3K, MAPK and TGFβ pathways. A) Western Blotting of selected components of the PI3K, MAPK and TGFβ pathways of wt and CyFIP1-/- ES cell clones. γ-Tubulin is shown as reference gene. **B)** Quantification analysis of total and phosphorylated protein levels showed significant decrease of phospho-Smad1/5 levels in CyFIP1-/- ES cells. No significant changes could be observed in the other proteins. Only a tendential decrease could be seen in the proteins which were related to the PI3K pathway and the phosphorylated MAPKs in CyFIP1-/- ES cells. Data were calibrated with γ-Tubulin levels and are expressed as means ± SEM; n = 3 per genotype. Statistical analysis with t-student's test: *p < 0.05

4.8 Biochemical Analysis of the WAVE Complex(es) in the Mouse

The WAVE complex is composed by the different isoforms of its 5 subunits but may be closely interacting with other unknown factors in order to be regulated in its activities. In this way the WAVE complex composition and function might be differently specified in different tissues. As mentioned in the introduction, Cyfip1/2 interacts with Profilin2 but not with Profilin1 (Witke, Podtelejnikov et al. 1998). The interaction of Profilin2 and the WAVE complex depends on the poly-L-proline binding domain of Profilin2 (Witke, Podtelejnikov et al. 1998). In pull-down assays with Profilin2-beads nearly all CyFIP1/2 is collected from brain lysates (Massimi 2008). Pull-down assays are useful for identifying the domains or post-translational regulatory mechanisms affecting protein-protein interactions and for identifying previously unknown binding partners by mass spectrometry sequencing of the pulled-down proteins.
Pull-down assays with Profilin2-beads were used in this thesis to investigate the question of subunit exchange and the regulatory mechanisms of the WAVE complex.

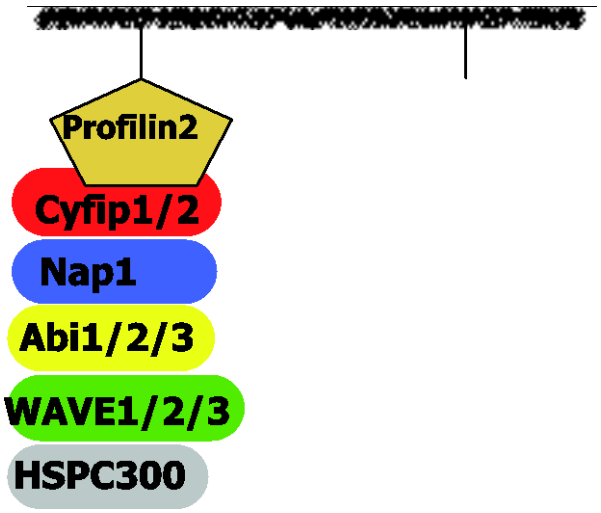

Figure 34: Scheme of a Profilin2 pull-down experiment. Profilin2 covalently bound to Sepharose 4B beads interacts with the WAVE complex when the beads are mixed with a mouse tissue lysate extracting it with its ligands from the total protein pool (Witke, Podtelejnikov et al. 1998)).

4.8.1 The WAVE complex in mouse tissues

Most WAVE complex subunits are represented by more than one isoform, which have a tissue specific pattern, with an expression overlap in some tissues. It is, therefore, possible to hypothesize that in every tissue one or more unique WAVE complexes are

formed. Pull-down assays with Profilin2-beads from brain, lung and kidney lysates were performed in order to dissect some of these complexes. In brain and lung the amount of free subunits (unbound fraction) was rather low and practically all of the subunits appear to be forming WAVE complexes bound to profilin2 (figure 35). In brain the complex incorporated essentially WAVE1, while in lungs only WAVE2 formed the complex, due to the different expression patterns of the WAVE subunits.

Surprisingly the WAVE complex in the kidney behaved differently from the other tissues. First of all in kidney the WAVE complex didn't bind to Profilin2 (figure 35). Secondly, no Abi1 was expressed (figure 35), implying that probably Abi2 is the main Abi component in kidney's WAVE complex, even though Abi2 has been characterized as the brain isoform (Grove et al., 2004).

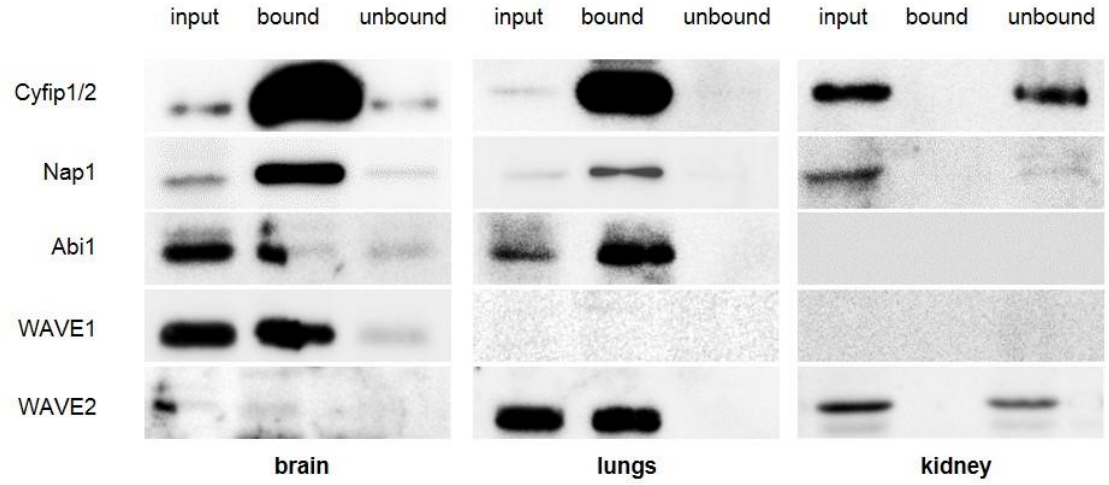

Figure 35: Different properties of the WAVE complex in brain, lungs and kidney. In brain and lungs the classical WAVE complex binds to Profilin2-beads. In kidney the WAVE complex doesn´t bind to Profilin2.

4.8.2 The WAVE complex regulation by different ionic conditions and signaling pathways

An interesting question is if the composition of the WAVE complex could change in response to different ionic conditions and signaling pathways. In order to address this question, Profilin2 pull-down assays were performed with different lysis buffers covering a range of conditions and signaling cascades. The control condition was a basic isotonic buffer with KCl, Tris/HCl pH 7.4 to keep the lysate buffered and TritonX-100 to lysate the tissues. The other buffers consisted of the basic buffer components

and some additional reagents: the second buffer was enriched in Mg^{2+} without Ca^{2+}. The absence of any free Ca^{2+} was ensured by the use of EGTA, which binds uniquely to Ca^{2+}, negatively affecting Ca^{2+}-dependent interactions and pathways. The third buffer, on the contrary, was enriched in both Mg^{2+} and Ca^{2+} and should therefore activate Ca^{2+}-dependent pathways. The fourth lysate was depleted of all divalent ions by using the strong wide spectrum chelator EDTA. The fifth type of lysate was depleted of all protein phosphorylation by digestion with CIP (calf intestinal phosphatase). The sixth one, was prepared with strong phosphatase inhibitors (NaF, Na_3VO_4 and Na-pyrophosphate) to preserve the physiological phosphorylation state of proteins. NaF is inhibiting serine and threonine phosphatases (PSPs). Na_3VO_4 has a high resemblance to phosphate due to the four oxygen atoms in a tetrahedral conformation and can inhibit tyrosine phosphatases (PTPs) through competitive inhibition. Na-pyrophosphate on the other hand has a high resemblance to the end product of phosphorylation (although it is missing the adenosine part) and can also inhibit phosphatases through competitive inhibition.

The results of the Profilin2 pull-down essay from brain extracts prepared in the different buffers are shown in figure 36. The bound fractions of each pull-down showed a surprisingly flexible composition of the WAVE complex. High Mg^{2+} in the absence of Ca^{2+} led to a strong binding of the entire WAVE complex to Profilin2 (column 2 vs. 1), whereas the addition of Ca^{2+} resulted in no binding at all (column 3). Sequestration of all divalent cations from the solution obtained with the addition of EDTA resulted in a very surprising effect, the braking of the pentameric WAVE complex in two parts, with the CyFIP/Nap1 core binding alone to Profilin2 and the Abi/WAVE part left in the unbound fraction (column 4). Dephosphorylation of the proteins in the lysate seemed to have only little influence on the binding pattern of the WAVE complex components (column 5 vs. 1). Finally, even more surprisingly, preservation of the phosphorylation state of proteins seemed to detach exclusively Abi1 from the complex, and at the same time to increase the binding of the CyFIP/Nap1 core similarly to when all divalent cations were removed by the addition of EDTA.

These results strongly pointed to a flexibility in the composition of the WAVE complex that in brain can also exist as a CyFIP/Nap1 complex alone or a CyFIP/Nap1/WAVE1 complex.

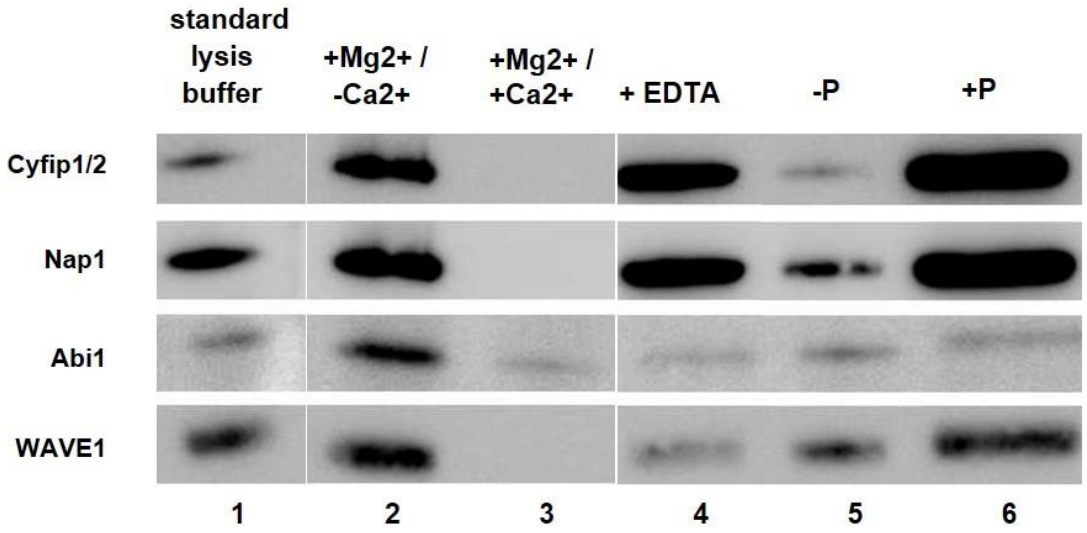

Figure 36: Differential composition of the WAVE complex binding to Profilin2 in different buffer conditions. Western blotting showing in Column 1 the binding of the WAVE complex in a basic isotonic buffer with 1% TritonX-100 for reference of the other columns; in Column 2 increased binding of the WAVE complex to Profilin2-beads in the presence of Mg^{2+} ions; in Column 3 loss of WAVE complex binding to Profilin2 in the presence of Ca^{2+}; in Column 4 uncoupling of CyFIP/Nap1 and Abi/WAVE sub-complexes when all divalent ions are sequestered from the solution; in Column 5 that treatment of the lysate with phosphatase (removing all phosphorylations) does not significantly affect the binding of the WAVE complex to Profilin2; in Columns 6 that in the presence of phosphatase inhibitors the binding of CyFIP/Nap1 to Profilin2 is enhanced, while the Abi subunit is specifically lost.

4.8.3 New candidate ligands of the WAVE complex

Since the data presented until now have shown that the WAVE complex has a quite flexible structure, it was sensible to think it might be interacting with yet unknown partners. In order to verify this hypothesis, a new approach was designed. CyFIP1/2 was immunoprecipitated from brain extracts with a specific monoclonal antibody previously generated and characterized in the lab (Massimi 2008) and new candidate ligands were identified by Maldi-TOF mass spectrometry after band elution from a polyacrylamide gel. Mass spectrometry is a technique that allows the identification of proteins by producing and separating ions by their unique mass-to-charge ratios. Although there is no possibility to distinguish if ligands directly interact with CyFIPs or with any of the other WAVE complex components, this approach allows at least identifying possible cellular processes in which the WAVE complex is involved and further expanding the current view of the WAVE complex as a static pentameric structure.

By mass spectrometry it was possible to identify among the immunoprecipitated material CyFIP1 and CyFIP2 as well as the classical complex components such as Nap1, Abi1/2 and WAVE1. Besides the WAVE complex, which was considered as a positive control for the whole experiment, many other possible novel ligands have been identified. For easiness of interpretation they are presented in figure 37 divided into four functional protein groups: actin-binding, membrane trafficking, signaling, and mRNA translation and transport.

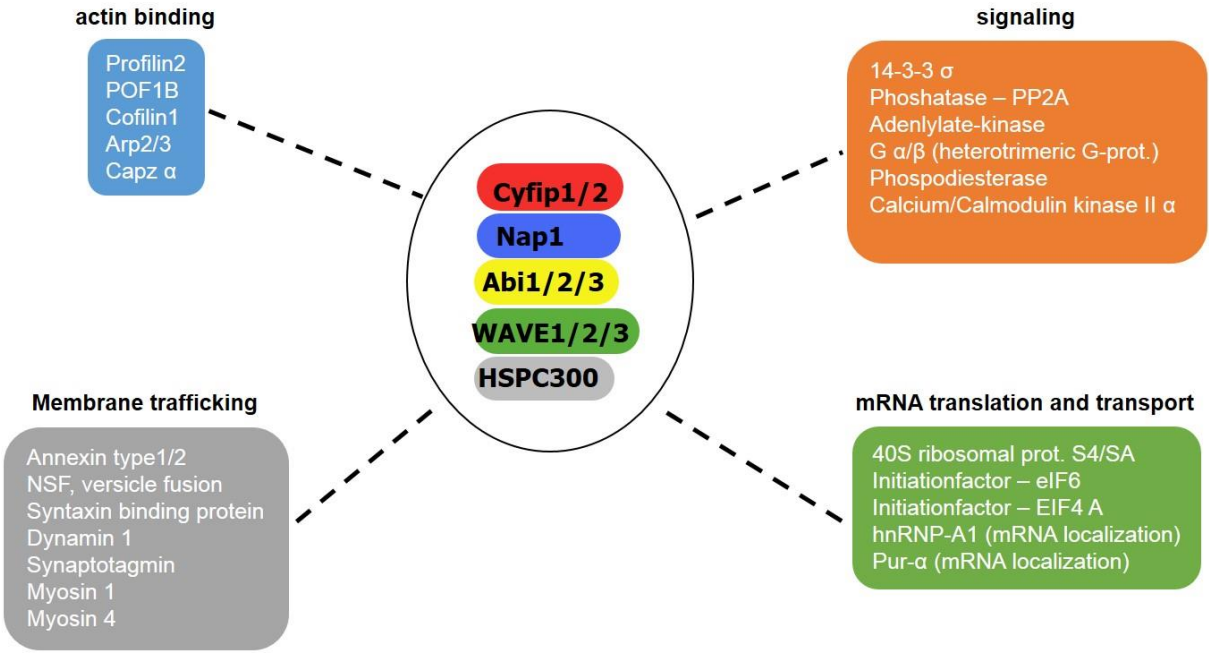

Figure 37: Novel candidate ligands for CyFIP1/2 and the WAVE complex identified by MALDI-TOF. The identified candidates are presented grouped according to four molecular pathways related to actin-binding, signaling, membrane trafficking and mRNA translation and transport.

In the group of actin-binding proteins were found besides the expected Profilin2 (Witke, Podtelejnikov et al. 1998) and Arp2/3 complex some interesting novel candidates such as Cofilin 1 and CapZ (figure 37). Also, surprisingly, POF1 was identified, a protein mutated in human premature ovarian failure (Lacombe, Lee et al. 2006), an infertility phenotype that has been previously described in CyFIP1+/- females (see Results 4.1). Among the membrane trafficking-related candidates, Myosin 1 and Myosin 4 were found, possibly pointing to a role of the WAVE complex in actin-based cargo transport (confirmed by the candidates concerning mRNA transport).

Interestingly proteins involved in translation initiation (e.g. eIF4A and eIF6) and mRNA transport in neurons (hnRNPA1, Pur-α) were also found, in line with the already shown

role of CyFIP1 in mRNA translational repression in spines in combination with FMRP (Napoli, Mercaldo et al. 2008).

5. Discussion

5.1 Relevance of genetic background for CyFIP1 deletion

The genetic background of the mouse is well known to dramatically influence the phenotype of single locus changes brought about by gene targeting. The influence of the genetic background is evident on the phenotype of the CyFIP1 knockout mouse model. The three strains used until now for this knockout show some substantial phenotypic differences. The widely used C57BL/6J and C57BL/6N strains are so-called inbred mouse strains which were generated by sister-brother matings for 20 or more consecutive generations, respectively at the Jackson Laboratories and at NIH, hence the last letter in the name (Green, Grueneberg et al. 1963). They have a great genetic stability and were generated to facilitate the comparison of data from different labs. The CD1 mice are outbred stocks, which have genetic variability. Inbred strains offer a defined genetic background, whereas outbred stocks offer a diverse gene pool, which is closer to the situation in most human studies. In C57BL/6J background the CyFIP1 knockout is embryonic lethal around E8.5. The CyFIP1 knockout in C57BL/6N background showed a much more severe phenotype, with embryonic lethality occurring as early as E6.5 and the embryos quickly reabsorbed. Moreover, an infertility phenotype of the heterozygous females appeared, which complicates the embryological studies. The infertility phenotype becomes much milder in CyFIP1 heterozygous females in the CD1 genetic background. In general, for embryological studies, the CD1 background is also much better, due to higher female fertility, better maternal behavior, and bigger litter size compared to the C57BL/6 strain. Therefore, the CD1 strain is ideal for studies where a high number of embryos is needed. Nevertheless, the lethality of the CyFIP1 knockout mouse in CD1 background occurred between E6.5 and E8.5, with the malformed mutant embryos still visible at E8.5, before being reabsorbed. The larger time range of embryonic death could be due the genetic variability of the outbred strain compared to the inbred C57BL/6. From the genetic point of view the two C57 strains were thought to be quite similar, but in the case of the CyFIP1 deletion a small genetic difference strongly affected the phenotype. More recent comparison of C57BL/6J and C57BL/6N demonstrated a range of genetic differences that have the potential to impact upon penetrance and expressivity of mutational effects in these strains. Sequence variants were identified which provide a set of candidate genes for the phenotypic differences observed between the two

strains (Simon, Greenaway et al. 2013). So the genetic background confirms being an important factor to consider when generating knockout mouse models.

5.2 CyFIP1 as a tumor suppressor

Cancer occurs when a dysregulation of important cellular processes like proliferation, apoptosis, differentiation and adhesion take place. A tumor suppressor is a gene that can control these important cellular processes in the direction opposite to carcinogenic alterations. CyFIP1 might indeed function as a tumor suppressor gene, as proposed in a previous report (Silva et al., 2009). Silva et al. published in 2009 that Cyfip1 is a putative invasion suppressor in epithelial cancers. They showed that CyFIP1 is deleted in human epithelial cancers and observed a reduced expression of Cyfip1 during invasion of epithelial tumors (Silva, Ezhkova et al. 2009). Silencing of WAVE complex components reduced cell-cell adhesion and adhesion to the extracellular matrix (Silva, Ezhkova et al. 2009).

Upon deletion of both CyFIP1 alleles, in fact, ES cells gain proliferative capacity, lose adhesion to extracellular matrix and maintain an undifferentiated morphology for a longer time. In order to uncover the molecular pathways responsible for the phenotype, two approaches were employed in this work: 1. An unbiased high throughput analysis using microarrays; 2. A biochemical study of signaling pathways selected by their relevance in the processes altered in the CyFIP1-/- cells. Contrary to many expectations, classical pathways involved in cell proliferation and growth such as the MAPK and the PI3K pathways did not result significantly activated in the CyFIP1-/- cells at the protein level (although the PI3K pathway at the mRNA level appeared to be up-regulated). Instead, a specific signaling cascade within the TGFβ pathway was found significantly reduced. The TGFβ pathway is vast and widespread, with roles from embryo development to adult organisms, and is known to be involved in cancer (Grady 2005). In particular Smad1/5, which are involved in TGFβ signaling, showed a significant reduction of their phosphorylation in CyFIP1-/- ES cells. It has been shown that conditional deletion of Smad1 and Smad5 in somatic cells of male and female gonads leads to metastatic tumor development in mice (Pangas, Li et al. 2008). The question is how CyFIP1 is connected to the TGFβ pathway. Experiments with CyFIP1

-/- ES cells in a special medium (Esgro, Millipore) to grow these cells without feeders and serum free showed a reduction of the CyFIP1-/- phenotype (data not shown). In these conditions ES cells reverted to nearly normal proliferation rates and EBs differentiated properly. This medium contains BMP4 and a GSK3β inhibitor. GSK3 (Glycogen synthase kinase-3) is a target of Akt and is known to play important roles in numerous signaling pathways that regulate a variety of cellular processes including cell proliferation, differentiation, apoptosis and embryonic development (Xu, Kim et al. 2009). In the microarray analysis only a non-significant up-regulation of GSK3β could be detected, but protein and phosphorylation levels have not yet been analyzed. BMP4 is an extracellular signaling molecule of the TGFβ superfamily of ligands that binds to heterodimeric complexes of type I and type II cell surface receptors (BMPRI and BMPRII), which in turn leads to phosphorylation of Smad1/5/8 (Ueki and Reh 2012). As mentioned before, in CyFIP1-/- ES cell a significant decrease in phosphorylation of Smad1/5 was observed, but the Esgro medium was able to rescue it. Therefore CyFIP1 must have a direct or indirect influence on the phosphorylation of the Smads. The gene Nipa1 is often found together with CyFIP1 as an autism risk gene because in human they are both in the 15q11.2 region (Doornbos, Sikkema-Raddatz et al. 2009). This region has been implicated in autism spectrum disorders (ASDs) associated with 15q13.2microduplication (van der Zwaag et al., 2009) and 15q11-q13 deletion at break points 1 and 3 in Prader-Willi and Angelman syndromes (Moreira, Griesi-Oliveira et al. 2014). This region encodes four genes: CyFIP, TUBGCP5, Nipa1 and Nipa2 (Murthy, Nygren et al. 2007). TUBGCP5, the Tubulin Gamma Complex Associated Protein 5 is a member of the gamma-tubulin complex which is a large multiprotein complex that is required for microtubule nucleation at the centrosome (Murphy, Preble et al. 2001). Nipa family members are integral membrane proteins which function as magnesium transporters (Xie, Zhang et al. 2014). Nipa1, Nipa3 and Nipa4 transport Mg^{2+} as well as other cations. Nipa2 is a highly selective magnesium transporter located in the cytomembrane and the early endosome (Goytain, Hines et al. 2008). Its function is to transfer extracellular Mg^{2+} into the cytoplasm (Quamme 2010). Nipa1 is also known to be an inhibitor of BMP signaling by interacting with the type II BMP receptor (Tsang, Edwards et al. 2009), although it is not known how Nipa1 itself is regulated. It was shown in cell culture experiments on human embryonic stem cells, that high concentration of magnesium in the medium resulted increased proliferation and increased apoptosis of the cells (Nguyen, Garcia et al. 2012). Low or high magnesium

concentrations in the cytoplasm are diverse discussed in the cancer field. It is well established that intracellular magnesium concentrations affect functions directly linked to those identified as the hallmarks of cancer (Hanahan and Weinberg 2000; Hanahan and Weinberg 2011). One can hypothesize that Nipa1 and/or Nipa2 are negatively regulated by CyFIP1. This hypothesis needs to be confirmed with further experiments. Finally, many transcription factors found up-regulated in CyFIP1-/- ES cells by the unbiased microarray screening presented in this thesis are connected to cancer. HMGA1 was found to be overexpressed in pancreatic adenocarcinomas (Liau, Jazag et al. 2007) and overexpression of HMGB2 was shown to be associated with tumor aggressiveness and prognosis of hepatocellular carcinoma (Kwon, Kim et al. 2010). Atf4 is overexpressed in human solid tumors, suggesting that it has an important function in tumor progression (Ye, Kumanova et al. 2010). TGIF1 splicing variant 8 was found overexpressed oral squamous cell carcinoma and is related to pathological and clinical behavior (Liborio, Ferreira et al. 2013). CtBP2 was shown to be overexpressed in colon, breast, and prostate cancer (Thomas, Jacobs et al. 2008), and increased levels have been linked to the loss of tumor suppressors such as APC, Hipk2, and ARF (alternative reading frame) (Ng, Thakker et al. 2004). An hypothesis that could explain the up-regulation of this panel of transcription factors involved in cell proliferation and adhesion, and consequently in cancer progression and invasiveness, could be that the suppression of the TGFβ pathway reduces the competition with the MAPK and PI3K pathways, which can take over, although the increase in transcription factor level should be verified at the protein level, as well as their translocation to the nuclear compartment.

5.3 Functions of CyFIP1 in embryonic development and cellular processes

Homozygous deletion of CyFIP1 resulted in an early embryonic lethal phenotype between E6.5 and E8.5. Most homozygous embryos appeared to die of severe defects in gastrulation and were quickly reabsorbed. Indeed, differentiation studies of ES cells into embryoid bodies showed substantial expansion of the endoderm, partially also at the expense of mesodermal differentiation. The formation of the primitive streak, of

meso-endodermal nature, is the important starting point of gastrulation in embryonic development.

These considerations also explain previous observations on CyFIP1-/- embryonic developmental alterations in the C57Bl/6J background (Massimi 2008). Massimi reported that CyFIP1 ko embryos have defects in somite formation, neural tube closure and anterior-posterior axis formation. These structures are of mesodermal origin or are induced by mesoderm formation. For example, the formation of the neural plate begins when the dorsal mesoderm signals to the ectodermal cells above it to elongate into columnar neural plate cells (Keller, Shih et al. 1992). Members of the TGFβ family of secreted growth factors regulate key processes during postimplantation mammalian development including embryonic axis patterning, organogenesis and specification of the germ line.

CyFIP1 controls important cell functions like proliferation, adhesion, differentiation and apoptosis. In CyFIP1-/- ES cells hyper-proliferation was observed and adhesion is impaired. CyFIP1-/- EBs show increased apoptosis rate and disturbed differentiation into mesoderm. CyFIP1-/- ES cells which were differentiated for three days on gelatine showed a more stem cell-like morphology and also the analysis of the molecular markers in these cells showed a defect of differentiation into hematopoietic cells, which are of mesodermal origin.

Transcription factors regulating proliferation and differentiation were found affected using a microarray approach. The transcription factor RNF4 is up-regulated in CyFIP-/- ES cells. It was shown that disruption of the RNF4 gene in chicken DT40 cells resulted in a gradual loss of proliferation capability (Hirota, Tsuda et al. 2014). The experiments performed on ES cells in this work showed a higher proliferation rate in the absence of CyFIP1. In CyFIP1-/- ES cells the transcription factor HMGB2 is significantly up-regulated. HMGB2, the high mobility group box 2, is a member of the non-histone chromosomal high-mobility group protein family. Interestingly, the transcription factor is known to regulate Oct4, a stem cell marker that is important in embryonic development. The knockout of HMGB2 in the sub-granular zone showed a down-regulation of Oct4 expression (Abraham, Bronstein et al. 2013). It has been shown that reduced expression of Oct4 in hESCs promoted up-regulation of markers indicative of mesoderm and endoderm differentiation, while elevated levels of Oct4 in hESCs promoted up-regulation of markers indicative of endoderm derivatives (Rodriguez, Velkey et al. 2007). This could be one biological mechanism behind what

was is seen in the CyFIP1-/- EBs, where a massive expansion of the endoderm takes place, but mesoderm formation is decreased. Indeed, Oct4 is up-regulated at the mRNA level in CyFIP1-/- ES cells (data not shown). Another transcription factor, which is also important in embryonic development and was found to be up-regulated in CyFIP1-/- ES cells, is TGIF1. TGIF1 function is required for gastrulation, and limits the transcriptional response to Nodal signaling during early embryogenesis (Powers, Taniguchi et al. 2010). The nodal family of proteins belongs to the TGFβ superfamily and is responsible for meso-endoderm induction, patterning of the nervous system, and determination of dorsal- ventral axis in vertebrate embryos (Schier 2003). A third developmental transcription factor that was found up-regulated is RBBP7, which is also named retinoblastoma (Rb) suppressor-associated protein 46 (RbAp46). This factor plays an important role in negatively regulating β-catenin expression and the β-catenin/TCF3 signaling pathway, presumably through regulation of GSK3 expression (Li and Wang 2006). RBBP7 is up-regulated in CyFIP1-/- ES cells and also in the EBs and may have an influence on the β–catenin pathway, which is decreased in CyFIP1-/- EBs, although GSK3 protein levels in the mutant cells have not been verified yet. Atf4 a transcription factor that was also shown to regulate proliferation, blocking it when inhibited (Ye, Kumanova et al. 2010), was found significantly up-regulated in CyFIP1-/- ES cells. The only significantly down-regulated transcription factor found in CyFIP1-/- ES cells is RNF2, the Ring Finger Protein 2. This is an essential component of a Polycomb group (PcG) multi-protein PRC1-like complex, a complex class required to maintain the transcriptionally repressive state of many genes, including Hox genes, throughout development. The down-regulation of RNF2 could be the reason why Hox genes like TGIF1 and possibly also other transcription factors were up-regulated in the mutant ES cells. RNF2-deficient mice show a similar phenotype to the CyFIP1-/- mice (Voncken, Roelen et al. 2003). They are early embryonic lethal, don´t undergo normal gastrulation and have problems with mesoderm formation (Voncken, Roelen et al. 2003).

It seems that several unrelated genes belonging to different signaling pathways are affected by CyFIP1 depletion. There could be several explanation for this counter-intuitive findings. One explanation could be that the effect of CyFIP1 depletion on the TGFβ pathway (discussed in 5.2) resulting in its down-regulation might imbalance the equilibrium between different and competitive pathways such as the PI3K and the MAPK pathways producing the described defects of the CyFIP1-/- ES cells. A second

possibility could be that in consequence of CyFIP1 depletion, one or more of the other WAVE complex subunits would be freed from the complex and therefore available to activate or inhibit other pathways. For example Abi1 is known to be in a tricomplex together with Eps8 and SOS1 (Innocenti, Tenca et al. 2002). Abi1 binds through its SH3 domain to the same binding site on SOS1 as Grb2, so that SOS1 can either form the tricomplex with Eps8 and Abi1 or form a functionally different Gbr2-SOS1 complex (Innocenti, Tenca et al. 2002). If Abi1 is freed from the WAVE complex due to the absence of CyFIP1 the complex with Gbr2 and SOS1 could not be formed in the correct amount because extra SOS1 would be sequestered in the tricomplex by the excess of available Abi1. All these hypotheses would have to be experimentally proved.

Finally, CyFIP2 was found increased 1.5 fold in CyFIP1-/- cells by microarray analysis. CyFIP2 is a direct target of p53 (Jackson, Cho et al. 2007). It was shown that CyFIP2 expression is sufficient to induce apoptotic cell death. The increase of CyFIP2 expression could therefore explain the apoptosis phenotype of CyFIP1-/- ES cells and embryoid bodies.

In conclusion CyFIP1 plays an important role in lineage determination by affecting developmental pathways that depend on TGFβ signaling, which explains the early failure of embryonic development. In this view CyFIP1 appears to regulate important cellular processes such as proliferation, adhesion, differentiation and apoptosis.

5.4 CyFIP and the WAVE complex

The classical WAVE complex consists of the five subunits CyFIP, Nap, WAVE, Abi, and HSPC300. Except for HSPC300, which has no known paralogues, each of the other subunits in mammals is a member of a protein family consisting of two or three paralogue genes, some of them also alternatively spliced. Considering all the different isoforms of each subunits, about 56 different WAVE complexes could be theoretically formed. Moreover, the new findings presented in this work suggest that the classical pentameric WAVE complex is only one possible complex. In fact in vivo a regulated exchange of subunits can occur. Under certain ionic conditions and in response to specific signaling the WAVE complex can break down. CyFIP and Nap appear to form a core complex around which the other subunits can assemble or not. When using a

physiological buffer rich in Mg^{2+}, an intact pentameric WAVE complex binds to Profilin2. However, when divalent cations are completely sequestrated the WAVE complex falls apart uncoupling Abi1 and WAVE1 from the CyFIP/Nap1 core, suggesting that Mg^{2+} is an essential co-factor for integrity of the pentameric WAVE complex. In more physiological conditions, when phosphorylation is preserved, the binding of Cyfip1/2 and Nap1 to Profilin2 is significantly increased by about 5-fold, while binding of WAVE1 is reduced and retention of Abi1 is virtually abolished. This suggests that phosphorylation triggers CyFIP/Nap1 binding to Profilin2, and secondly that phosphorylation uncouples the other subunits from the CyFIP/Nap1 complex.

Several conclusions can be drawn from the experiments presented in this work: first, different signals (phosphorylation, divalent ions) can control the stoichiometry of the WAVE complex in different ways. Secondly, phosphorylation appears to be a major regulatory mechanism of WAVE complex formation and subunit exchange. Finally, the results also prove that binding of the WAVE complex to Profilin2 occurs through the CyFIP/Nap1 core complex, directly or indirectly through another yet unidentified ligand. This explains how the WAVE complex in its full conformation can recruit Profilin2, when it is known that neither Abi nor WAVE when incorporated in the WAVE complex are able to bind to Profilin2, their PLP stretches being buried in the structure (Davidson and Insall 2013) (Insall, personal communication).

These data are a fundamental finding in view of the other roles that the WAVE complex subunits might have in the cell and shed light on the possible interpretations of the CyFIP1 knockout phenotype. For example, phosphorylated Abi1 can activate PI3-kinase by stabilizing the PI3-kinase regulatory p85 subunit and thereby trigger downstream signaling events via the PI3K/Akt pathway (Dubielecka, Machida et al. 2010). However, a role of Abi1 phosphorylation for its incorporation in the WAVE complex has not been formally shown. In this view, it is possible that the stable CyFIP/Nap1 core complex can function to sequester the other subunits, thereby regulating the corresponding signaling pathways. The Chen et al. model of the WAVE complex structure suggests that activation of WAVE1 is basically mediated by a desequestration of the VCA-domain from CyFIP1 (Chen, Borek et al. 2010). The phenotype originated by the deletion of CyFIP1 and commented in the previous sections can therefore be also explained in this view. The reduction or complete depletion of the WAVE complex has freed the other subunits to activate without control other pathways, which have to be analyzed more in detail in the future. A similar

sequestration effect of the WAVE complex towards the Arp2/3 complex was described in a recent report where depletion of the WAVE complex in cells hyperactivated N-WASP-Arp2/3-driven 3D migration (Tan, Li et al. 2013).

In certain tissues the CyFIP/Nap1 complex might be differently regulated. As mentioned above, Profilin2 binds the classical WAVE complex with high efficiency from brain through the CyFIP/Nap1 core subunits. On the contrary, in kidney CyFIP and Nap1 are expressed, but no CyFIP/Nap1 complex could bind to Profilin2-beads. This leads to hypothesize the existence of a different modification of the WAVE complex in kidney or the presence of tissue-specific intermediary ligands.

The diverse phenotypes of the knockout mouse models for the WAVE complex subunits also argue against a single common genetic pathway. Nap1 mutant embryos show a severe defect at E8.5 in axis polarity (Rakeman 2006), CyFIP1 mutants show early defects around E6.5 in mesodermal lineage formation, Abi1 mutants die around E11.5 because of vascularization defects (Ring, Ginsberg et al. 2011), while Abi2 mutants are viable and show neuronal deficits (Grove, Demyanenko et al. 2004). WAVE1 mutants are viable (Soderling, Langeberg et al. 2003), but WAVE2 mutants die around E10.5 from angiogenesis defects (Yamazaki, Suetsugu et al. 2003). CyFIP2 null mutants die at birth (Hauck, unpublished). Information on HSPC300/Brk1, WAVE3 and Abi3 knockout mice are not available yet. This shows that in vivo the WAVE complex can serve quite distinct cellular pathways, although it is possible that the different subunits can compensate each other only in certain functions and cell types, but not others due to expression, splicing, or modification differences. Judging from the similar phenotypes, the mouse CyFIP1 and Nap1 genes and Abi1 and WAVE2 genes seem to function in closely connected pathways and tissues. The genetic data from knockout studies suggest that in vivo a functional link between Cyfip1 and Nap1 as well as Abi1 and WAVE2 exists, with the other subunits such as WAVE1 and 3, Abi2 and 3, and HSPC300/Brk1 having specific functions and possibly being exchangeable complex ligands.

In summary the WAVE complex composition and complexity differs in tissues and cells. The WAVE complex that is bound to Profilin2 changes in response to different signaling pathways. The WAVE complex is not a stable pentameric complex, it undergoes dynamic turnover.

5.5 Infertility disorder of CyFIP1+/- females

In this thesis work the novel infertility phenotype (POI) of CyFIP1 heterozygous females and a first evaluation of the morphological and biochemical features associated with the ovaries of CyFIP1+/- mice is described. The lower amount of CyFIP1 in the ovary leads to a down-regulation of the components of the WAVE complex, a higher number of atretic follicles and corpora lutea, and smaller antral and pre-ovulatory follicles. These findings provide a first insight into the early infertility phenotype of the CyFIP1 heterozygous females. Two potential mechanisms may be involved in the development of POI: (1) abnormalities in primordial follicle activation and (2) increased rates of apoptosis of oocytes (Sullivan and Castrillon 2011). The premutation of FMR1 is well known in the context of infertility disorders. A mouse model carrying the human FMR1 premutation allele showed that FMR1 premutation causes primary ovarian failure (Lu, Lin et al. 2012). FMR1 premutation RNA can cause a reduction in the number of growing follicles in ovaries and is sufficient to impair female fertility (Lu, Lin et al. 2012). In the CyFIP1-/- knockout a solid molecular phenotype seems to be a decreased signaling of the TGFβ pathway. Smad1/5 phosphorylation was significantly down-regulated in CyFIP1-/- ES cells. Interestingly, it has been shown that Smad1/5 play a key role also in female fertility. Double Smad1;Smad5 knockout females become infertile and develop metastatic granulosa cell tumors (Pangas, Li et al. 2008). The Anti-Mullerian Hormone (AMH) is also a member of the transforming growth factor-β (TGF-β) family and activates BMP-specific R-Smads (Smad 1, 5 and 8) (di Clemente, Josso et al. 2003). In patients with primary ovarian failure, the Anti-Mullerian Hormone is absent or reduced (Visser, Schipper et al. 2012). The AMH levels in CyFIP1+/- females have to be tested in future. In addition, the microarray results from CyFIP1-/- differentiated ES cells for 3 days on gelatine showed a significant up-regulation of the transcription factor RHOX9, which is a member of the Reproductive Homeobox gene family and important in the reproductive system. RHOX9, together with RHOX5, was found to be expressed in follicular cells, is constitutively expressed in ovarian cells (Lee, Lee et al. 2013) and mRNA levels of RHOX9 were fairly consistently expressed during follicular development. RHOX9 knockout mice have no observable phenotype and ovulate normally (Takasaki, Rankin et al. 2001). So deletion of RHOX9 seems to be compensated by other RHOX genes (Takasaki, Rankin et al. 2001). But overexpression may influence follicle development. RHOX9, also named

Gpbox (RHOXF1 in human), was discussed in a paper as a new candidate gene for premature ovarian failure (Suzumori, Pangas et al. 2007).

From the biochemical point of view, POF1B was found by mass spectrometry as a new candidate ligand of the WAVE complex. Disrupted binding of POF1B (Premature Ovarian Failure Protein 1B) to non-muscle actin filaments is associated with premature ovarian failure (Lacombe, Lee et al. 2006). In human POF1B is located on the X chromosome, like FMR1, and these two genes have been formally demonstrated to be responsible for premature ovarian failure (Bione and Toniolo 2000). One additional possibility could be that the WAVE complex is regulating female fertility via its interaction with POF1B, which might also be part of the complex. Further experiments are needed to prove this hypothesis, as well as the TGFβ pathway down-regulation.

In summary the heterozygous deletion of CyFIP1 shows similar effects on ovary function as the premutation of FMR1 and CyFIP1-mediated regulation of or CyFIP1 interaction with genes important for follicle development and female fertility, such as RHOX9 and POF1B, could be relevant for the infertility phenotype of the CyFIP1+/- mouse.

5.6 Conclusions and outlook

The work presented in this thesis provides solid grounds to unravel the function of CyFIP1 and the WAVE complex in cells and during embryonic development. A novel and unexpected role of CyFIP1 in lineage determination via the TGFβ pathway was found, which explains the early failure of embryonic development. CyFIP1 is required during embryogenesis for mesodermal differentiation and has additional activities in controlling proliferation and adhesion. CyFIP1 also controls apoptosis and overall behaves as a tumor suppressor gene.

In addition, in the female reproductive system of the mouse CyFIP1 plays a fundamental role and decreased CyFIP1 causes an infertility phenotype similar to a POF syndrome.

Although CyFIP1 role as an actin nucleation promoting factor has been previously demonstrated, the knockout approach has shown that by itself or through the WAVE

complex it is indirectly regulating important signaling pathways, such as the TGFβ pathway.

Finally, at the biochemical level the WAVE complex is not a stable pentameric complex, CyFIP/Nap1 build a core complex around which the other subunits assemble. Different signals (phosphorylation, divalent ions) can control the stoichiometry of the WAVE complex in different ways. Other proteins seem to interact with the WAVE complex, either due to its function in specific cellular processes (translational regulation, cargo/mRNA transport, signaling) or to allow its role in actin polymerization (for example in brain interacts with Profilin2 but not in kidney, where some other mechanism might be used)

To address the open questions about CyFIP1 function further experiments will be needed. A reporter mouse line like a CyFIP1-LacZ insertion would be a helpful tool to characterize the distribution of CyFIP1 in the mouse tissues and to distinguish the different expression pattern of CyFIP1 and CyFIP2. A conditional CyFIP1 mouse model would be a great tool to analyze the function of CyFIP1 more specifically. The knockout of CyFIP1 in the brain would be very useful to distinguish the functions of CyFIP1 and CyFIP2 in the brain and to answer the question if they have overlapping functions or they act in completely different neuronal cell types or compartments. Electrophysiological analysis would address the question of synaptic and network physiology of neurons lacking CyFIP1. Specific knockout of CyFIP1 in neuronal subtypes would help to study the involvement of CyFIP1 in autism spectrum disorder.

A further step would be the CyFIP1 and CyFIP2 double knockout mouse model for in vitro and/or in vivo studies. An interesting question is what would happen to the WAVE complex when there is no CyFIP at all: can the complex exist without CyFIP? What happens to the other components of the WAVE complex when they are freed from the WAVE complex due to CyFIP1 depletion? An interesting question is if in brain and kidney and perhaps other tissues have distinct from the classical WAVE complex other ligands and how would these complexes relate to actin nucleation.

In conclusion in this work for the first time a molecular pathway was found, the TGFβ pathway, which consistently explains all the different phenotypes of CyFIP1 depletion (infertility of heterozygote females, embryonic development defects, cellular alterations such as proliferation, adhesion and apoptosis), although it is still missing the mechanism how CyFIP1 is affecting this signaling pathway. This will be the object of future studies.

6. References

Abraham, A. B., R. Bronstein, et al. (2013). "Aberrant neural stem cell proliferation and increased adult neurogenesis in mice lacking chromatin protein HMGB2." PloS one **8**(12): e84838.
Aldrich, R. A., A. G. Steinberg, et al. (1954). "Pedigree demonstrating a sex-linked recessive condition characterized by draining ears, eczematoid dermatitis and bloody diarrhea." Pediatrics **13**(2): 133-139.
Bagutti, C., A. M. Wobus, et al. (1996). "Differentiation of embryonal stem cells into keratinocytes: comparison of wild-type and beta 1 integrin-deficient cells." Dev Biol **179**(1): 184-196.
Bain, G., W. J. Ray, et al. (1996). "Retinoic acid promotes neural and represses mesodermal gene expression in mouse embryonic stem cells in culture." Biochemical and biophysical research communications **223**(3): 691-694.
Bear, J. E., J. F. Rawls, et al. (1998). "SCAR, a WASP-related protein, isolated as a suppressor of receptor defects in late Dictyostelium development." J Cell Biol **142**(5): 1325-1335.
Beddington, S. P. (1981). "An autoradiographic analysis of the potency of embryonic ectoderm in the 8th day postimplantation mouse embryo." J Embryol Exp Morphol **64**: 87-104.
Ben-Shachar, S., B. Lanpher, et al. (2009). "Microdeletion 15q13.3: a locus with incomplete penetrance for autism, mental retardation, and psychiatric disorders." Journal of medical genetics **46**(6): 382-388.
Bione, S. and D. Toniolo (2000). "X chromosome genes and premature ovarian failure." Seminars in reproductive medicine **18**(1): 51-57.
Blagg, S. L., M. Stewart, et al. (2003). "PIR121 regulates pseudopod dynamics and SCAR activity in Dictyostelium." Curr Biol **13**(17): 1480-1487.
Bogdan, S., O. Grewe, et al. (2004). "Sra-1 interacts with Kette and Wasp and is required for neuronal and bristle development in Drosophila." Development **131**(16): 3981-3989.
Bozdagi, O., T. Sakurai, et al. (2012). "Haploinsufficiency of Cyfip1 produces fragile X-like phenotypes in mice." PloS one **7**(8): e42422.
Braude, P., S. Pickering, et al. (2002). "Preimplantation genetic diagnosis." Nat Rev Genet **3**(12): 941-953.
Braun, A., A. Aszodi, et al. (2002). "Genomic organization of profilin-III and evidence for a transcript expressed exclusively in testis." Gene **283**(1-2): 219-225.
Bruce, S. J., B. B. Gardiner, et al. (2007). "Dynamic transcription programs during ES cell differentiation towards mesoderm in serum versus serum-freeBMP4 culture." BMC genomics **8**: 365.
Carlsson, L., L. E. Nystrom, et al. (1977). "Actin polymerizability is influenced by profilin, a low molecular weight protein in non-muscle cells." J Mol Biol **115**(3): 465-483.
Carpenedo, R. L., C. Y. Sargent, et al. (2007). "Rotary suspension culture enhances the efficiency, yield, and homogeneity of embryoid body differentiation." Stem cells **25**(9): 2224-2234.
Chen, Z., D. Borek, et al. (2010). "Structure and control of the actin regulatory WAVE complex." Nature **468**(7323): 533-538.
Chesarone, M. A. and B. L. Goode (2009). "Actin nucleation and elongation factors: mechanisms and interplay." Current Opinion in Cell Biology **21**(1): 28-37.
Clifford, S., C. Dissanayake, et al. (2007). "Autism spectrum phenotype in males and females with fragile X full mutation and premutation." Journal of autism and developmental disorders **37**(4): 738-747.
Comiskey, M., C. Y. Goldstein, et al. (2003). "Evidence that HLA-G is the functional homolog of mouse Qa-2, the Ped gene product." Hum Immunol **64**(11): 999-1004.
Cooper, M. D., H. P. Chae, et al. (1968). "Wiskott-Aldrich syndrome. An immunologic deficiency disease involving the afferent limb of immunity." Am J Med **44**(4): 499-513.
Coucouvanis, E. and G. R. Martin (1995). "Signals for death and survival: a two-step mechanism for cavitation in the vertebrate embryo." Cell **83**(2): 279-287.
Coucouvanis, E. and G. R. Martin (1999). "BMP signaling plays a role in visceral endoderm differentiation and cavitation in the early mouse embryo." Development **126**(3): 535-546.
Dahl, J. P., J. Wang-Dunlop, et al. (2003). "Characterization of the WAVE1 knock-out mouse: implications for CNS development." J Neurosci **23**(8): 3343-3352.
Dang, S. M., M. Kyba, et al. (2002). "Efficiency of embryoid body formation and hematopoietic development from embryonic stem cells in different culture systems." Biotechnology and bioengineering **78**(4): 442-453.
Dani, C., A. G. Smith, et al. (1997). "Differentiation of embryonic stem cells into adipocytes in vitro." J Cell Sci **110 (Pt 11)**: 1279-1285.
Davidson, A. J. and R. H. Insall (2013). "SCAR/WAVE: A complex issue." Communicative & integrative biology **6**(6): e27033.

Davidson, K. C., A. M. Adams, et al. (2012). "Wnt/beta-catenin signaling promotes differentiation, not self-renewal, of human embryonic stem cells and is repressed by Oct4." Proceedings of the National Academy of Sciences of the United States of America **109**(12): 4485-4490.
di Clemente, N., N. Josso, et al. (2003). "Components of the anti-Mullerian hormone signaling pathway in gonads." Molecular and Cellular Endocrinology **211**(1-2): 9-14.
Di Nardo, A., R. Gareus, et al. (2000). "Alternative splicing of the mouse profilin II gene generates functionally different profilin isoforms." J Cell Sci **113 Pt 21**: 3795-3803.
Doetschman, T. C., H. Eistetter, et al. (1985). "The in vitro development of blastocyst-derived embryonic stem cell lines: formation of visceral yolk sac, blood islands and myocardium." Journal of embryology and experimental morphology **87**: 27-45.
Doornbos, M., B. Sikkema-Raddatz, et al. (2009). "Nine patients with a microdeletion 15q11.2 between breakpoints 1 and 2 of the Prader-Willi critical region, possibly associated with behavioural disturbances." European journal of medical genetics **52**(2-3): 108-115.
dos Remedios, C. G., D. Chhabra, et al. (2003). "Actin binding proteins: regulation of cytoskeletal microfilaments." Physiol Rev **83**(2): 433-473.
Drukker, M., C. Tang, et al. (2012). "Isolation of primitive endoderm, mesoderm, vascular endothelial and trophoblast progenitors from human pluripotent stem cells." Nature biotechnology **30**(6): 531-542.
Dubielecka, P. M., K. I. Ladwein, et al. (2011). "Essential role for Abi1 in embryonic survival and WAVE2 complex integrity." Proceedings of the National Academy of Sciences of the United States of America **108**(17): 7022-7027.
Dubielecka, P. M., K. Machida, et al. (2010). "Abi1/Hssh3bp1 pY213 links Abl kinase signaling to p85 regulatory subunit of PI-3 kinase in regulation of macropinocytosis in LNCaP cells." FEBS letters **584**(15): 3279-3286.
Duncan, M., L. Cummings, et al. (1993). "Germ cell deficient (gcd) mouse as a model of premature ovarian failure." Biol Reprod **49**(2): 221-227.
Eden, S., R. Rohatgi, et al. (2002). "Mechanism of regulation of WAVE1-induced actin nucleation by Rac1 and Nck." Nature **418**(6899): 790-793.
Eistetter, H. R. (1989). Pluripotent Embryonal Stem Cell Lines can be established from disaggregated Mouse Morulae. Development Growth & Differentiation**:** 275-282.
Ennis, S., D. Ward, et al. (2006). "Nonlinear association between CGG repeat number and age of menopause in FMR1 premutation carriers." Eur J Hum Genet **14**(2): 253-255.
Eppig, J. J. (2001). "Oocyte control of ovarian follicular development and function in mammals." Reproduction **122**(6): 829-838.
Erlacher (2009). "Genetic analysis of the FLRT family of proteins during early mouse embryonic development.".
Evans, M. J. and M. H. Kaufman (1981). "Establishment in culture of pluripotential cells from mouse embryos." Nature **292**(5819): 154-156.
Faix, J. and R. Grosse (2006). "Staying in shape with formins." Dev Cell **10**(6): 693-706.
Fan, P. D. and S. P. Goff (2000). "Abl interactor 1 binds to sos and inhibits epidermal growth factor- and v-Abl-induced activation of extracellular signal-regulated kinases." Molecular and Cellular Biology **20**(20): 7591-7601.
Faure, S., M. A. Lee, et al. (2000). "Endogenous patterns of TGFbeta superfamily signaling during early Xenopus development." Development **127**(13): 2917-2931.
Fraichard, A., O. Chassande, et al. (1995). "In vitro differentiation of embryonic stem cells into glial cells and functional neurons." J Cell Sci **108 (Pt 10)**: 3181-3188.
Gautreau, A. (2004). "Purification and architecture of the ubiquitous Wave complex." Proceedings of the National Academy of Sciences **101**(13): 4379-4383.
Gerecht-Nir, S., S. Cohen, et al. (2004). "Bioreactor cultivation enhances the efficiency of human embryoid body (hEB) formation and differentiation." Biotechnology and bioengineering **86**(5): 493-502.
Ginis, I., Y. Luo, et al. (2004). "Differences between human and mouse embryonic stem cells." Developmental biology **269**(2): 360-380.
Gleicher, N. and D. H. Barad (2010). "The FMR1 gene as regulator of ovarian recruitment and ovarian reserve." Obstet Gynecol Surv **65**(8): 523-530.
Goley, E. D. and M. D. Welch (2006). "The ARP2/3 complex: an actin nucleator comes of age." Nature Reviews Molecular Cell Biology **7**(10): 713-726.
Gordon, K. J. and G. C. Blobe (2008). "Role of transforming growth factor-beta superfamily signaling pathways in human disease." Biochimica et biophysica acta **1782**(4): 197-228.

Goytain, A., R. M. Hines, et al. (2008). "Functional characterization of NIPA2, a selective Mg2+ transporter." American journal of physiology. Cell physiology **295**(4): C944-953.
Grabel, L. B. and J. E. Casanova (1986). "The outgrowth of parietal endoderm from mouse teratocarcinoma stem-cell embryoid bodies." Differentiation; research in biological diversity **32**(1): 67-73.
Grady, W. M. (2005). "Transforming growth factor-beta, Smads, and cancer." Clinical cancer research : an official journal of the American Association for Cancer Research **11**(9): 3151-3154.
Green, M. C., H. Grueneberg, et al. (1963). "A Revision of the Standardized Genetic Nomenclature for Mice." The Journal of heredity **54**: 159-162.
Grove, M., G. Demyanenko, et al. (2004). "ABI2-deficient mice exhibit defective cell migration, aberrant dendritic spine morphogenesis, and deficits in learning and memory." Mol Cell Biol **24**(24): 10905-10922.
Guan, K., J. Rohwedel, et al. (1999). "Embryonic stem cell differentiation models: cardiogenesis, myogenesis, neurogenesis, epithelial and vascular smooth muscle cell differentiation in vitro." Cytotechnology **30**(1-3): 211-226.
Gustafsson, C. M. and T. Samuelsson (2001). "Mediator--a universal complex in transcriptional regulation." Molecular microbiology **41**(1): 1-8.
Hanahan, D. and R. A. Weinberg (2000). "The hallmarks of cancer." Cell **100**(1): 57-70.
Hanahan, D. and R. A. Weinberg (2011). "Hallmarks of cancer: the next generation." Cell **144**(5): 646-674.
Hegert, C., J. Kramer, et al. (2002). "Differentiation plasticity of chondrocytes derived from mouse embryonic stem cells." J Cell Sci **115**(Pt 23): 4617-4628.
Heldin, C. H., K. Miyazono, et al. (1997). "TGF-beta signalling from cell membrane to nucleus through SMAD proteins." Nature **390**(6659): 465-471.
Hetzer, M. and I. W. Mattaj (2000). "An ATP-dependent, Ran-independent mechanism for nuclear import of the U1A and U2B" spliceosome proteins." The Journal of cell biology **148**(2): 293-303.
Hirao, N., S. Sato, et al. (2006). "NESH (Abi-3) is present in the Abi/WAVE complex but does not promote c-Abl-mediated phosphorylation." FEBS letters **580**(27): 6464-6470.
Hirota, K., M. Tsuda, et al. (2014). "SUMO-targeted ubiquitin ligase RNF4 plays a critical role in preventing chromosome loss." Genes to cells : devoted to molecular & cellular mechanisms **19**(10): 743-754.
Holmes, C. and W. L. Stanford (2007). "Concise review: stem cell antigen-1: expression, function, and enigma." Stem cells **25**(6): 1339-1347.
Honore, B., P. Madsen, et al. (1993). "Cloning and expression of a novel human profilin variant, profilin II." FEBS Lett **330**(2): 151-155.
Hubner, K., G. Fuhrmann, et al. (2003). "Derivation of oocytes from mouse embryonic stem cells." Science **300**(5623): 1251-1256.
Illumina.
Innocenti, M., P. Tenca, et al. (2002). "Mechanisms through which Sos-1 coordinates the activation of Ras and Rac." The Journal of cell biology **156**(1): 125-136.
Itskovitz-Eldor, J., M. Schuldiner, et al. (2000). "Differentiation of human embryonic stem cells into embryoid bodies compromising the three embryonic germ layers." Molecular medicine **6**(2): 88-95.
Jackson, R. S., 2nd, Y. J. Cho, et al. (2007). "CYFIP2, a direct p53 target, is leptomycin-B sensitive." Cell cycle **6**(1): 95-103.
Kang, S. M., M. S. Cho, et al. (2007). "Efficient induction of oligodendrocytes from human embryonic stem cells." Stem cells **25**(2): 419-424.
Kaufman, M. H. (1992). The Atlas of Mouse Development. London, Academic Press.
Kehler, J., K. Hubner, et al. (2005). "Generating oocytes and sperm from embryonic stem cells." Semin Reprod Med **23**(3): 222-233.
Keller, G. M. (1995). "In vitro differentiation of embryonic stem cells." Current opinion in cell biology **7**(6): 862-869.
Keller, R., J. Shih, et al. (1992). "Planar induction of convergence and extension of the neural plate by the organizer of Xenopus." Developmental dynamics : an official publication of the American Association of Anatomists **193**(3): 218-234.
Kerkhoff, E. (2006). "Cellular functions of the Spir actin-nucleation factors." Trends Cell Biol **16**(9): 477-483.

Kim, H. J., A. B. DiBernardo, et al. (2006). "WAVE1 is required for oligodendrocyte morphogenesis and normal CNS myelination." The Journal of neuroscience : the official journal of the Society for Neuroscience **26**(21): 5849-5859.
Kobayashi, K., S. Kuroda, et al. (1998). "p140Sra-1 (specifically Rac1-associated protein) is a novel specific target for Rac1 small GTPase." J Biol Chem **273**(1): 291-295.
Kramer, J., C. Hegert, et al. (2000). "Embryonic stem cell-derived chondrogenic differentiation in vitro: activation by BMP-2 and BMP-4." Mech Dev **92**(2): 193-205.
Kron, S. J., D. G. Drubin, et al. (1992). "Yeast actin filaments display ATP-dependent sliding movement over surfaces coated with rabbit muscle myosin." Proc Natl Acad Sci U S A **89**(10): 4466-4470.
Kuhn, J. R. and T. D. Pollard (2005). "Real-time measurements of actin filament polymerization by total internal reflection fluorescence microscopy." Biophys J **88**(2): 1387-1402.
Kurosawa, H. (2007). "Methods for inducing embryoid body formation: in vitro differentiation system of embryonic stem cells." Journal of bioscience and bioengineering **103**(5): 389-398.
Kwiatkowski, D. J. and G. A. Bruns (1988). "Human profilin. Molecular cloning, sequence comparison, and chromosomal analysis." J Biol Chem **263**(12): 5910-5915.
Kwon, J. H., J. Kim, et al. (2010). "Overexpression of high-mobility group box 2 is associated with tumor aggressiveness and prognosis of hepatocellular carcinoma." Clinical cancer research : an official journal of the American Association for Cancer Research **16**(22): 5511-5521.
Lacombe, A., H. Lee, et al. (2006). "Disruption of POF1B binding to nonmuscle actin filaments is associated with premature ovarian failure." American journal of human genetics **79**(1): 113-119.
Laemmli, U. K. (1970). "Cleavage of structural proteins during the assembly of the head of bacteriophage T4." Nature **227**(5259): 680-685.
Lebensohn, A. M. and M. W. Kirschner (2009). "Activation of the WAVE complex by coincident signals controls actin assembly." Molecular cell **36**(3): 512-524.
Lee, S. E., S. Y. Lee, et al. (2013). "Rhox in mammalian reproduction and development." Clinical and experimental reproductive medicine **40**(3): 107-114.
Li, G. C. and Z. Y. Wang (2006). "Retinoblastoma suppressor associated protein 46 (RbAp46) attenuates the beta-catenin/TCF signaling through up-regulation of GSK-3beta expression." Anticancer research **26**(6B): 4511-4518.
Liau, S. S., A. Jazag, et al. (2007). "Overexpression of HMGA1 promotes anoikis resistance and constitutive Akt activation in pancreatic adenocarcinoma cells." British journal of cancer **96**(6): 993-1000.
Liborio, T. N., E. N. Ferreira, et al. (2013). "TGIF1 splicing variant 8 is overexpressed in oral squamous cell carcinoma and is related to pathologic and clinical behavior." Oral surgery, oral medicine, oral pathology and oral radiology **116**(5): 614-625.
Ling, V. and S. Neben (1997). "In vitro differentiation of embryonic stem cells: immunophenotypic analysis of cultured embryoid bodies." Journal of cellular physiology **171**(1): 104-115.
Lu, C., L. Lin, et al. (2012). "Fragile X premutation RNA is sufficient to cause primary ovarian insufficiency in mice." Human molecular genetics **21**(23): 5039-5047.
Machesky, L. M., S. J. Atkinson, et al. (1994). "Purification of a cortical complex containing two unconventional actins from Acanthamoeba by affinity chromatography on profilin-agarose." J Cell Biol **127**(1): 107-115.
Macpherson, J., A. Murray, et al. (1999). "Fragile X syndrome: of POF and premutations." J Med Genet **36**(2): 171-172.
Maltsev, V. A., J. Rohwedel, et al. (1993). "Embryonic stem cells differentiate in vitro into cardiomyocytes representing sinusnodal, atrial and ventricular cell types." Mech Dev **44**(1): 41-50.
Maltsev, V. A., A. M. Wobus, et al. (1994). "Cardiomyocytes differentiated in vitro from embryonic stem cells developmentally express cardiac-specific genes and ionic currents." Circ Res **75**(2): 233-244.
Maltsev, V. A., A. M. Wobus, et al. (1994). "Cardiomyocytes differentiated in vitro from embryonic stem cells developmentally express cardiac-specific genes and ionic currents." Circulation research **75**(2): 233-244.
Martin, G. R. (1981). "Isolation of a pluripotent cell line from early mouse embryos cultured in medium conditioned by teratocarcinoma stem cells." Proc Natl Acad Sci U S A **78**(12): 7634-7638.
Massimi, M. (2008). Characterization of Profilin2 Complexes in the Mouse, EMBL Monterotondo Italy.
Maye, P., S. Becker, et al. (2000). "Indian hedgehog signaling in extraembryonic endoderm and ectoderm differentiation in ES embryoid bodies." Mech Dev **94**(1-2): 117-132.

Miki, H., K. Miura, et al. (1996). "N-WASP, a novel actin-depolymerizing protein, regulates the cortical cytoskeletal rearrangement in a PIP2-dependent manner downstream of tyrosine kinases." EMBO J **15**(19): 5326-5335.
Miki, H., T. Sasaki, et al. (1998). "Induction of filopodium formation by a WASP-related actin-depolymerizing protein N-WASP." Nature **391**(6662): 93-96.
Mockrin, S. C. and E. D. Korn (1980). "Acanthamoeba profilin interacts with G-actin to increase the rate of exchange of actin-bound adenosine 5'-triphosphate." Biochemistry **19**(23): 5359-5362.
Moreira, D. P., K. Griesi-Oliveira, et al. (2014). "Investigation of 15q11-q13, 16p11.2 and 22q13 CNVs in autism spectrum disorder Brazilian individuals with and without epilepsy." PloS one **9**(9): e107705.
Mullins, R. D., J. A. Heuser, et al. (1998). "The interaction of Arp2/3 complex with actin: nucleation, high affinity pointed end capping, and formation of branching networks of filaments." Proceedings of the National Academy of Sciences of the United States of America **95**(11): 6181-6186.
Mullins, R. D., W. F. Stafford, et al. (1997). "Structure, subunit topology, and actin-binding activity of the Arp2/3 complex from Acanthamoeba." J Cell Biol **136**(2): 331-343.
Murphy, S. M., A. M. Preble, et al. (2001). "GCP5 and GCP6: two new members of the human gamma-tubulin complex." Molecular biology of the cell **12**(11): 3340-3352.
Murthy, S. K., A. O. Nygren, et al. (2007). "Detection of a novel familial deletion of four genes between BP1 and BP2 of the Prader-Willi/Angelman syndrome critical region by oligo-array CGH in a child with neurological disorder and speech impairment." Cytogenetic and genome research **116**(1-2): 135-140.
Napoli, I., V. Mercaldo, et al. (2008). "The fragile X syndrome protein represses activity-dependent translation through CYFIP1, a new 4E-BP." Cell **134**(6): 1042-1054.
Nefsky, B. and A. Bretscher (1992). "Yeast actin is relatively well behaved." Eur J Biochem **206**(3): 949-955.
Ng, D., N. Thakker, et al. (2004). "Oculofaciocardiodental and Lenz microphthalmia syndromes result from distinct classes of mutations in BCOR." Nature genetics **36**(4): 411-416.
Nguyen, T. Y., S. Garcia, et al. (2012). "Effects of magnesium on growth and proliferation of human embryonic stem cells." Conference proceedings : ... Annual International Conference of the IEEE Engineering in Medicine and Biology Society. IEEE Engineering in Medicine and Biology Society. Annual Conference **2012**: 723-726.
Nishimura, Y., C. L. Martin, et al. (2007). "Genome-wide expression profiling of lymphoblastoid cell lines distinguishes different forms of autism and reveals shared pathways." Human molecular genetics **16**(14): 1682-1698.
Nourse, M. B., D. E. Halpin, et al. (2010). "VEGF induces differentiation of functional endothelium from human embryonic stem cells: implications for tissue engineering." Arteriosclerosis, thrombosis, and vascular biology **30**(1): 80-89.
Obermann, H., I. Raabe, et al. (2005). "Novel testis-expressed profilin IV associated with acrosome biogenesis and spermatid elongation." Mol Hum Reprod **11**(1): 53-64.
Padrick, S. B., H. C. Cheng, et al. (2008). "Hierarchical regulation of WASP/WAVE proteins." Molecular cell **32**(3): 426-438.
Paliwal, S., R. C. Kovi, et al. (2007). "The alternative reading frame tumor suppressor antagonizes hypoxia-induced cancer cell migration via interaction with the COOH-terminal binding protein corepressor." Cancer research **67**(19): 9322-9329.
Pangas, S. A., X. Li, et al. (2008). "Conditional deletion of Smad1 and Smad5 in somatic cells of male and female gonads leads to metastatic tumor development in mice." Molecular and Cellular Biology **28**(1): 248-257.
Parameswaran, M. and P. P. Tam (1995). "Regionalisation of cell fate and morphogenetic movement of the mesoderm during mouse gastrulation." Dev Genet **17**(1): 16-28.
Pathania, M., E. C. Davenport, et al. (2014). "The autism and schizophrenia associated gene CYFIP1 is critical for the maintenance of dendritic complexity and the stabilization of mature spines." Translational psychiatry **4**: e374.
Pedersen, T. and H. Peters (1968). "Proposal for a classification of oocytes and follicles in the mouse ovary." Journal of reproduction and fertility **17**(3): 555-557.
Pilo Boyl, P., A. Di Nardo, et al. (2007). "Profilin2 contributes to synaptic vesicle exocytosis, neuronal excitability, and novelty-seeking behavior." EMBO J **26**(12): 2991-3002.
Pittman, A. J., J. A. Gaynes, et al. (2010). "nev (cyfip2) is required for retinal lamination and axon guidance in the zebrafish retinotectal system." Developmental biology **344**(2): 784-794.

Porter, A. G. and R. U. Janicke (1999). "Emerging roles of caspase-3 in apoptosis." Cell death and differentiation **6**(2): 99-104.
Powers, S. E., K. Taniguchi, et al. (2010). "Tgif1 and Tgif2 regulate Nodal signaling and are required for gastrulation." Development **137**(2): 249-259.
Quamme, G. A. (2010). "Molecular identification of ancient and modern mammalian magnesium transporters." American journal of physiology. Cell physiology **298**(3): C407-429.
Rakeman, A. S. (2006). "Axis specification and morphogenesis in the mouse embryo require Nap1, a regulator of WAVE-mediated actin branching." Development **133**(16): 3075-3083.
Ring, C., M. H. Ginsberg, et al. (2011). "Abl-interactor-1 (Abi1) has a role in cardiovascular and placental development and is a binding partner of the alpha4 integrin." Proceedings of the National Academy of Sciences of the United States of America **108**(1): 149-154.
Rodriguez, R. T., J. M. Velkey, et al. (2007). "Manipulation of OCT4 levels in human embryonic stem cells results in induction of differential cell types." Experimental biology and medicine **232**(10): 1368-1380.
Rohwedel, J., V. Maltsev, et al. (1994). "Muscle cell differentiation of embryonic stem cells reflects myogenesis in vivo: developmentally regulated expression of myogenic determination genes and functional expression of ionic currents." Dev Biol **164**(1): 87-101.
Rossant, J. (1987). "Cell lineage analysis in mammalian embryogenesis." Curr Top Dev Biol **23**: 115-146.
Rujano, M. A., P. Pina, et al. (2004). "Retinoic acid-induced differentiation into astrocytes and glutamatergic neurons is associated with expression of functional and activable phospholipase D." Biochem Biophys Res Commun **316**(2): 387-392.
Saller, E., E. Tom, et al. (1999). "Increased apoptosis induction by 121F mutant p53." EMBO J **18**(16): 4424-4437.
Sasaki, S., D. Mori, et al. (2005). "Complete loss of Ndel1 results in neuronal migration defects and early embryonic lethality." Molecular and Cellular Biology **25**(17): 7812-7827.
Schenck, A., B. Bardoni, et al. (2003). "CYFIP/Sra-1 controls neuronal connectivity in Drosophila and links the Rac1 GTPase pathway to the fragile X protein." Neuron **38**(6): 887-898.
Schenck, A., B. Bardoni, et al. (2001). "A highly conserved protein family interacting with the fragile X mental retardation protein (FMRP) and displaying selective interactions with FMRP-related proteins FXR1P and FXR2P." Proc Natl Acad Sci U S A **98**(15): 8844-8849.
Schier, A. F. (2003). "Nodal signaling in vertebrate development." Annual review of cell and developmental biology **19**: 589-621.
Schmitt, R. M., E. Bruyns, et al. (1991). "Hematopoietic development of embryonic stem cells in vitro: cytokine and receptor gene expression." Genes Dev **5**(5): 728-740.
Schroeder, I. S., A. Rolletschek, et al. (2006). "Differentiation of mouse embryonic stem cells to insulin-producing cells." Nat Protoc **1**(2): 495-507.
Shen, M. M. and P. Leder (1992). "Leukemia inhibitory factor is expressed by the preimplantation uterus and selectively blocks primitive ectoderm formation in vitro." Proceedings of the National Academy of Sciences of the United States of America **89**(17): 8240-8244.
Shi, Y., K. Alin, et al. (1995). "Abl-interactor-1, a novel SH3 protein binding to the carboxy-terminal portion of the Abl protein, suppresses v-abl transforming activity." Genes Dev **9**(21): 2583-2597.
Shukla, S., R. Nair, et al. (2010). "Synthesis and organization of hyaluronan and versican by embryonic stem cells undergoing embryoid body differentiation." The journal of histochemistry and cytochemistry : official journal of the Histochemistry Society **58**(4): 345-358.
Silva, J. M., E. Ezhkova, et al. (2009). "Cyfip1 is a putative invasion suppressor in epithelial cancers." Cell **137**(6): 1047-1061.
Simon, M. M., S. Greenaway, et al. (2013). "A comparative phenotypic and genomic analysis of C57BL/6J and C57BL/6N mouse strains." Genome biology **14**(7): R82.
Soderling, S. H., L. K. Langeberg, et al. (2003). "Loss of WAVE-1 causes sensorimotor retardation and reduced learning and memory in mice." Proc Natl Acad Sci U S A **100**(4): 1723-1728.
Solaimani Kartalaei, P., T. Yamada-Inagawa, et al. (2015). "Whole-transcriptome analysis of endothelial to hematopoietic stem cell transition reveals a requirement for Gpr56 in HSC generation." The Journal of experimental medicine **212**(1): 93-106.
Soto, M. C., H. Qadota, et al. (2002). "The GEX-2 and GEX-3 proteins are required for tissue morphogenesis and cell migrations in C. elegans." Genes Dev **16**(5): 620-632.
Srinivas, S. (2006). "The anterior visceral endoderm-turning heads." Genesis **44**(11): 565-572.
Steffen, A., K. Rottner, et al. (2004). "Sra-1 and Nap1 link Rac to actin assembly driving lamellipodia formation." EMBO J **23**(4): 749-759.

Stoecker, S. (2010). Function of the Cytoplasmic FMRP Interacting Protein 1 (CyFIP1) in mouse embryonic development. Diploma Thesis, University of Bonn.
Stovold, C. F., T. H. Millard, et al. (2005). "Inclusion of Scar/WAVE3 in a similar complex to Scar/WAVE1 and 2." BMC cell biology **6**(1): 11.
Strubing, C., G. Ahnert-Hilger, et al. (1995). "Differentiation of pluripotent embryonic stem cells into the neuronal lineage in vitro gives rise to mature inhibitory and excitatory neurons." Mech Dev **53**(2): 275-287.
Stumpf, M., C. Waskow, et al. (2006). "The mediator complex functions as a coactivator for GATA-1 in erythropoiesis via subunit Med1/TRAP220." Proceedings of the National Academy of Sciences of the United States of America **103**(49): 18504-18509.
Suetsugu, S., H. Miki, et al. (1999). "Identification of two human WAVE/SCAR homologues as general actin regulatory molecules which associate with the Arp2/3 complex." Biochem Biophys Res Commun **260**(1): 296-302.
Sullivan, S. D. and D. H. Castrillon (2011). "Insights into primary ovarian insufficiency through genetically engineered mouse models." Seminars in reproductive medicine **29**(4): 283-298.
Sumitomo, A., R. Ishino, et al. (2010). "The transcriptional mediator subunit MED1/TRAP220 in stromal cells is involved in hematopoietic stem/progenitor cell support through osteopontin expression." Molecular and Cellular Biology **30**(20): 4818-4827.
Suzumori, N., S. A. Pangas, et al. (2007). "Candidate genes for premature ovarian failure." Current medicinal chemistry **14**(3): 353-357.
Takaki, M., S. Nakayama, et al. (2006). "In vitro formation of enteric neural network structure in a gut-like organ differentiated from mouse embryonic stem cells." Stem cells **24**(6): 1414-1422.
Takasaki, N., T. Rankin, et al. (2001). "Normal gonadal development in mice lacking GPBOX, a homeobox protein expressed in germ cells at the onset of sexual dimorphism." Molecular and Cellular Biology **21**(23): 8197-8202.
Takenawa, T. and H. Miki (2001). "WASP and WAVE family proteins: key molecules for rapid rearrangement of cortical actin filaments and cell movement." J Cell Sci **114**(Pt 10): 1801-1809.
Tam, P. P. and R. S. Beddington (1987). "The formation of mesodermal tissues in the mouse embryo during gastrulation and early organogenesis." Development **99**(1): 109-126.
ten Berge, D., W. Koole, et al. (2008). "Wnt signaling mediates self-organization and axis formation in embryoid bodies." Cell stem cell **3**(5): 508-518.
Thomas, G., K. B. Jacobs, et al. (2008). "Multiple loci identified in a genome-wide association study of prostate cancer." Nature genetics **40**(3): 310-315.
Thrasher, A. J. (2002). "WASp in immune-system organization and function." Nat Rev Immunol **2**(9): 635-646.
Tsang, H. T., T. L. Edwards, et al. (2009). "The hereditary spastic paraplegia proteins NIPA1, spastin and spartin are inhibitors of mammalian BMP signalling." Human molecular genetics **18**(20): 3805-3821.
Ueki, Y. and T. A. Reh (2012). "Activation of BMP-Smad1/5/8 signaling promotes survival of retinal ganglion cells after damage in vivo." PloS one **7**(6): e38690.
Visser, J. A., I. Schipper, et al. (2012). "Anti-Mullerian hormone: an ovarian reserve marker in primary ovarian insufficiency." Nature reviews. Endocrinology **8**(6): 331-341.
Voncken, J. W., B. A. Roelen, et al. (2003). "Rnf2 (Ring1b) deficiency causes gastrulation arrest and cell cycle inhibition." Proceedings of the National Academy of Sciences of the United States of America **100**(5): 2468-2473.
Walsh, C. A., E. M. Morrow, et al. (2008). "Autism and brain development." Cell **135**(3): 396-400.
Wang, E. L., Z. R. Qian, et al. (2010). "Increased expression of HMGA1 correlates with tumour invasiveness and proliferation in human pituitary adenomas." Histopathology **56**(4): 501-509.
Wang, W., N. Lian, et al. (2009). "Atf4 regulates chondrocyte proliferation and differentiation during endochondral ossification by activating Ihh transcription." Development **136**(24): 4143-4153.
Winder, S. J. (2005). "Actin-binding proteins." Journal of Cell Science **118**(4): 651-654.
Witke, W. (2004). "The role of profilin complexes in cell motility and other cellular processes." Trends Cell Biol **14**(8): 461-469.
Witke, W., A. V. Podtelejnikov, et al. (1998). "In mouse brain profilin I and profilin II associate with regulators of the endocytic pathway and actin assembly." EMBO J **17**(4): 967-976.
Witke, W., J. D. Sutherland, et al. (2001). "Profilin I is essential for cell survival and cell division in early mouse development." Proc Natl Acad Sci U S A **98**(7): 3832-3836.

Wobus, A. M., G. Wallukat, et al. (1991). "Pluripotent mouse embryonic stem cells are able to differentiate into cardiomyocytes expressing chronotropic responses to adrenergic and cholinergic agents and Ca2+ channel blockers." Differentiation **48**(3): 173-182.
Xie, H., Y. Zhang, et al. (2014). "Functional study of NIPA2 mutations identified from the patients with childhood absence epilepsy." PloS one **9**(10): e109749.
Xu, C., N. G. Kim, et al. (2009). "Regulation of protein stability by GSK3 mediated phosphorylation." Cell cycle **8**(24): 4032-4039.
Yamada, G., C. Kioussi, et al. (1994). "Regulated expression of Brachyury(T), Nkx1.1 and Pax genes in embryoid bodies." Biochemical and biophysical research communications **199**(2): 552-563.
Yamazaki, D., S. Suetsugu, et al. (2003). "WAVE2 is required for directed cell migration and cardiovascular development." Nature **424**(6947): 452-456.
Yan, C., N. Martinez-Quiles, et al. (2003). "WAVE2 deficiency reveals distinct roles in embryogenesis and Rac-mediated actin-based motility." EMBO J **22**(14): 3602-3612.
Ye, J., M. Kumanova, et al. (2010). "The GCN2-ATF4 pathway is critical for tumour cell survival and proliferation in response to nutrient deprivation." The EMBO journal **29**(12): 2082-2096.
Yokota, Y., C. Ring, et al. (2007). "Nap1-Regulated Neuronal Cytoskeletal Dynamics Is Essential for the Final Differentiation of Neurons in Cerebral Cortex." Neuron **54**(3): 429-445.
Zhang, T. F., S. Q. Yu, et al. (2003). "Inducible expression of RbAp46 activates c-Jun NH2-terminal kinase-dependent apoptosis and suppresses progressive growth of tumor xenografts in nude mice." Anticancer research **23**(6C): 4621-4627.

7. Appendix

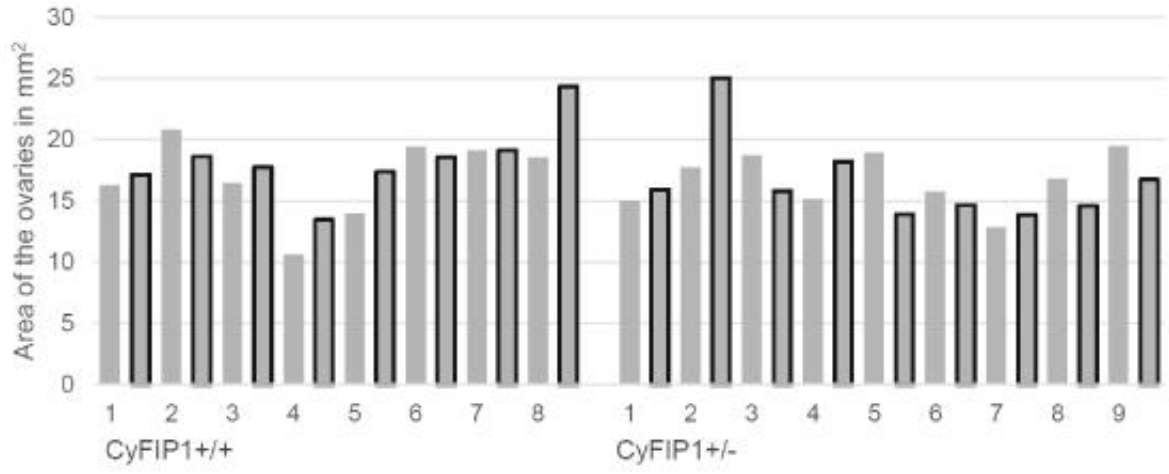

Figure 38: Graphical representation of the surface area of the analyzed ovaries. Left: Ovaries from wt mice. Right: Ovaries from CyFIP1+/- mice. Grey columns: first ovary from the examined mouse. Black framed grey columns: second ovary from the examined mouse. The surface area varied strongly from mouse to mouse, independently of the genotype and no significant differences could be observed.

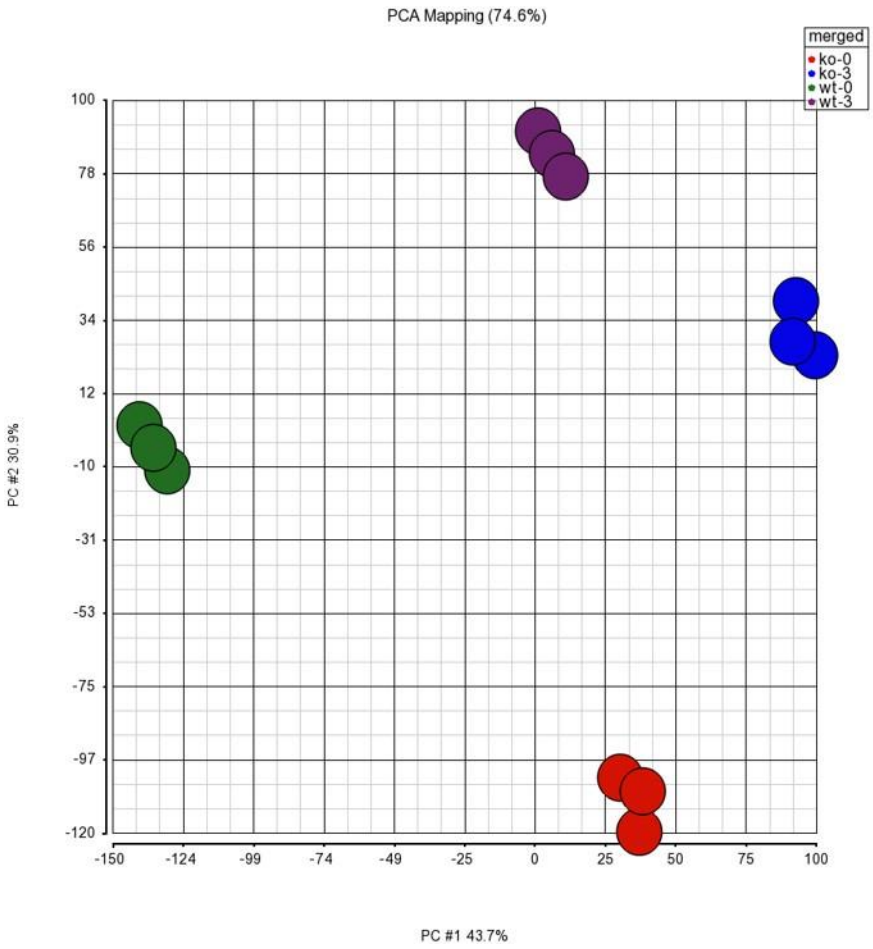

Figure 39: Principal component analysis (PCA) mapping for the microarray data. The gene expression data after normalization for each genotype and time point are represented by circles of different color. Each

colored circle represents data from one clone. wt-0 green: Wild type ES cells; ko-0 red: CyFIP1-/- ES cells; wt-3 purple: Differentiated wild type ES cells for 3 days on gelatine; ko-3 blue: Differentiated CyFIP1-/- ES cells for 3 days on gelatine. The three clones for each type show very little variance, therefore a mean of the three could be used for further analyses.